NASA/TM–20210016636

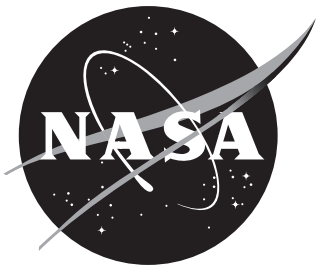

Solving Two-Equation Turbulence Models

With a Perspective on Solving Transport Equations

R. C. Swanson
Langley Research Center, Hampton, Virginia

October 2021

NASA STI Program Report Series

Since its founding, NASA has been dedicated to the advancement of aeronautics and space science. The NASA scientific and technical information (STI) program plays a key part in helping NASA maintain this important role.

The NASA STI program operates under the auspices of the Agency Chief Information Officer. It collects, organizes, provides for archiving, and disseminates NASA's STI. The NASA STI program provides access to the NTRS Registered and its public interface, the NASA Technical Reports Server, thus providing one of the largest collections of aeronautical and space science STI in the world. Results are published in both non-NASA channels and by NASA in the NASA STI Report Series, which includes the following report types:

- TECHNICAL PUBLICATION. Reports of completed research or a major significant phase of research that present the results of NASA Programs and include extensive data or theoretical analysis. Includes compilations of significant scientific and technical data and information deemed to be of continuing reference value. NASA counterpart of peer-reviewed formal professional papers but has less stringent limitations on manuscript length and extent of graphic presentations.

- TECHNICAL MEMORANDUM. Scientific and technical findings that are preliminary or of specialized interest, e.g., quick release reports, working papers, and bibliographies that contain minimal annotation. Does not contain extensive analysis.

- CONTRACTOR REPORT. Scientific and technical findings by NASA-sponsored contractors and grantees.

- CONFERENCE PUBLICATION. Collected papers from scientific and technical conferences, symposia, seminars, or other meetings sponsored or co-sponsored by NASA.

- SPECIAL PUBLICATION. Scientific, technical, or historical information from NASA programs, projects, and missions, often concerned with subjects having substantial public interest.

- TECHNICAL TRANSLATION. English-language translations of foreign scientific and technical material pertinent to NASA's mission.

Specialized services also include organizing and publishing research results, distributing specialized research announcements and feeds, providing information desk and personal search support, and enabling data exchange services.

For more information about the NASA STI program, see the following:

- Access the NASA STI program home page at http://www.sti.nasa.gov

- Help desk contact information:

https://www.sti.nasa.gov/sti-contact-form/
and select the "General" help request type.

NASA/TM–20210016636

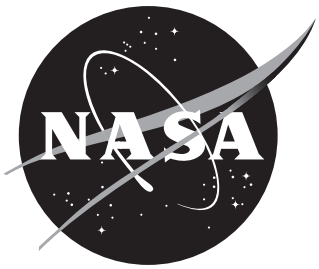

Solving Two-Equation Turbulence Models
With a Perspective on Solving Transport Equations

R. C. Swanson
Langley Research Center, Hampton, Virginia

National Aeronautics and
Space Administration

October 2021

Available from:

NASA STI Program / Mail Stop 148
NASA Langley Research Center
Hampton, VA 23681-2199
Fax: 757-864-6500

Abstract

There are three principal objectives of this report. The first objective is to explore and evaluate the performance of the solution algorithm for the Reynolds-averaged Navier-Stokes (RANS) equations with two-equation turbulence models. The RANS and turbulence modeling equations are solved in a weakly coupled manner. A Runge-Kutta/Implicit scheme is the basis of the solution algorithm for both sets of equations. This scheme is used as a smoother for a multigrid method when solving the mean flow form of the conservation equations. Throughout this report, emphasis is given to reducing the residuals to machine zero in all flow calculations to eliminate error due to numerical integration of the discrete governing equations. The second objective of this report is to investigate frequently used two-equation models when solving the RANS equations. In this study, we consider the 2006 Wilcox and the 2003 Menter Shear Stress Transport (SST) models. Computations for flows over two different airfoils are examined to compare these turbulence models. Effects on modeling the physics of each flow due to variations in the models, such as using either strain rate or vorticity in the turbulence production term, are considered and discussed. The final objective is to provide a perspective on solving transport equations for turbulence modeling. Aspects of solving such stiff systems of equations, as well as various numerical difficulties and possible techniques to overcome them, are considered. Discussion is also provided concerning what is called 'numerical compatibility,' which is an essential requirement when designing an effective solution algorithm for solving transport equations.

Contents

1 Introduction

Reliable and sufficient convergence for steady-state and unsteady (using dual-time stepping approach) computations of turbulent flows continues to be a challenge in computational fluid dynamics. Convergence frequently becomes much more difficult when applying transport equation models to determine the effects of turbulence on the mean flow. This problem often becomes acute when considering turbulence models with more than one transport equation. Moreover, frequently in engineering applications the residual for the turbulence model is only reduced between two to five orders of magnitude. The results from such calculations clearly cannot be representative, in general, of the solutions of the transport equations. Thus, it is essential that the convergence behavior with these models be dramatically improved; otherwise, we cannot use such models (certainly not on any routine basis) or determine the relative benefits of one model with respect to another.

In this report we consider the Reynolds-averaged Navier-Stokes (RANS) equations. The RANS equations are based on the Reynolds expansion for the dependent variables density and pressure and Favre mass-averaged expansion for all other dependent flow variables. These expansions of the variables are substituted into the conservation of momentum equations and time averaged [1] to obtain the RANS equations. The same procedure is followed for the conservation of mass and energy equations. By using the mass-averaged flow variables, the time-averaged compressible equations can retain essentially the same form as their laminar flow counterparts. The resulting mean flow momentum equations are simply augmented by an additional stress term (a Reynolds stress), and the mean flow energy equation includes an additional heat flux term (Reynolds heat flux) and work term due to the Reynolds stresses. The energy equation also includes turbulence kinetic energy terms, which are often neglected when considering subsonic and transonic flows. Then, to close the system of equations, some form of modeling is required to determine the Reynolds stresses and Reynolds heat fluxes.

Currently, in engineering applications, partial differential equations (PDEs) of a transport type are generally used in modeling the effects of turbulence. One approach for modeling the additional terms (Reynolds stresses) appearing in the RANS equations is to invoke the eddy viscosity hypothesis (the Boussinesq approximation) in which the Reynolds stress tensor is proportional to the mean strain rate tensor. This constitutive relation requires the determination of a viscosity coefficient that is called an eddy viscosity. The eddy viscosity depends on two scales: a velocity scale and a length scale. These scales can be determined using transport equations. Usually, turbulence modeling formulations use one or two equations to determine the scales. For one-equation models, the velocity scale comes from solving for either the turbulence kinetic energy k or a quantity that can be related to k. The length scale for these models comes from an algebraic method that depends on physical location and whether the flow is a wall-bounded shear layer or a free shear layer. Two-equation models are often considered since the two scales can be computed from the two transport equations, one for k and the other for a quantity related to the length scale, such as the dissipation rate of k. Two advantages in using one-equation or two-equation models are that they avoid the necessity of solving directly for the Reynolds stresses and simplify considerably the modeling and the solution requirements (e.g., typical Reynolds stress models require solving six equations for the Reynolds stresses and one equation for the length scale). Further discussion of the history of turbulence modeling is given in Appendix A and also in the paper by Speziale [2]. The focus in this paper concerns two-equation models.

In the last several years, significant effort has been dedicated to evaluating the one-equation model of Spalart and Allmaras [3–5], both in terms of its applications and numerical behavior. The improved solvability of the single transport equation of the model using the SA negative form is a major factor for the wide use of this turbulence model. While two-equation models, such as those of Wilcox [1, 6, 7] and Menter [8]–[13] continue to be applied frequently, very little attention has been directed to how to solve the associated transport equations reliably and efficiently. Although a number of papers have considered such models, along with a number of variations of them [14], there

are generally few details and discussion about various numerical issues and convergence behavior (i.e., as revealed by convergence plots for both the mean flow and turbulence modeling equations). While there are a few papers that consider some numerical issues and show convergence histories, such as those of Mor-Yossef [15, 16] and Wasserman et al. [17], there remains a need to have additional comprehensive evaluations. A requirement in any further evaluations is that all residuals of the discrete equations must be reduced to machine zero (i.e., fully converged) to eliminate any adverse effects due to numerical integration errors. We consider two-equation models in the present investigation because numerical difficulties are frequently experienced when solving the governing equations for the mean flow and two-equation models. Further, study of such models allows extensive examination of modeling and numerical issues arising from a transport equation for a length scale, which is also present in considerably more complicated second-order closure turbulence models, such as Reynolds stress models. These models solve directly for the Reynolds stresses, removing the Boussinesq approximation and the assumption of isotropic turbulence inherent in first-order closure models.

The initial work, forming the foundation for this paper, was primarily performed by the author during summer visits to Deutsches Zentrum für Luft- und Raumfahrt (DLR) in Braunschweig, Germany. There are three principal objectives in this paper. A key objective is to investigate the efficacy and reliability of a numerical algorithm for solving the mean conservation equations and the transport equations for modeling the effects of turbulence. The mean flow and and turbulence modeling equations are solved in a weakly coupled manner. A Runge-Kutta/Implicit (RK/Implicit) scheme is the basis of the solution algorithm for both sets of equations. This scheme can be viewed as a member of the general class of implicit Runge-Kutta schemes, which includes Diagonally Implicit Runge-Kutta (DIRK) schemes. It is used as a smoother for a multigrid method when solving the mean flow equations. In this report, emphasis is placed on obtaining fully converged solutions in all flow computations. This is considered an essential requirement when evaluating and comparing various turbulence models to remove the influence of errors due to numerical integration of the governing equations. In addition, by consistently reducing the residuals of the discrete equations to machine zero, there is support for the assertion that the numerical scheme is contractive.

The second objective of this report is to evaluate two first-order turbulence modeling formulations based on the k-ω model. For representative first-order models, we have chosen the 2006 Wilcox model and the 2003 Menter Shear Stress Transport (SST) model. The Wilcox model includes transport equations for the turbulence kinetic energy k and its specific dissipation rate ω. This k-ω model is also part of the SST model of Menter. With the Menter model, there is a blend of both the k-ω and the k-ϵ models, where ϵ is the rate of dissipation of turbulence kinetic energy. The Wilcox k-ω model is used near a surface boundary, and the k-ϵ model is applied automatically (due to blending) in the vicinity of the boundary-layer edge. There are certain advantages of each model. For example, the k-ω model has good stability properties and predictive capability for the logarithmic layer in pressure gradient flows, and the k-ϵ model yields better representation in the wake region of the boundary layer and also for free shear flows. While these are certainly compelling arguments for the blended formulation, Wilcox argues in support of the elegance of the single model approach, which avoids the blending and seems to give equally good predictions for a number of canonical problems involving turbulent flows. One particularly important issue with both of these turbulence models is the singular type behavior of the ω equation when approaching a solid wall boundary. Thus, there is a need for careful consideration and assessment of this behavior on the numerical solution algorithm, including the impact of the boundary condition.

To evaluate these turbulence models, we consider computations for turbulent flows over two different airfoils. Computations are performed for both subsonic and transonic flows over the RAE 2822 airfoil at low angles of attack. Since often accuracy and convergence issues are encountered when computing high angle of attack aerodynamic flows, it is important to evaluate the two-equation turbulence models when considering such flows. Thus, numerical solutions with these models are also obtained for low-speed flow over the NACA 4412 airfoil at 13.87 degrees angle of attack. For

all flow cases, we examine the effects of mesh refinement in which the number of mesh cells on each successive grid is doubled in each coordinate direction. In addition, we consider and discuss the effects on representing the physics of each flow due to variations in the turbulence models, such as using either strain rate or vorticity in the turbulence production term of the transport equations.

The final objective is to provide a perspective on solving transport equations for turbulence modeling. Here, aspects of solving the stiff system of equations as well as various numerical difficulties and possible techniques for overcoming such issues are considered. Discussion is also provided concerning what one may call 'numerical compatibility,' which is a principal requirement when designing an efficient and reliable algorithm for solving transport equations.

In Section 2, the integral form of the RANS equations and the corresponding boundary conditions of the continuous problem are defined. Some fundamental discussion of the two-equation turbulence models being considered is given in Section 3.4, setting the stage for Sections 3.1 and 3.2 that define the 2006 Wilcox model and the 2003 Menter SST model. Details concerning the spatial discretization of the governing equations and the numerical solution algorithm are presented and discussed in Section 4. The following two sections, Sections 5 and 6, show and discuss the computational results for flows over the RAE 2822 and NACA 4412 airfoils. For each flow case computed, the convergence histories for both the mean flow and turbulence modeling equations are displayed. The effects of mesh refinement on the numerical solutions, which include surface pressure and skin-friction distributions, pressure contours and streamlines, eddy viscosity contours and velocity profiles (NACA 4412 airfoil flow) are considered. These sections also include discussion on the additional subjects of turbulence production limiter, changing the form of numerical dissipation and the stress limiter of the Wilcox model. Before making concluding remarks in the last section, we present observations and perspectives on solving transport equations in Section 7.

2 Governing Equations

In this paper, all applications are for two-dimensional (2-D) airfoil flows. We consider the RAE 2822 and NACA 4412 airfoils. These particular airfoils are frequently considered when evaluating turbulence models. However, we point out that both the mathematical formulation and the numerical methods described herein have been extended to three-dimenional (3-D) turbulent flows. In this paper, we consider the 2-D RANS equations that govern turbulent compressible flows.

2.1 Mathematical Formulation

Assuming a volume fixed in space and time, the integral form of these equations can be written as

$$\iiint_{\mathcal{V}} \frac{\partial \mathbf{W}}{\partial t} d\mathcal{V} + \iint_{\mathcal{S}} \mathcal{F} \cdot \mathbf{n} d\mathcal{S} = 0, \tag{1}$$

where the symbol ∂ indicates partial differentiation, $\mathbf{W}$ is the state vector of conservative variables,

$$\mathbf{W} = \left[\begin{array}{cccccc} \rho & \rho u & \rho v & \rho w & \rho E \end{array} \right]^T; \tag{2}$$

$\mathcal{F}$ is the flux density tensor, and $\mathcal{V}$, $\mathcal{S}$, and $\mathbf{n}$ denote the volume, surface, and outward facing normal of the control volume. One can split the flux density tensor into a convective contribution $\mathcal{F}_c$ and a viscous contribution $\mathcal{F}_v$, which are given by

$$\mathcal{F}_c = \begin{bmatrix} \rho \mathbf{q} \\ \rho u\, \mathbf{q} + p\, \mathbf{e}_x \\ \rho v\, \mathbf{q} + p\, \mathbf{e}_y \\ \rho w\, \mathbf{q} + p\, \mathbf{e}_z \\ \rho H\, \mathbf{q} \end{bmatrix}, \qquad \mathcal{F}_v = - \begin{bmatrix} 0 \\ \bar{\tau} \cdot \mathbf{e}_x \\ \bar{\tau} \cdot \mathbf{e}_y \\ \bar{\tau} \cdot \mathbf{e}_z \\ \bar{\tau} \cdot \mathbf{q} - \nabla \cdot \mathbf{Q} \end{bmatrix}, \tag{3}$$

where ∇ is the gradient operator, $\mathbf{q}$ is the velocity vector with Cartesian components (u, v, w), and the unit vectors $(\mathbf{e}_x, \mathbf{e}_y, \mathbf{e}_z)$ are associated with the Cartesian coordinates (x, y, z). The variables ρ and p represent density and pressure, respectively. The H is the total specific enthalpy, which is defined by

$$H = E + \frac{p}{\rho}, \quad H = h + \frac{\mathbf{q} \cdot \mathbf{q}}{2}, \tag{4}$$

where h represents the specific enthalpy. The stress tensor $\bar{\tau}$ and the heat flux vector $\mathbf{Q}$ are given by

$$\bar{\tau} = \begin{bmatrix} \tau_{xx} & \tau_{xy} & \tau_{xz} \\ \tau_{yx} & \tau_{yy} & \tau_{yz} \\ \tau_{zx} & \tau_{zy} & \tau_{zz} \end{bmatrix}, \qquad \mathbf{Q} = \hat{k} \nabla T = -\hat{k} \begin{bmatrix} \partial T/\partial x \\ \partial T/\partial y \\ \partial T/\partial z \end{bmatrix}, \tag{5}$$

with $\hat{k}$ denoting the coefficient of thermal conductivity and T representing the temperature. The elements of the stress tensor $\bar{\tau}$ are defined by

$$\tau_{ij} = \mu \left(\frac{\partial u_i}{\partial x_j} + \frac{\partial u_j}{\partial x_i} - \frac{2}{3} \delta_{ij} \frac{\partial u_k}{\partial x_k} \right) \qquad (i, j, k = 1, 2, 3) \tag{6}$$

where μ is the molecular viscosity, δ_{ij} is the kronecker delta, and the subscripts i, j, k refer to the x, y, z directions, respectively. It is convenient to express the stress tensor in terms of dyadic products,

$$\begin{aligned} \bar{\tau} = & \tau_{xx}\mathbf{e}_x\mathbf{e}_x + \tau_{xy}\mathbf{e}_x\mathbf{e}_y + \tau_{xz}\mathbf{e}_x\mathbf{e}_z \\ & \tau_{yx}\mathbf{e}_y\mathbf{e}_x + \tau_{yy}\mathbf{e}_y\mathbf{e}_y + \tau_{yz}\mathbf{e}_y\mathbf{e}_z \\ & \tau_{zx}\mathbf{e}_z\mathbf{e}_x + \tau_{zy}\mathbf{e}_z\mathbf{e}_y + \tau_{zz}\mathbf{e}_z\mathbf{e}_z. \end{aligned} \tag{7}$$

In order to close the system given by Eq. (1), we use the equation of state for an ideal gas,

$$p = \rho R T, \tag{8}$$

where R is the specific gas constant.

To derive the mean flow form of the conservation equations, which include the Navier-Stokes (momentum) equations, we first substitute the appropriate Favre variables and Reynolds variables for the instantaneous flow variables. Then, time averaging (in the sense of Reynolds) is applied to the equations. Details of this procedure are given in Wilcox [1] and also Rubesin and Rose [18]. The particular nondimensionalization of the equations is presented in Appendix B.

Frequently, in particular for subsonic and transonic flows, the turbulence kinetic energy contributions to the mean flow energy equation are neglected. Then, the mean flow equations are determined by simply replacing the coefficient μ by $\mu_\ell + \mu_t$ and replacing the coefficient $\hat{k}$ according to

$$\hat{k} \rightarrow C_p \left[\frac{\mu_\ell}{Pr_\ell} + \frac{\mu_t}{Pr_t} \right] \tag{9}$$

The subscripts ℓ and t refer to molecular and turbulent values of the viscosity and thermal conductivity coefficients. The C_p is the specific heat at constant pressure, and Pr is the Prandtl number.

2.2 Physical Boundary Conditions for the Mean Flow Variables

For viscous flows, both the no-penetration and the no-slip conditions

$$\mathbf{q} \cdot \mathbf{n} = 0, \quad \mathbf{q} \cdot \mathbf{t} = 0 \tag{10}$$

must be satisfied. Here, $\mathbf{n}$ and $\mathbf{t}$ are the unit normal and tangential vectors to the solid surface boundary, respectively. In addition, a boundary condition is required to determine the surface temperature.

For this boundary condition, either the wall temperature is set to a specified value or the adiabatic condition

$$\mathbf{Q} \cdot \mathbf{n} = 0 \tag{11}$$

is imposed, where $\mathbf{Q}$ is the heat flux vector given in Eq. (5).

3 Two-Equation Turbulence Models

The following sections present the two-equation models considered in this report. First, the 2006 Wilcox model and a variation introduced herein are defined. The next section defines the 2003 Menter SST model. In the last section, comparisons are made between the 2006 Wilcox and 2003 Menter models. In so doing, possible sources of differences in the computational results with the models are identified.

3.1 Wilcox k-ω Models

In this section, we describe the Wilcox k-ω model and delineate the specific assumptions associated with the form of the model that we have applied. A stress limiter (with parameter) for the specific dissipation rate is defined. The effect of the stress-limiter parameter on the extent of flow separation is discussed in the results section.

A detailed discussion of the 2006 version of the Wilcox k-ω model is given in the third edition of the book on turbulence modeling by Wilcox [6]. See also Wilcox [7]. This version of the model is an extension to the 1998 version, which is describe in the second edition of the book on turbulence modeling by Wilcox [1]. The principal changes in the 1998 model are the inclusion of a cross-diffusion term and a stress limiter. Before writing the two transport equations of this model, we present the relevant constitutive relations and define the associated quantities. In general, the mean-molecular-stress tensor $\bar{t}_{ij}$ and the Reynolds-stress tensor τ_{ij} are given by

$$\bar{t}_{ij} = 2\mu\bar{S}_{ij}, \qquad \tau_{ij} = 2\mu_t\bar{S}_{ij} - \frac{2}{3}\bar{\rho}k\delta_{ij}, \qquad \bar{S}_{ij} = S_{ij} - \frac{1}{3}\frac{\partial\tilde{u}_k}{\partial x_k}\delta_{ij}. \tag{12}$$

where μ is the molecular viscosity, μ_t is the turbulent viscosity, $\bar{\rho}$ is the mean density, k is the turbulence kinetic energy per unit mass, and δ_{ij} is the kronecker delta. The overbar and tilde indicate Reynolds-averaged and mass-averaged quantities, respectively. The mean strain-rate tensor S_{ij} in Eq. (12) and the mean rotation tensor Ω_{ij} are defined as follows:

$$S_{ij} = \frac{1}{2}\left(\frac{\partial\tilde{u}_i}{\partial x_j} + \frac{\partial\tilde{u}_j}{\partial x_i}\right), \qquad \Omega_{ij} = \frac{1}{2}\left(\frac{\partial\tilde{u}_i}{\partial x_j} - \frac{\partial\tilde{u}_j}{\partial x_i}\right). \tag{13}$$

The equation for the turbulence kinetic energy can be written as

$$\frac{\partial}{\partial t}(\bar{\rho}k) + \frac{\partial}{\partial x_j}(\bar{\rho}\tilde{u}_j k) = \mathcal{P} - \beta^*\bar{\rho}k\omega + \frac{\partial}{\partial x_j}\left[\left(\mu + \sigma_k\frac{\bar{\rho}k}{\omega}\right)\frac{\partial k}{\partial x_j}\right]. \tag{14}$$

The equation for the specific dissipation rate is given by

$$\frac{\partial}{\partial t}(\bar{\rho}\omega) + \frac{\partial}{\partial x_j}(\bar{\rho}\tilde{u}_j\omega) = \alpha\frac{\omega}{k}\mathcal{P} - \beta\bar{\rho}\omega^2 + \sigma_d\frac{\bar{\rho}}{\omega}\frac{\partial k}{\partial x_j}\frac{\partial\omega}{\partial x_j} + \frac{\partial}{\partial x_j}\left[\left(\mu + \sigma_\omega\frac{\bar{\rho}k}{\omega}\right)\frac{\partial\omega}{\partial x_j}\right]. \tag{15}$$

Here, $\mathcal{P}$ represents the turbulence production term,

$$\mathcal{P} = \tau_{ij}\frac{\partial\tilde{u}_i}{\partial x_j}, \tag{16}$$

and substituting for τ_{ij}, the production term becomes

$$\mathcal{P} = 2\mu_t S_{ij}\frac{\partial \tilde{u}_i}{\partial x_j} - \frac{2}{3}\mu_t\left(\frac{\partial \tilde{u}_k}{\partial x_k}\,\delta_{ij}\right)\frac{\partial \tilde{u}_i}{\partial x_j} - \frac{2}{3}\bar{\rho}k\frac{\partial \tilde{u}_i}{\partial x_j}\delta_{ij}. \tag{17}$$

Note that repeated indices imply the standard summation convention. The first, second, and last terms of the right-hand sides of Eqs. (14) and (15) represent the production, destruction, and diffusion of turbulence, respectively. The third term in Eq. (15) is a cross-diffusion term. The coefficient of the production term in Eq. (15) uses the parameter α, which is consistent with the notation of Wilcox. It should be mentioned that often Menter, as well as the Turbulence Modeling Resource (TMR) website [19], replaces this parameter with γ.

In this report, in which only low-speed and transonic flows are considered, we neglect the term that contains k in the Reynolds-stress tensor, which is important for high Mach number flows. Thus, the production term defined in Eq. (16) becomes

$$\mathcal{P} = 2\mu_t \bar{S}_{ij}\frac{\partial \tilde{u}_i}{\partial x_j}. \tag{18}$$

Then, expanding the production term in Eq. (18), it can easily be shown that this term, which depends on the strain rate tensor, can be expressed as

$$\mathcal{P} = \mu_t(2\,\bar{S}_{ij}\bar{S}_{ij}). \tag{19}$$

The production term of Eq. (19) is frequently approximated by

$$\mathcal{P} = \mu_t(2\,S_{ij}S_{ij}), \tag{20}$$

which is exact if the flow is incompressible (i.e., volumetric dilatation is zero). In terms of the mean rotation tensor Ω_{ij} defined in Eq. (13),

$$\mathcal{P} = \mu_t(2\,\Omega_{ij}\Omega_{ij}). \tag{21}$$

The $S_{ij}S_{ij}$ and $\Omega_{ij}\Omega_{ij}$ are double dot products of the mean strain-rate and mean rotation tensors with themselves. Thus, the production term in Eq. (21) can be written in terms of the square of the magnitude of the vorticity vector,

$$\mathcal{P} = \mu_t\,|\nabla \times \mathbf{q}|^2. \tag{22}$$

To compare the effect of using strain rate or vorticity in the production term, we use the approximations of Eqs. (20) and (21), respectively.

The cross-diffusion term, which does not appear in earlier versions of the Wilcox model, is of particular importance for free-shear flows. As revealed subsequently and discussed in the results section, it is also beneficial in the neighborhood of a stagnation point. As noted earlier, the second principal modification to the 1998 version of the Wilcox model is the introduction of a stress limiter. With this modification the turbulent viscosity μ_t depends on the limited $\hat{\omega}$ rather than strictly the ω. The modified ω used in computing μ_t is given by

$$\hat{\omega} = \max\left\{\omega, \quad C_{lim}\sqrt{\frac{2\bar{S}_{ij}\bar{S}_{ij}}{\beta^*}}\right\}, \qquad C_{lim} = 0.95, \tag{23}$$

where $\bar{S}_{i,j}$ is the zero trace version of the mean strain-rate tensor. When we use vorticity in the approximation of the production term, then $(2\bar{S}_{ij}\bar{S}_{ij})^{1/2}$ is replaced by the magnitude of the vorticity vector. Wilcox [7] indicates that the alternative of vorticity instead of strain rate is preferred in a

number of implementations of this turbulence model. The turbulent viscosity μ_t and eddy viscosity ν_t are given by

$$\mu_t = \frac{\bar{\rho}k}{\hat{\omega}}, \quad \nu_t = \frac{k}{\hat{\omega}}, \tag{24}$$

The introduction of the stress limiter is quite important for separated flows. In particular, it reduces the magnitude of the eddy viscosity when the production of turbulence energy exceeds the dissipation rate, which allows larger separation bubbles (as demonstrated by Huang [20]). Furthermore, Wilcox [7] points out that the success of the 2006 version of the model demonstrates that a more elegant model formulation is possible without any need for blending functions, such as those used in the SST model [10].

The remaining modifications in the 1998 model involve the closure coefficients. The closure coefficients for the 2006 k-ω model are as follows:

$$\alpha = \frac{13}{25}, \quad \beta = \beta_o f_\beta, \quad \beta^* = \frac{9}{100}, \quad \sigma_k = \frac{3}{5}, \quad \sigma_\omega = \frac{1}{2}, \quad \sigma_{do} = \frac{1}{8}, \quad \beta_o = 0.0708, \tag{25}$$

$$Pr_t = \frac{8}{9}, \quad f_\beta = \frac{1+85\chi_\omega}{1+100\chi_\omega}, \quad \chi_\omega \equiv \left| \frac{\Omega_{ij}\Omega_{jk}\hat{S}_{ki}}{(\beta^*\omega)^3} \right|, \quad \hat{S}_{ki} = S_{ki} - \frac{1}{2}\frac{\partial \tilde{u}_m}{\partial x_m}\delta_{ki},$$

$$\sigma_d = \begin{cases} 0, & \frac{\partial k}{\partial x_j}\frac{\partial \omega}{\partial x_j} \le 0 \\ \sigma_{do}, & \frac{\partial k}{\partial x_j}\frac{\partial \omega}{\partial x_j} > 0 \end{cases}$$

where Pr_t is the turbulent Prandtl number. As indicated in the TMR website [19],

$$\alpha = \frac{\beta_o}{\beta^*} - \frac{\sigma_\omega \kappa^2}{\sqrt{\beta^*}}, \tag{26}$$

and the value of α corresponds to a von Kàrmàn constant of 0.4.

In general, an important consideration when applying turbulence models is the effect of initialization on the numerical solution process. For example, when initializing a computation with free-stream conditions, numerical difficulties (e.g., convergence stall or even divergence of the iterative procedure for steady-state solutions) can occur in regions where ω becomes small, which allows disturbances in the strain rate to result in large values of the turbulent viscosity. Menter [9] considers a transport-type equation for the eddy viscosity ν_t to show that the production term becomes very large when ω goes to zero and ν_t is finite. In order to prevent this from occurring, especially during the initial stages of a calculation, Menter suggests applying a constraint on the production term. Let P_k and D_k denote the production and destruction contributions in Eqs. (14) and (15). Then, according to Menter a suitable limiter on the turbulence production is given by

$$\tilde{P}_k = \min(P_k,\, 20D_k) = \min(P_k,\, 20\beta^*\bar{\rho}k\omega). \tag{27}$$

This limiter works well in turbulent airfoil flow applications, and it is used in previous versions of the Wilcox model. With the introduction of the stress limiter, the need for such a production limiter (e.g., avoiding anomolous behavior at a stagnation point) is eliminated. Therefore, unless otherwise stated, we do not use Eq. (27) in the present implementation of the model. We do prevent ω from being zero during the numerical solution process.

3.2 Menter SST Model

In this section, we describe and discuss Menter SST models and delineate the specific assumptions associated with the form of the model that we have applied. As with the use of a stress limiter and the accompanying definition of the turbulent viscosity μ_t in the Wilcox model, we also encounter

in this model a specific modification of the standard representation of μ_t. It is this change in the magnitude of μ_t that attempts to include the influence of adverse pressure gradients on a turbulent flow. How this modification differs from that used with the Wilcox 2006 model is discussed. In so doing, a suggestion is made that the essential difference in these two forms of linear turbulence models is primarily a consequence of augmenting the sensitivity of the models to adverse pressure gradients rather than due to the blending of the k-ω and k-ϵ models employed in versions of the SST model. The equation for the turbulence kinetic energy is given by

$$\frac{\partial}{\partial t}(\bar{\rho}k) + \frac{\partial}{\partial x_j}(\bar{\rho}\tilde{u}_j k) = \mathcal{P} - \beta^* \bar{\rho} k\omega + \frac{\partial}{\partial x_j}\left[(\mu + \sigma_k \mu_t)\frac{\partial k}{\partial x_j}\right]. \tag{28}$$

The equation for the specific dissipation rate is given by

$$\begin{aligned}\frac{\partial}{\partial t}(\bar{\rho}\omega) + \frac{\partial}{\partial x_j}(\bar{\rho}\tilde{u}_j \omega) = \frac{\alpha}{\nu_t}\mathcal{P} - \beta\bar{\rho}\omega^2 + 2(1-F_1)\sigma_{\omega 2}\frac{\bar{\rho}}{\omega}\frac{\partial k}{\partial x_j}\frac{\partial \omega}{\partial x_j} \\ + \frac{\partial}{\partial x_j}\left[(\mu + \sigma_\omega \mu_t)\frac{\partial \omega}{\partial x_j}\right],\end{aligned} \tag{29}$$

and the production term $\mathcal{P}$ is given by

$$\mathcal{P} = 2\mu_t S_{ij}\frac{\partial \tilde{u}_i}{\partial x_j} - \frac{2}{3}\mu_t\left(\frac{\partial \tilde{u}_k}{\partial x_k}\delta_{ij}\right)\frac{\partial \tilde{u}_i}{\partial x_j} - \frac{2}{3}\bar{\rho}k\frac{\partial \tilde{u}_i}{\partial x_j}\delta_{ij}. \tag{30}$$

which is the same as given previously in Eq. (17) for the 2006 Wilcox model. For the Menter SST model, as with the 2006 Wilcox model, we neglect the kinetic energy term in the Reynolds stress. In addition, we apply the approximations of the turbulence production term $\mathcal{P}$ given in Eqs. (20) and (21). The mean strain-rate tensor S_{ij} replaces the tensor $\bar{S}_{ij}$, which includes the volumetric dilatation. The shear stress τ_{ij}, mean strain-rate tensor and mean rotation tensor are also the same as defined previously in Eqs. (12) and (13). For the 2003 version of the Menter SST model, there is a change in the limiter on the turbulence production term relative to previous versions. The factor of 20, as in Eq. (27), is reduced to 10, and it is applied to both the k and ω equations.

The first, second, and last terms of the right-hand sides of Eqs. (28) and (29) represent the production, destruction, and diffusion of turbulence, respectively. The third term in Eq. 29 is a cross-diffusion term. The turbulent viscosity of this model is given by

$$\mu_t = \frac{\bar{\rho}a_1 k}{\max(a_1\omega, SF_2)}, \tag{31}$$

where a_1 is a closure coefficient, S is given by

$$S = \sqrt{2S_{ij}S_{ij}}, \tag{32}$$

and F_2 is a blending function that will be defined subsequently. In previous versions of the SST model, S is replaced with the magnitude of vorticity Ω, which is defined by

$$\Omega = \sqrt{2\Omega_{ij}\Omega_{ij}}. \tag{33}$$

Additional discussion associated with the modified turbulent viscosity is included at the end of this section.

In this model, there is a blending of the constants for the k-ω (inner layer) and k-ϵ (outer layer) models. Moreover, each of the constants is a blending of those associated with the two models, and any constant ϕ is determined by

$$\phi = F_1\phi_1 + (1-F_1)\phi_2,$$

with ϕ_1 and ϕ_2 denoting the two members of the sets of two constants. Additional functions are as follows:

$$F_1 = \tanh(arg_1^4), \tag{34}$$

$$arg_1 = \min\left[\max\left(\frac{\sqrt{k}}{\beta^* \omega d}, \frac{500\nu}{d^2\omega}\right), \frac{4\bar{\rho}\sigma_{\omega_2} k}{CD_{k\omega} d^2}\right], \tag{35}$$

$$CD_{k\omega} = \max\left(2\bar{\rho}\sigma_{\omega 2}\frac{1}{\omega}\frac{\partial k}{\partial x_j}\frac{\partial \omega}{\partial x_j}, 10^{-10}\right), \tag{36}$$

$$F_2 = \tanh(arg_2^2), \tag{37}$$

$$arg_2 = \max\left(2\frac{\sqrt{k}}{\beta^* \omega d}, \frac{500\nu}{d^2\omega}\right) \tag{38}$$

The closure coefficients for the 2003 version of the Menter SST model are as follows:

$$\alpha_1 = 5/9, \quad \alpha_2 = 0.44, \tag{39}$$

$$\sigma_{k1} = 0.85, \quad \sigma_{\omega 1} = 0.5, \quad \beta_1 = 0.075 \tag{40}$$

$$\sigma_{k2} = 1.0, \quad \sigma_{\omega 2} = 0.856, \quad \beta_2 = 0.0828 \tag{41}$$

$$\beta^* = 0.09, \quad a_1 = 0.031$$

and again the turbulent Prandtl number $Pr_t = \frac{8}{9}$. One particular change in these closure coefficients of this version of the model, relative to the 1994 version [10], is that the von Kármán constant κ no longer explicitly appears. The coefficients α_1 and and α_2 in the 1994 version are determined by the following:

$$\alpha_1 = \frac{\beta_1}{\beta^*} - \frac{\sigma_{\omega 1}\kappa^2}{\beta^*}, \quad \alpha_2 = \frac{\beta_2}{\beta^*} - \frac{\sigma_{\omega 2}\kappa^2}{\beta^*}. \tag{42}$$

These equations for α_1 and α_2 are derived based on a flat-plate solution. Substituting the closure coefficients of the 1994 SST model into Eq. (42), we obtain $\alpha_1 = 0.553$ and $\alpha_2 = 0.440$. There is a slight change for the first coefficient ($\alpha_1 = 0.556$) in the 2003 SST model, but the second coefficient remains the same. The implicit dependence of the values of α on the von Kármán constant represents a departure from the usual explicit dependence on κ generally occurring in eddy viscosity models (i.e., models invoking the Boussinesq approximation). Menter does not delineate in [12] why this change was made and what the possible impact of the change is.

Menter determined the modified turbulent viscosity in Eq. (31) by introducing the effect of shear-stress transport. The modification is based on the Bradshaw assumption [21] that $\tau = \bar{\rho} a_1 k$. The motivation of this approach is based upon the success of the Johnson and King (J-K) model [22] for boundary layers exposed to adverse pressure gradients. The J-K model uses an algebraic turbulence model in combination with a transport equation for principal shear-stress. Without the change of μ_t in Eq. (31), its value would be too large in boundary layers with adverse pressure gradients. The k could be significantly larger than the corresponding dissipation. With Eq. (31), the μ_t is decreased because the invariant measure of strain rate S is greater than $a_1\omega$.

3.3 Boundary Conditions

Here, we complete the description of the turbulence models previously given by defining the boundary conditions. As a starting and reference point, we again define the boundary-value problem of this report for turbulent flow over an airfol immersed in a finite domain. Consider the finite domain $D \subset R^m$, where m indicates the dimensionality of the space, and $m = 2$ for the turbulent flows being investigated. Let $\mathbf{W}_t$ denote the solution vector of the dependent variables k and ω. These

variables must be defined at the solid surface boundary and the boundary ∂D, which is the outer boundary of D.

The boundary conditions for the model are the following. On a solid wall boundary $k = k_w$, which is zero. When approaching a smooth solid wall, the asymptotic behavior of ω (see Ref. [6]) is given by

$$\omega_w \rightarrow \frac{6\,\nu_w}{\beta_0\,d^2}, \quad d \rightarrow 0, \tag{43}$$

where d is the distance from the wall. In numerical computations, the asymptotic behavior is replaced by the following approximate boundary condtion

$$\omega = \omega_w = \frac{60\mu_1}{\rho_1\beta_0(d_1)^2}, \tag{44}$$

where ρ_1 and μ_1 are the values of density and molecular viscosity at the center of the mesh cell adjacent to the wall, and d_1 is the distance to the wall. This determination of ω_w differs by a factor of 10 from the smooth wall boundary condition of Wilcox [6], which uses the asymptotic behavior of Eq. (43). The factor of 10 was introduced by Menter [10] to simulate this boundary condition when using the first mesh point away from the wall boundary, and having ${\Delta y_1}^+ < 3$. Let a_∞ denote the free-stream speed of sound. Then, in the free-stream (Ref. [23]),

$$k = k_\infty = 9 \times 10^{-9}\,a_\infty^2, \quad \omega = \omega_\infty = 1 \times 10^{-6}\,\left(\frac{a_\infty^2}{\nu_\infty}\right). \tag{45}$$

3.4 Discussion about Turbulence Models

In this discussion, the initial focus is on the basic differences of the 2003 Menter SST model relative to previous versions. Next, the basic differences of the 2006 Wilcox k-ω turbulence model relative to previous versions are delineated. How the changes in certain terms of the Wilcox model relate to the corresponding terms of the Menter model are also addressed.

3.4.1 Aspects and differences of the 2003 Menter model

An interesting factor of the blending functions F_1 and F_2 used in the SST model is that they have a dependence on the commonly used algebraic length scale, which is defined by the distance from a solution point to the nearest wall boundary. Thus, both the length scale associated with the second transport equation and an algebraic length scale are used in the model. This introduction of another length scale into the model is not consistent with a primary objective of two-equation turbulence models.

An important feature of the SST model is that it accounts for the effect of principal turbulent shear-stress transport, which allows the history, sometimes called memory, effects of turbulence to be included in the modeling. It is these effects that are extremely important in boundary layers exposed to adverse pressure gradients. To fully realize the role played in this transport of the Reynolds shear stresses, we identify the factors affecting these stresses.

As pointed out by Hinze [24], one can view the Reynolds stresses as being comprised of two parts. The first part is a consequence of the local state of the flow, which is associated with the local mean velocity gradient. That is, in standard two-equation turbulence models, which are based upon the Boussinesq approximation, there is the assumption that the momentum exchange processes are determined only by the local gradient of the mean velocity. The second part of the Reynolds stresses is due to the history effects of the turbulence that occur in the developing regions of turbulent flows. In such regions, there is insufficient time for the turbulence to adapt to additional changes in the local normal gradients associated with the transport of shear stresses. Moreover, these additional

changes cannot occur locally because of rapid fluctuations in the streamwise direction of the flow. Downstream of the developing region of the flow, the dynamics of the turbulence can change, and the memory effects of the turbulence can be substantial. Then, these effects are included in the Reynolds shear stress. For additional discussion about history effects and their influence on a turbulent flow, see Hinze [25].

As in all previous versions of the SST model, the eddy viscosity ν_t is also modified in the 2003 Menter SST model. Unlike earlier versions of the SST model in which there is a functional dependence on the magnitude of the vorticity, the modification now depends on the invariant measure of strain rate S. It is this change in the eddy viscosity that accounts for the effects of transporting the principal shear stress. The basis of the change is the Bradshaw assumption that the turbulent shear stress is proportional to the turbulence kinetic energy. In adverse pressure gradient flows, the eddy viscosity is required to satisfy this assumption. Moreover, when $S > a_1\omega$ in Eq. (31), the denominator of ν_t produces a departure from the standard definition of ν_t as k/ω. The modification produces a decrease of ν_t in wall-bounded shear layers when the production of turbulence exceeds its dissipation. As a consequence, the turbulent shear stress τ is reduced in regions of adverse pressure gradients, and the extent of possible flow separation is increased.

The 2003 Menter SST model continues to include a production limiter, which alleviates difficulties that can be experienced in numerical computations due to a significant imbalance between the production and destruction of turbulence. Such difficulties can prevent convergence in steady-state calculations or unsteady ones using a dual time stepping solution algorithm. As seen in the description of 2003 SST model, the limiting factor of the production limiter is decreased by a factor of two relative to previous versions of the model.

3.4.2 Changes of the 2006 Wilcox model

There are two principal changes that occur with the 2006 version of the Wilcox model. One change is the introduction of a cross-diffusion term in the specific dissipation rate (ω) equation. This change was made to reduce the sensitivity of the model to free-stream k and ω values. Regarding such sensitivity, Wilcox indicates that one would expect that in any physical problem there would be some sensitivity to the free-stream turbulence level (e.g., consider stagnation point heat transfer effects). The introduction of the cross-diffusion term does require some special consideration of adverse effects on the spreading rate of free shear flows, such as the far wake, plane jet and mixing layer. Thus, in this version of the Wilcox model, the cross-diffusion coefficient σ_d is reduced and changes are made in other closure coefficients, as explained in Ref. [7]. These changes allow satisfactory agreement with measurements of the spreading rates of free-shear flows. There is the additional requirement that the coefficient σ_d be suppressed when the cross-diffusion term is close to a solid boundary of a wall-bounded shear flow.

It should be noted that the Menter SST model does not experience any special issues in free-shear flows due to the cross-diffusion term. This is because of the blending functions of the model. As indicated by Wilcox [7], these functions cause all the closure coefficients to assume values appropriate for the k-ω model near solid boundaries and to approach the asymptotic values of the k-ϵ value at the outer part of a boundary layer and in free-shear flows.

The other change in the 2006 version of the Wilcox model is the inclusion of a stress limiter in the determination of the eddy viscosity. As with the Menter SST model, the modification of the ν_t depends on the invariant measure of strain rate, but it has a premultiplying factor of $C_{lim}/\sqrt{\beta^*}$, as seen in Eq. (23). The introduction of the stress limiter is necessary to overcome the previous weakness of the model concerning the prediction of the correct shock location in a transonic flow. Thus, the model has an improved representation of the adverse pressure gradient produced by the shock wave. There is also numerical evidence that there is no longer a need for a production limiter.

In previous versions of the Wilcox model, there was an apparent need to include this production limiter when strain rate instead of vorticity was used in the production term. Otherwise, one observes

the stagnation point anomaly, which corresponds to an overproduction of the turbulence kinetic energy. Such an anomaly can affect the stagnation point location, and thus, the computed flow field downstream. The necessity of applying the production limiter in a flow field when using the 1988 version of the Wilcox k-ω model is revealed in the section on computational results. With the Wilcox k-ω 2006 model, computational results indicate that there is no longer a need to introduce the Menter production limiter when considering strain rate in the turbulence production term. In a sense, this limiter seems to provide similar benefits to that of the direct limiting (production limiter) in the SST model.

In this report, the values of the stress limiter introduced into the eddy viscosity are given by Wilcox. These values depend on whether strain rate or vorticity is used in computing the turbulence production term of the two-equation model. The choice of the values was determined by calibration based on a range of flows. It should be indicated that there is some sensitivity to the choice of the value regarding both the prediction of turbulent flows as well as solving the governing transport equations of the model.

4 Numerical Scheme

To solve the Reynolds-averaged Navier-Stokes (RANS) equations, we use a multigrid algorithm with the RK/Implicit scheme as a smoother. The k-ω turbulence model requires the solution of two transport-type equations. In the present work, we do not directly couple the solution of the fluid dynamic equations and the additional equations of the turbulence model. They are solved by first updating the equations of the turbulence model and then updating the equations of the mean flow. For details see Swanson and Rossow [26]. The transport-type equations of the k-ω model are solved with the RK/Implicit scheme.

4.1 Discretization

We apply a finite-volume approach to discretize the fluid dynamic equations and use the approximate Riemann solver of Roe [27] to obtain a second-order discretization of the advection terms. The viscous terms are discretized with a second-order central difference approximation.

The discretization of the advective terms in the mean flow equations uses central differencing with the Roe numerical dissipation. For flows with shock waves, we use the limiter of Swanson, Radespiel, and Turkel [28]. A first-order approximation is used for the advective terms of the transport equations of the turbulence model. Using first order avoids the necessity of applying a limiter, which in general is a highly nonlinear function.

When solving transport equations, it is quite common to used a first-order discretization of the convective terms. The question does arise as to whether a second-order approximation is necessary. There are two principal reasons why it may be essential to use second order. The obvious one is that the convective terms play a major role in representing the physics of the turbulent flow. At this time, there still seems to be a need to make a delineation of a set of physical problems and their numerical solutions that clearly substantiate the benefit of using a second-order approximation. The second reason is that the grid is highly irregular in a crucial part of the flow. For example, consider the trailing edge of a single element airfoil. However, in this case, it has been shown by Rossow and Swanson [29] that simply improving the grid removes the need for second-order to reduce the truncation error.

4.2 Discrete Boundary Conditions and Initial Solution

In all the applications, the same boundary conditions were imposed for the fluid dynamic equations. On the surface, the no-penetration and no-slip conditions were applied. At the outer boundary, Riemann invariants were used. A far-field vortex effect was included to specify the velocity for an

inflow condition at the outer boundary. The calculations were performed on the solution grid with the initial solution given as the free-stream conditions.

An important element in the development of an accurate and efficient algorithm for solving the Euler and Navier-Stokes equations is the selection of proper boundary conditions. The choice of conditions must be consistent with physical constraints of the problem of interest as well as the interior discrete formulation. Moreover, the physical conditions, in general, must be supplemented with a sufficient number of numerical relations to allow determination of all dependent variables. In addition to defining the conditions at wall boundaries, which can be solid or porous, the infinite domain problem must be adequately simulated in the case of external flows. This is usually done by delineating boundaries at some distance from the primary region of consideration, and then prescribing suitable boundary conditions for that location. In the case of a lifting airfoil, the outer boundary position must be sufficiently far to not compromise the development of the lift. For example, five airfoil chords would be too close where as 20 chords would be satisfactory if the far-field vortex effect is taken into account. Even for inviscid nonlifting flow over a circular cylinder, an outer boundary placed too close can cause inaccurate prediction of the flow over the aft portion of the cylinder.

In this work, all wall boundaries are assumed to be solid. Since inviscid as well as viscous flow problems are computed in the results section, the wall boundary procedures for both types of flow are discussed here. For inviscid flows, the tangency (or no-penetration) condition

$$\mathbf{q} \cdot \mathbf{n} = 0, \tag{46}$$

where $\mathbf{q}$ is the velocity vector and $\mathbf{n}$ is the unit normal to the surface, must be satisfied. Now, consider the vector momentum equation

$$\rho \frac{D\mathbf{q}}{Dt} = -\nabla p, \tag{47}$$

where $D\mathbf{q}/Dt$ denotes the substantial derivative of $\mathbf{q}$, and ∇ is the gradient operator. Clearly, along the surface boundary the substantial derivative of $\mathbf{q} \cdot \mathbf{n}$ must vanish. If one subtracts from this equation the inner product of the unit normal and Eq. (47), then

$$\rho \mathbf{q} \cdot (\mathbf{q} \cdot \nabla) = \mathbf{n} \cdot \nabla p. \tag{48}$$

Using the transformation

$$(x, y) \rightarrow (\xi, \eta)\,,$$

taking $\eta(x, y) = \text{constant}$ to conincide with the surface boundary, and noting that the contravariant velocity component

$$V = -\frac{y_\xi}{J^{-1}} u + \frac{x_\xi}{J^{-1}} v$$

is zero because of Eq. (46), one obtains from Eq. (48) that

$$p_\eta = \frac{1}{\left(x_\xi^2 + y_\xi^2\right)} \left[\left(x_\xi x_\eta + y_\xi y_\eta\right) p_\xi + \left(y_\eta u - x_\eta v\right) \left(\rho v x_{\xi\xi} - \rho u y_{\xi\xi}\right) \right]. \tag{49}$$

At a solid boundary, a row of auxiliary cells is created exterior to the domain of the flow. Approximating the normal pressure gradient of Eq. (49) with a three-point centered difference at the surface, the auxiliary cell pressure is obtained. The density at this cell is equated to the density at the first point off the surface. The Cartesian velocity components are determined from

$$\left[\begin{array}{c} u \\ v \end{array} \right]_{i,1} = \left[\begin{array}{cc} \bar{x}_\xi & -\bar{y}_\xi \\ \bar{y}_\xi & -\bar{x}_\xi \end{array} \right]_w \left[\begin{array}{c} q_t \\ q_n \end{array} \right]_{i,2}$$

where q_t and q_n are the tangential and normal velocity components, the subscript w means wall, the indices $(i, 1)$ and $(i, 2)$ refer to the centers of the auxiliary and the first interior cells, respectively.

The overbar means the quantity is divided by $\sqrt{x_\xi^2 + y_\xi^2}$. Thus, the tangency condition of Eq. (46) is enforced. Finally, the total internal energy is computed using the relation

$$\rho E = \frac{1}{\gamma - 1} p + \frac{1}{2} \rho \left(u^2 + v^2 \right).$$

In the case of viscous flows, the no-slip condition is required, and this is imposed by treating the Cartesian velocity components as antisymmetric functions with respect to the solid surface. Thus,

$$u_{i,1} = -u_{i,2}, \qquad v_{i,1} = -v_{i,2}. \tag{50}$$

The surface values of pressure p and temperature T are computed using the reduced normal momentum and energy equations

$$\frac{\partial p}{\partial \eta} = 0, \qquad \frac{\partial T}{\partial \eta} = 0, \tag{51}$$

where η is the coordinate normal to the surface. As part of the boundary conditions, we include the option to specify the wall temperature instead of imposing the adiabatic condition of Eq. (51).

To compute the unknown flow variables at the outer boundary of an external aerodynamics problem, characteristic theory, some simplifying assumptions, and the concept of a point vortex are considered. By considering the two-dimensional Euler equations, a point on the outer boundary, and assuming a locally homentropic flow, the one-dimensional equations of gas dynamics are derived for the direction normal to the boundary. The elements of the solution vector are proportional to the local tangential velocity component and the Riemann invariants

$$R^+ = q_n + \frac{2c}{\gamma - 1}, \qquad R^- = q_n - \frac{2c}{\gamma - 1},$$

respectively, where the tangential and normal velocity components are defined as

$$q_t = u \ \cos\theta + v \ \sin\theta, \qquad q_n = -u \ \sin\theta + v \ \cos\theta,$$

respectively.

Again we introduce a row of auxiliary (boundary) cells exterior to the domain. At a boundary cell, one can compute the normal velocity component q_n and the speed of sound c from the relations

$$q_n = \frac{1}{2} \left(R^+ + R^- \right), \quad c = \frac{(\gamma - 1)}{4} \left(R^+ - R^- \right), \tag{52}$$

where the characteristic variables R^+ and R^- are appropriately determined. Assume that the flow normal to the boundary is subcritical. If inflow occurs, the characteristic variables corresponding to the ingoing characteristics are specified. Since we actually have a two-dimensional system, an additional quantity must be given. It follows directly that one should specify the entropy s (the flow has been assumed to be locally homentropic). In practice, for convenience, we define $s^* = p/\rho^\gamma$, which has the same functional dependence as entropy, and use this variable in place of entropy. So, for an inflow situation, we set

$$q_t = q_{t\infty}, \quad R^+ = R^+_\infty, \quad s^* = s^*_\infty, \tag{53}$$

and extrapolate R^- from the interior. If outflow occurs at the boundary, there is only one ingoing characteristic (corresponding to R^+); and thus, we set $R^+ = R^+_\infty$, and extrapolate from the interior q_t, R^-, and s^*. In the particular case of supersonic flow, all characteristics are ingoing if there is inflow, and they are outgoing if there is outflow. Therefore, we specify the dependent variables with their free-stream values if inflow occurs, and we use extrapolation to determine the boundary flow variables if outflow occurs.

At a distance far enough away from a two-dimensional lifting body, one can view the body as a point vortex with strength proportional to the circulation associated with the lift. One can then compute the components of the induced velocity at the far-field boundary due to the vortex. Moreover, as given in Ref. [30], the effective velocity components at the far-field boundary are computed as

$$u = u_\infty \cos\alpha + F \sin\phi, \quad v = v_\infty \sin\alpha - F\cos\phi, \tag{54}$$

where

$$F = c_l \, \frac{c}{4\pi} \frac{\bar{\beta}}{R} \left[1 - M_\infty^2 \sin^2(\phi - \alpha)\right]^{-1}, \quad \bar{\beta} = \sqrt{1 - M_\infty^2},$$

the subscript ∞ refers to free-stream values, α is the angle of attack, R and ϕ are the magnitude and angle of the position vector originating from a reference point at the body (i.e., quarter-chord point for airfoil) and extending to the far-field boundary point, c is the body length, and c_l is the lift coefficient. The polar angle ϕ is defined to be positive in the counterclockwise direction relative to a reference line (i.e., coinciding with chord for airfoil) emanating from the leading edge of the body and proceeding downstream. The Cartesian velocity components u and v of Eq. (54) are used to compute the local tangential and normal velocity components required in the boundary conditions.

4.3 Solver: RK/Implicit Scheme

To obtain an explicit update to the solution vector for the flow equations, we use a three-stage RK scheme.

$$\begin{aligned} \mathbf{W}^{(0)} &= \mathbf{W}^n \\ \mathbf{W}^{(q)} &= \mathbf{W}^{(0)} - \alpha_q \Delta t \, \mathbf{R}(\mathbf{W}^{(q-1)}), \quad q = 1, 2, 3 \\ \mathbf{W}^{n+1} &= \mathbf{W}^{(3)}. \end{aligned} \tag{55}$$

The update for the q-th stage of a RK scheme is given by

$$\mathbf{W}^{(q)} = \mathbf{W}^{(0)} + \Delta\mathbf{W}^{(q)}, \tag{56}$$

where the change in the solution vector $\mathbf{W}$ is

$$\Delta\mathbf{W}^{(q)} = \mathbf{W}^{(q)} - \mathbf{W}^{(0)} = -\alpha_q \frac{\Delta t}{\mathcal{V}} \mathcal{L}\, \mathbf{W}^{(q-1)}, \tag{57}$$

and $\mathcal{L}$ is the complete difference operator for the system of equations. Here α_q is the RK coefficient of the q-th stage, Δt is the time step, and $\mathcal{V}$ is the volume of the mesh cell being considered. To extend the support of the difference scheme, we consider implicit residual smoothing for the system of equations. This is a generalization of the original scalar approach defined by Jameson [31], which considered changes in each conservative variable. Applying the residual smoothing technique for the system, we have the following:

$$\mathcal{L}_i \, \overline{\Delta\mathbf{W}}^{(q)} = \Delta\mathbf{W}^{(q)}, \tag{58}$$

where $\mathcal{L}_i$ is an implicit operator. By approximately inverting the operator $\mathcal{L}_i$ we obtain

$$\overline{\Delta\mathbf{W}}^{(q)} = -\alpha_q \frac{\Delta t}{\mathcal{V}} \mathcal{P}\, \mathcal{L}\, \mathbf{W}^{(q-1)} \tag{59}$$

where $\mathcal{P}$ is a preconditioner defined by the approximate inverse $\widetilde{\mathcal{L}}_i^{-1}$. The change $\overline{\Delta\mathbf{W}}^{(q)}$ replaces the explicit update appearing in Eq. (56). Thus, each stage in the RK scheme is now preconditioned by an implicit operator. Unlike the scalar residual smoothing procedure, which uses a diffusion

operator for the implicit operator $\mathcal{L}_i$, a first-order upwind approximation based either on the Roe scheme [27] or the matrix dissipation of Swanson and Turkel [32] in conjunction with central differencing is used for the convective derivatives in the implicit operator.

One approach for deriving the implicit operator $\mathcal{L}_i$, which allows the determination of the implicit preconditioner $\mathcal{P}$, is as follows. Consider the integral form of the conservation laws, and apply a finite volume discretization method. Then, this equation can be written as

$$\frac{\partial \mathbf{W}}{\partial t} + \frac{1}{\mathcal{V}} \sum_k \mathbf{F}_k^{n+1} S_k = 0, \tag{60}$$

where $\mathcal{V}$ represents the volume of a discretization cell, k is the summation index over all faces of a discretization cell. For each cell face, $\mathbf{F}_k$ denotes the flux density vector normal to the face and S_k is the surface area. Rather than solve this nonlinear system, we now apply linearization to (60). Consider a Taylor series expansion in time of the normal flux density vector, which is given by

$$\mathbf{F}_k^{n+1} = \mathbf{F}_k^n + \left(\frac{\partial \mathbf{F}_k}{\partial \mathbf{W}} \right)^n \Delta \mathbf{W} + O(\Delta t^2). \tag{61}$$

Substituting for $\mathbf{F}_k^{n+1}$ in Eq. (60), and performing the inner product on each cell face, we obtain

$$\frac{\Delta \mathbf{W}}{\Delta t} + \frac{1}{\mathcal{V}} \sum_k A_k^n \, S_k \Delta \mathbf{W} = -\frac{1}{\mathcal{V}} \sum_k F_k^n \, S_k, \tag{62}$$

with A_k^n denoting the flux Jacobian. This equation can be rewritten as

$$\left(I + \frac{\Delta t}{\mathcal{V}} \sum_k A_k^n \, S_k \right) \Delta \mathbf{W} = -\frac{\Delta t}{\mathcal{V}} \sum_k F_k^n \, S_k = \mathbf{R}(\mathbf{W}^n). \tag{63}$$

Thus, the implicit operator $\mathcal{L}_i$ is defined by

$$\mathcal{L}_i = I + \frac{\Delta t}{\mathcal{V}} \sum_k A_k^n \, S_k. \tag{64}$$

To determine an approximate inverse of $\mathcal{L}_i$, and thus, obtain a suitable implicit preconditioner $\mathcal{P}$, the linear system of Eq. (63) can be approximately solved. Flexibility in devising a suitable solution method for computing the approximate $\mathcal{L}_i^{-1}$ can be obtained by introducing an implicit parameter ε. Then, Eq. (64) becomes

$$\mathcal{L}_i = I + \varepsilon \frac{\Delta t}{\mathcal{V}} \sum_k A_k^n \, S_k \tag{65}$$

. By substituting for the implicit operator in Eq. (58), we obtain for for the q-th stage of the RK scheme

$$\left[I + \varepsilon \frac{\Delta t}{\mathcal{V}} \sum_k A_k^n \, S_k \right] \overline{\Delta \mathbf{W}}^{(q)} = -\alpha_q \frac{\Delta t}{\mathcal{V}} \sum_k F_k^{(q-1)} \, S_k = \widehat{\mathbf{R}}^{(q-1)}, \tag{66}$$

where $\widehat{\mathbf{R}}^{(q-1)}$ represents the residual function for the $(q-1)$-th stage, and ε is an implicit parameter. The parameter ε is taken to be 0.7. Analysis and discussion concerning choosing ε is given in Swanson et al. [33]. $\mathbf{A}_n$ is the flux Jacobian associated with $\mathbf{F}_n$ at a cell face. The matrix $\mathbf{A}_n$ can be decomposed into $\mathbf{A}_n^+$ and $\mathbf{A}_n^-$, which are associated with the positive and negative eigenvalues of A_n and defined by

$$\mathbf{A}_n^+ = \frac{1}{2} \left(\mathbf{A}_n + |\mathbf{A}_n| \right), \quad \mathbf{A}_n^- = \frac{1}{2} \left(\mathbf{A}_n - |\mathbf{A}_n| \right). \tag{67}$$

If we substitute for $\mathbf{A}_n$ in Eq. (66) using the definitions of Eq. (67), then the implicit scheme can be written as

$$\left[I + \varepsilon \frac{\Delta t}{\mathcal{V}} \sum_k \mathbf{A}_n^+ \, S_k \right] \overline{\Delta \mathbf{W}}_{i,j}^{(q)} = \widehat{\mathbf{R}}_{i,j}^{(q-1)} - \varepsilon \frac{\Delta t}{\mathcal{V}} \sum_k \mathbf{A}_n^- \, \overline{\Delta \mathbf{W}}_{NB}^{(q)} \, S_k, \tag{68}$$

where the indices (i, j) indicate the cell of interest, and NB refers to all the direct neighbors of the cell being considered. Consider traversing the boundary of a mesh cell in a counterclockwise manner, with the positive surface normal vector always pointing outward from the cell. Then, as discussed by Rossow [34], the quantity $\mathbf{A}_n^- \, \overline{\Delta \mathbf{W}}$ represents the flux density change associated with waves having a negative wave speed (i.e., waves that enter the cell (i, j) from outside). Only the neighbor cells NB can contribute to these changes in flux density. Similarly, the quantity $\mathbf{A}_n^+ \, \overline{\Delta \mathbf{W}}$ represents flux density changes associated with positive wave speeds (i.e., waves that leave the cell (i, j)). These flux density changes are determined only by information from within the cell (i, j).

Before describing the method to determine the inverse of the implicit operator in Eq. (68), it is important to indicate that one can make a direct connection between this RK/Implicit algorithm and the general class of implicit Runge-Kutta schemes. In particular, consider a multistage diagonally implicit Runge-Kutta (DIRK) scheme given by selecting a desired Butcher tableau [35]. Also, see Alexander [36]. As shown by Langer [37], this DIRK scheme can be used to derive essentially the same algorithm that is derived here.

To solve Eq. (68) for the changes in conservative variables $\overline{\Delta \mathbf{W}}_{i,j}^{(q)}$, the 4×4 matrix on the left-hand side of Eq. (68) must be inverted. It is sufficient to approximate the inverse of the implicit operator. An adequate approximate inverse is obtained with two symmetric Gauss-Seidel sweeps. To initialize the iterative process, the unknowns are set to zero.

We consider two approaches for approximating the inverse of the implicit operator. One method is to apply two sweeps of point symmetric Gauss-Seidel (SGS) relaxation. The other is to apply radial line (or j-line) SGS sweeps. We should point out that when referring to this type of SGS in the text the modifiers line and j-line are used interchangeably. When computing boundary-layer and free shear-layer turbulent flows, the computational grid is usually strongly clustered to adequately resolve the steep flow-field gradients, which produces a strong grid anisotropy and a high degree of stiffness in the discrete flow equations. Line solvers are frequently employed with structured grid solvers in the direction of strongest coupling to relieve the stiffness associated with the grid anisotropy. Even on unstructured grids line solvers can be applied. By constructing artificial lines in an unstructured grid that extend only through the regions of strongest coupling, Mavriplis [38] has demonstrated effective reduction of the numerical stiffness.

With line SGS, we apply the implicit operator across the wake line (the line emanating from the trailing edge of an airfoil), which we call a fully implicit treatment. It is also possible to lag the boundary condition at the wake line rather than extending the line solve across the wake line. This approach can also work well provided local relaxation or subiterations are performed to compensate for the lagging of the wake boundary condition. Although this may be a more convenient option, from the implementation point of view, for multiblock structured grid methods, we use the fully implicit method in this paper to obtain a measure of the best possible convergence with the line SGS relaxation as the smoother for the multigrid method. Furthermore, a variation on this wake treatment can be applied with unstructured grid methods by appropriate ordering of unknowns.

The solution algorithm is composed of a nonlinear outer part and a linear inner part. A three-stage Runge-Kutta scheme is used in the outer part, and the linear system of the inner part is approximately solved with a combination of point and line symmetric Gauss-Seidel (SGS) relaxation. Complete details of the scheme are presented in the papers of Rossow [39] and Swanson et al. [26, 33].

In all the applications of this report, a relaxation parameter, which is denoted as ε, is assigned a value of 0.5. Thus, there is an overrelaxation when approximately solving the linear system. When representing the effects of turbulence with algebraic or one-equation models, we use two SGS

sweeps with lexicographic ordering to approximate the inverse of the implicit preconditioner. Other types of ordering of the solution points, such as red-black ordering, require more relaxation sweeps in general. When using a two-equation model, such as the k-ω model, it seems to be necessary to increase the number of relaxation sweeps. This requirement depends on mesh density and flow complexity (e.g., transonic flow with shock wave). For all calculations herein we have used either two or four SGS relaxation sweeps. The Courant-Friedrichs-Lewy (CFL) number for both the mean flow and the transport equations in the pseudotime integration is between 1.0×10^3 and 1.0×10^6.

Due to the upwind approximation used for the implicit operator, the coefficients for the RK scheme are also based on an upwind scheme. The three-stage RK scheme with the coefficients

$$[\alpha_1, \alpha_2, \alpha_3] = [0.15, 0.4, 1.0] \tag{69}$$

given in Ref. [40] is applied. In the application of the three-stage RK/implicit scheme as the smoother of a full approximation storage (FAS) multigrid method, the CFL number is increased to 1000 after 10 multigrid cycles. During the first 10 cycles the CFL is 16. A W-type cycle is used to execute the multigrid. Details of the multigrid method are given in the paper by Swanson et al. [33].

5 Computational Results: RAE 2822 Airfoil

A series of computations for turbulent, viscous flow over the RAE 2822 and the NACA 4412 airfoils were performed. This section covers the RAE 2822, while the next section covers the NACA 4412. These two airfoil flows were selected because they are frequently considered when attempting to validate turbulence models, which is due to the extensive amount of experimental data available. There were two objectives in these numerical evaluations. One was to examine the computational results using two k-ω type turbulence models. The other objective was to evaluate the convergence behavior for the discrete mean flow (RANS) and turbulence transport equations. In solving these equations, we used structured meshes with a C-type topology. There is a weak grid clustering in the neighborhood of the shock wave for the RAE 2822.

Table 1: Flow conditions for RAE 2822 airfoil.

Cases	M_∞	α (deg.)	Re_c	x_{tr}/c
Case 1	0.676	1.93	5.7×10^6	0.11
Case 9	0.730	2.79	6.5×10^6	0.03
Case 10	0.750	2.81	6.2×10^6	0.03

5.1 **Wilcox Model** (RAE 2822 Airfoil)

We considered three mesh densities. The finest mesh consists of 1280 cells around the airfoil (1024 cells on the airfoil) and 256 cells in the normal direction. Each successive mesh was generated by eliminating every other mesh point in each coordinate direction, starting with the finesh mesh. The normal mesh spacing at the surface of the finest mesh is approximately 3×10^{-6}, and the maximum surface cell aspect ratio is about 560. The airfoil solutions were calculated with the Case 1, Case 9 and and Case 10 flow conditions (see Table 1) from the experimental investigation of Cook, McDonald and Firmin [41]. For Case 1, the flow is primarily subsonic with a relatively small region of supersonic flow. The other two cases are transonic. In Case 9, there is a fairly strong shock wave occurring on the upper surface of the airfoil. Whereas, in Case 10, there is a sufficiently strong shock on the upper surface to cause significant flow separation behind the shock.

5.1.1 Strain rate for production of turbulence

Figure 1 shows the Case 1 convergence histories, both mean flow and turbulence modeling equations, on the three successively refined grids. The L_2 norm of the residual of the continuity equation is used as a measure of convergence for the mean flow equations. We also show the convergence of the lift coefficient C_L with each multigrid cycle. The computations were performed using the 2006 Wilcox model with strain rate for the turbulence production term. Unless otherwise noted, strain rate is used in all computations. In addition, numerical dissipation for the solution algorithm is from the Roe scheme, if not specified otherwise. Again, this scheme also includes low-speed preconditioning. The limiter of Ref. [28] is always employed when the flow is transonic. The far field vortex (FFV) effect is used in the outer boundary condition for all calculations. Transition (Tr) is set at the experimental value. Prior to the transition location, the production terms in the transport equations are set to zero. Although not shown, the convergence behavior with vorticity instead of strain rate is essentially the same. A fully converged solution (i.e., residuals reduced to machine zero or essentially this level) is attained in less than 125 multigrid cycles on all the grids. Further, as is evident in Fig. 1(a), there is also very rapid convergence of the lift coefficient (C_L). Table 2 presents the number of multigrid cycles for convergence and the corresponding convergence rate on each grid. Here, it is emphasized that obtaining a fully converged solution has been a primary objective so that the evaluation of a turbulence model can be accomplished without the effects of numerical integration error in the solution process. Moreover, in so doing, the benefits of one two-equation model relative to another in representing the physics of a turbulent flow can be established.

Table 2: Computational performance for Case 1 using the 2006 Wilcox k-ω turbulence model.

Grid	MG Cycles	Convergence Rate
320×64	108	0.7342
640×128	112	0.7440
1280×256	119	0.7571

Table 3: Computed lift and drag coefficients with 2006 Wilcox k-ω turbulence model for RAE 2822 airfoil (Case 1).

Grid	C_L	C_D	$(C_D)_p$	$(C_D)_v$
320×64	0.613228	0.00785059	0.00233432	0.00551628
640×128	0.605578	0.00805834	0.00234649	0.00571186
1280×256	0.600708	0.00827414	0.00243063	0.00584351

The surface pressure (C_p) and skin-friction (C_f) distributions computed when using the 2006 Wilcox k-ω model are displayed in Fig. 2. The surface pressures are quite similar on the three grids, exhibiting relatively small differences only in the neighborhood of the transition location, and they show good agreement with the experimental data. We emphasize that the transition location is set according to the experiment, rather than allowing the model to determine when the flow becomes turbulent. The differences near transition are a consequence of the flow acceleration over the upper airfoil surface and the transitioning of the flow. These factors result in a weak compression wave. It is interesting that for the 2006 Wilcox model the solution is essentially the same for Case 1 whether strain rate or vorticity is used in the production term. Note, the skin-friction coefficient C_f is the wall shear stress divided by the dynamic pressure based on boundary-layer edge values. In Table 3, we give the computed lift and drag values when using the 2006 Wilcox model.

Table 4: Computational performance for Case 9 using the 2006 Wilcox k-ω turbulence model.

Grid	MG Cycles	Convergence Rate
320×64	90	0.6901
640×128	77	0.6482
1280×256	65	0.5982

Table 5: Computed lift and drag coefficients with 2006 Wilcox k-ω turbulence model for RAE 2822 airfoil (Case 9).

Grid	C_L	C_D	$(C_D)_p$	$(C_D)_v$	x_{sep}/c
320×64	0.867173	0.0181325	0.0128358	0.00529665	0.572465
640×128	0.861471	0.0181334	0.0126105	0.00552288	0.571014
1280×256	0.856833	0.0181409	0.0124887	0.00565220	0.568675

For Case 9, the convergence plots for the mean flow and turbulence equations are presented in Fig. 3. Here, as for Case 1, we observe rapid convergence (less than 125 cycles) on all grids. The convergence performance for this case is presented in Table 4. In Fig. 4, the computed surface pressure and skin-friction distributions for Case 9 are displayed. The primary differences in the C_p results for the three grids is barely discernible in the vicinity of the upper surface shock. The aerodynamic coefficients for Case 9 are presented in Table 5.

Table 6: Computational performance for Case 10 using the 2006 Wilcox k-ω turbulence model.

Grid	MG Cycles	Convergence Rate
320×64	122	0.7606
640×128	115	0.7480
1280×256	101	0.7185

The final set of RAE 2822 airfoil results is for Case 10. This case is especially important because the shock is stronger; and thus, it tests the response of a turbulence model to varying shock strength and more extensive flow separation. Figure 5 displays the convergence behavior of the governing equations when using the 2006 Wilcox model. As in Case 9, we observe a notable acceleration in the convergence on the finest mesh. The convergence rates are given in Table 6.

Table 7: Computed lift and drag coefficients with 2006 Wilcox k-ω turbulence model for RAE 2822 airfoil (Case 10).

Grid	C_L	C_D	$(C_D)_p$	$(C_D)_v$	x_{sep}/c
320×64	0.852050	0.0291260	0.0239743	0.00515168	0.619553
640×128	0.843506	0.0288574	0.0234993	0.00535809	0.613754
1280×256	0.837403	0.0287605	0.0232980	0.00546251	0.608413

Figure 6 shows the computed C_p and C_f distributions. Comparing the results for the three grids, we discover similar trends to Case 9 as the mesh is refined. However, now the shock is predicted downstream of the experimental data. Even so, there is reasonable agreement with the available skin-friction data. The C_L and C_D values are included in Table 7.

Table 8: Computed lift and drag coefficients with 2006 Wilcox k-ω turbulence model for RAE 2822 airfoil. Vorticity is used in production term. Mesh density is 1280×256 cells.

Cases	C_L	C_D	$(C_D)_p$	$(C_D)_v$
Case 1	0.584657	0.00797389	0.00246787	0.00550602
Case 9	0.807128	0.0156078	0.0104005	0.00520733
Case 10	0.750109	0.0234890	0.0185019	0.00498701

5.1.2 Vorticity for production of turbulence

Now, we examine the effect on the surface pressure and skin-friction distributions of Case 9 and Case 10 when strain rate is replaced with vorticity. Consider Case 9 and compare Figs. 4 and 7 for strain rate and vorticity, respectively. Due to the vorticity replacement, the shock is displaced slightly upstream, but there is still satisfactory agreement with the data.

For Case 10, a comparison of Figs. 6 and 8 exhibits a significant upstream movement of the shock when vorticity is being used in turbulence production. The skin-friction distribution shows the expected increase in the extent of flow separation associated with the shifting of the shock. These same effects have been observed in Ref. [42] in which a different algorithm was used for solving the transport equations. The aerodynamic coefficients for Cases 9 and 10 using vorticity are given in Table 8.

We should note that vorticity is frequently used in the production term of one-equation turbulence models (e.g., SA model of Spalart and Allmaras). With the two-equation model of Wilcox, it has worked well for both subsonic and transonic airfoil flows. At the same time, it is important to understand that there are some possible disadvantages with using vorticity to replace strain rate in the turbulence production term. As indicated by Wilcox in his 2007 AIAA paper [7], using vorticity seems to be satisfactory for shock-separated flow computations up to approximately a Mach number of 3. He also points out that it has detrimental effects on hypersonic shock-induced separation, as well as some attached boundary layers and some free shear flows. Durbin [43] notes that using vorticity can produce spurious production in rotating or swirling flows.

It is interesting to compare the surface C_p variations for both Cases 9 and 10 with those obtained by Mor-Yossef [44, 45] using a full Reynolds stress model based upon the work of Eisfeld [46]. The predicted shock locations for these two cases seem to be nearly the same as obtained with the Wilcox k-ω model using vorticity. Mor-Yossef does not include the values of the C_L and C_D.

5.1.3 Turbulence production limiter

An important consideration in various two-equation turbulence models is the application of a limiter on the turbulence production term. For example, such a limiter is essential in general for the 1988 Wilcox turbulence model. Menter has included such a limiter (see description of Menter on the early development [10] of the SST model). Details of his implementation of the limiter have been described previously in this report for the 2003 version of the SST model.

Figure 9 shows turbulent viscosity contours for Case 9 using the 1988 Wilcox model both with and without a limiter. It is clear from this figure that when using the strain rate in the production term and no limiter that there is an anomalous behavior in the neighborhood of the shock. Although not shown, the requirement of a production limiter can be removed by applying vorticity rather than strain rate. Alternatively, such behavior with strain rate can be avoided by including a stress limiter. In the versions of the 2006 Wilcox model considered herein, a stress limiter is incorportated. This stress limiter removes any necessity for the introduction of a production limiter, as shown in Fig. 10 for the 2006 Wilcox model. In a sense, the stress limiter seems to be playing a similar role as the production limiter.

5.1.4 Stress limiter of the k-ω model

The stress limiter of the k-ω model has a significant effect on not only the representation of the physics for this strong transonic case (Case 10) but also the convergence of the solution for the mean flow and turbulence model equations. The influence of the stress limiter parameter C_{lim} on convergence and shock location is discussed in Swanson and Rossow [26]. They varied C_{lim} between 0.0 and 0.95 and showed the significant effect it has on both the convergence rate and the shock location. As pointed out in Ref. [26], it may be possible to improve the convergence through the use of a smoother switching from the unlimited specific dissipation rate to the limited one. Based upon the results of Ref. [26], we have used a value of 0.95 for C_{lim} in all calculations of this report. With the stress limiter, the k-ω model can produce essentially the same results obtained with Menter's SST model [11]. Without this limiter the shock location is predicted too far downstream.

Table 9: Computational performance on 1280×256 grid with Matrix dissipation for Cases 1, 9, and 10 using the 2006 Wilcox k-ω turbulence model.

Case	MG Cycles	Convergence Rate
1	136	0.7826
9	102	0.7070
10	125	0.7642

Table 10: Computed lift and drag coefficients with 2006 Wilcox k-ω turbulence model for RAE 2822 airfoil. Vorticity is used in production term. Matrix formulation for numerical dissipation. Grid has 1280×256 cells.

Cases	C_L	C_D	$(C_D)_p$	$(C_D)_v$
Case 1	0.584424	0.00798121	0.0024698	0.00551139
Case 9	0.806973	0.0156109	0.0104010	0.00520996
Case 10	0.749676	0.0234770	0.0184874	0.00498967

5.1.5 Behavior with matrix dissipation

We also performed calculations for the k-ω model on the 1280×256 grid using matrix dissipation with a pressure limiter. Vorticity is used in the production term of the transport equations. Table 9 shows the computational effort for the three RAE cases. The computed aerodynamic coefficients are given in Table 10. Consider a comparison of these results with the corresponding ones using the Roe rather than the matrix form for the numerical dissipation. See Table 8. The computations on the finest grid seem to be impervious to whether the pressure switch of the matrix dissipation or the general limiter [28] of the Roe dissipation is used for shock capturing. For Case 1, we observe a somewhat slower convergence with the matrix form. This may be a consequence of the fact that the matrix form in the residual does not include low-speed preconditioning whereas the Roe form does.

5.2 Menter SST Model (RAE 2822 Airfoil)

This section concerns computations with the 2003 Menter SST model for the RAE 2822 airfoil flows. Here again, unless otherwise stated, the production term of the turbulence model depends on strain rate.

Table 11: Computational performance for Case 1 using the 2003 Menter SST turbulence model.

Grid	MG Cycles	Convergence Rate
320×64	117	0.7556
640×128	106	0.7306
1280×256	115	0.7473

Table 12: Computed lift and drag coefficients with 2003 Menter SST turbulence model for RAE 2822 airfoil (Cases 1, 9 and 10).

Case	Grid	C_L	C_D	$(C_D)_p$	$(C_D)_v$	x_{sep}/c
1	320×64	0.590067	0.00781976	0.00233480	0.00548497	–
1	640×128	0.603580	0.00792761	0.00232047	0.00560687	–
1	1280×256	0.598711	0.00802810	0.00237207	0.00565604	–
9	320×64	0.816835	0.0158616	0.0108925	0.00496914	0.546605
9	640×128	0.807070	0.0157002	0.0105277	0.00517251	0.545416
9	1280×256	0.800513	0.0156612	0.0103689	0.00529232	0.543642
10	320×64	0.767978	0.0244646	0.0197081	0.00475648	0.572465
10	640×128	0.762655	0.0242471	0.0192944	0.00495272	0.568207
10	1280×256	0.756988	0.0241231	0.0190518	0.00507129	0.567302

Figure 11 shows the convergence behavior of the mean flow and turbulence model equations for Case 1. It is evident that the convergence rates are nearly the same as the mesh is refined, and these rates are quite similar to those obtained with the 2006 Wilcox model. Specific details of the convergence performance are given in Table 11.

The surface variations of C_p and C_f for the essentially subsonic flow of Case 1 on the three grids considered are shown in Fig. 12. Consider a comparison of the computed aerodynamic coefficients contained in Table 12 with the corresponding values calculated with the 2006 Wilcox model given in Table 3. These tables reveal that the coefficients calculated for Case 1 with the two turbulence models are quite similar.

For Cases 9 and 10, the convergence histories and surface distributions of C_p and C_f are displayed in Figs. 13 – 16. There is generally similar convergence behavior for Cases 9 and 10 using the SST model, although not as monotonic, as when employing the Wilcox k-ω model. This is evident by comparing Figs. 13 and 15 with Fig. 3 for Case 9, and Fig. 5 for Case 10.

When we consider these two transonic cases computed using the Menter SST model with strain rate, the importance of including the effects of principal turbulent shear stress transport for such adverse pressure gradient flows is revealed. As seen in Figs. 14 and 16, both cases show an upstream shifting of the shock location compared to the results with the Wilcox model, which are shown in Figs. 4 and 6. In fact, there is a dramatic difference in the shock location for Case 10.

The differences in the solutions for Cases 9 and 10 is further emphasized by considering the lift and drag coefficients (C_L and C_D) given in Tables 5, 7 and 12. For Case 9, the C_L and C_D computed using the Wilcox model are about 7% and 16% higher, respectively, than the values obtained with the Menter model. The C_L and C_D for Case 10 using the Wilcox model are about 11% and 19% higher than the corresponding values determined with the Menter model. Note, if vorticity is used in the production term of the Wilcox model, the coefficients presented in Table 8 are close to those calculated using the Menter model. Furthermore, one can see by comparing Figs. 7 and 8 for the Wilcox model using vorticity with Figs. 14 and 16 for the Menter SST model using strain rate that the shock location is nearly the same.

To further examine the flow fields computed with the 2006 Wilcox and 2003 Menter SST models, we display the turbulent viscosity contours in the RAE 2822 airfoil trailing edge region for Cases 9 and 10. The contours are shown in Figs. 17 and 18. They are quite similar, even though the Wilcox model uses vorticity and the Menter model uses strain rate in the production term.

6 Computational Results: NACA 4412 Airfoil

In the continuation of the investigation of the 2006 Wilcox k-ω and 2003 Menter SST turbulence models, we consider the low-speed flow over the NACA 4412 airfoil at a high angle of attack. The flow conditions are $M_\infty = 0.09$, $\alpha = 13.87°$, and $Re_c = 1.52 \times 10^6$. This particular case was selected because convergence difficulties are often experienced for high lift airfoil flows. Such difficulties seem to be a consequence of disturbances generated in the trailing edge separation region. As indicated on the TMR website [19], the experimental data of Coles and Wadcock [47, 48] were obtained in a relatively small wind tunnel, which could have an important effect on the data. For this reason, this validation case is considered somewhat weak. Nevertheless, this particular test case has been considered frequently in evaluating turbulence models.

The grids used for the calculations are from the TMR website [19], and they consists of 448×128, 896×256, and 1792×512 cells with the outer boundary located at 100 chords. These are also structured meshes with a C-type topology. The normal grid spacings at the wall boundary for the three grids are about 7.8×10^{-6}, 3.9×10^{-6}, and 1.95×10^{-6} chords, respectively. Boundary conditions are the same as described for the RAE 2822 airfoil flow. Even though the outer boundary is 100 chords from the airfoil surface, we have included the effect of using the far-field vortex condition. The influence of this condition is also examined.

Before performing the computations for this case, we examined the effect of the free-stream turbulence level on the solution for the RAE 2822 Case 1 when using the Wilcox 2006 model. The magnitude of the free-stream value of the turbulence dissipation rate ω was varied by factors of 10 to 1000. This variation did not reveal any significant effect on the numerical solution. Thus, with the 2006 Wilcox model, there seems to be at most weak sensitivity to free-stream turbulence level, which was considered to be an issue with previous versions of the Wilcox model.

6.1 **Wilcox Model** (NACA 4412 Airfoil)

The initial series of computations for turbulent, viscous flow over the NACA 4412 airfoil were performed with the 2006 Wilcox model. As for the RAE 2822 airfoil flows, the principal objectives are to not only compare computed solutions with the experimental data of Coles and Wadcock [47] but also to evaluate the convergence behavior when using the RK/Implicit scheme. Previously, it was demonstrated that for an airfoil flow with sufficiently high shock strength there is a delay in separation when using the 2006 Wilcox model with strain rate for the production term. In this section, we show that there can be a delay in separation for a subsonic airfoil flow, whether strain rate or vorticity is used in the production term.

Table 13: Computational performance for flow over NACA 4412 airfoil using the 2006 Wilcox model. Strain rate used in production term.

Grid	MG Cycles	Convergence Rate
448×128	97	0.7363
896×256	102	0.7484
1792×512	140	0.8113

Figures 19 and 20 show convergence histories for the mean flow and turbulence model equations when applying the 2006 Wilcox model using strain rate or vorticity in the production term. For

both calculations, low-speed preconditioning was applied. The final level of the mean flow residual is somewhat higher than observed in the computations for the RAE airfoil flows. This is a consequence of roundoff errors. As indicated in Ref. [26], such roundoff errors occurring at low Mach numbers can be avoided by introducing a gauge pressure. The convergence level is attained in about 140 cycles with strain rate and 150 cycles with vorticity. In both calculations, we observe the expected rapid convergence of the lift coefficient (C_L). Table 13 presents the the number of multigrid cycles and convergence rate for each grid when using strain rate. If vorticity replaces strain rate, the convergence rates are about the same on the two finer grids.

We should point out that throughout this investigation three to four iterations of the turbulence modeling equations were performed for each RK stage of the mean flow equations. Additional updates of the eddy viscosity can be beneficial to overcome convergence slowdown or convergence difficulties, but this has not been necessary for the current study.

In Figs. 21 and 22, a comparison is made of surface pressure (C_p) and skin-friction (C_f) distributions computed with either strain rate or vorticity. The two surface pressure variations exibit fairly good agreement with each other. They also show good agreement with the experimental data except in the trailing edge (TE) region. There are slight differences of the C_p values in the TE region. The C_f distributions are quite similar, except for differences of the peak value and flow separation location. Using vorticity, the peak C_f is about 20% smaller, and the separation location is at 0.88 chords instead of 0.89 chords. In Table 14, we present the computed lift and drag coefficients using the 2006 Wilcox model with either strain rate or vorticity. These results compare favorably with those from the NASA TMR, which were calculated with the NASA computer codes CFL3D (structured grids) and FUN3D (unstructured grids). As indicated in the table, the C_L and C_D values determined with the Wilcox (k-ω) model and strain rate are 8.5% higher and 23.4% lower, respectively, than those obtained with the Menter SST turbulence model.

Table 14: Computed lift and drag coefficients with the 1988 and 2006 versions of the Wilcox model and the 2003 Menter SST model for the NACA 4412 airfoil. Grid with 896×256 cells from NASA TMR. The notation k–ω-V means vorticity in the production term of a Wilcox model, and plim delineates that the production limiter is used. The superscript $*$ indicates results from the TMR website.

Code	Model	C_L	C_D	$(C_D)_p$	$(C_D)_v$	x_{sep}/c
CFL3D*	2006 k–ω–plim	1.7572	0.02549	0.01762	0.007865	0.89
FUN3D*	2006 k–ω–plim	1.7528	0.02650	0.01864	0.007865	0.89
FLOMG	1988 k–ω–plim	1.79690	0.0250879	0.0166555	0.00843241	0.924
FLOMG	1988 k–ω–V	1.79689	0.0250882	0.0166559	0.00843226	0.924
FLOMG	2006 k–ω	1.75365	0.0252050	0.0174919	0.00771308	0.889
FLOMG	2006 k–ω–plim	1.75749	0.0249440	0.0172363	0.00770768	0.891
FLOMG	2006 k–ω–V	1.73793	0.0246438	0.0169300	0.00771377	0.881
CFL3D*	SST	1.616	0.0311	0.0242	0.00687	0.78
FUN3D*	SST	1.615	0.0320	0.0252	0.00684	0.78

The velocity profiles computed with strain rate and vorticity in the production term of the 2006 Wilcox model are displayed for the two finer grids (mesh densities of 896×256 and 1792×512) in Figs. 23 – 26. No limiter of the production was used in these calculations. Here, as mentioned earlier, the stress limiter of the turbulence model is sufficient to prevent any anomalous behavior at the stagnation point when using strain rate. Moreover, we observe the expected small differences between the results using the strain rate and vorticity. These velocity profiles are quite similar to

those presented on the NASA Turbulence Modeling Resource (TMR) website [19], which used the production limiter. It is also evident that the inclusion of the production limiter (which appears unnecessary) does have only a small effect on the aerodynamic coefficients in this particular case. From the table, we see that the flow separates at about $x/c = 0.89$ when using the 2006 Wilcox model, which is much later than the flow separation point predicted with the Menter SST model ($x/c = 0.78$).

Figure 27 exhibits the contours of the turbulent viscosity and streamlines for the leading edge region of the NACA 4412 airfoil when using the 2006 Wilcox model with strain rate. These contours and the ones that follow are for the 896×256 grid. Pressure contours and streamline patterns for both the leading edge and trailing edge regions are displayed in Fig. 28. There is a relatively small separation bubble on the upper surface of the airfoil. Figure 29(a) shows the turbulent viscosity contours computed with the 2006 Wilcox model. If these contours for the trailing edge and near wake regions are compared with those computed with the 2003 Menter model, which are shown in Figure 29(b), we observe a significant difference in the magnitude of the turbulent viscosity. This is a reflection of the separation location and the behavior of each model in the wake. Solutions and the associated surface and skin-friction distributions, as well as the velocity profiles, for the Menter SST model are presented in the subsequent subsection.

6.2 **Menter SST Model** (NACA 4412 Airfoil)

In all the computations for flow over the NACA 4412 airfoil using the 2003 Menter SST model, numerical results are calculated with central differencing and Roe dissipation and applying low-speed preconditioning. Strain rate is used in the production terms of the turbulence model. Although not shown in detail, essentially the same results have also been obtained with matrix dissipation. Furthermore, the previously stated requirement to reduce the residual to at least essentially machine zero is enforced. Even though the outer boundary of the computational domain is located at 100 chords from the airfoil, the far-field vortex effects have been included. Such effects have proven to have only a relatively small impact on just the pressure drag.

The computational performance with the 2003 Menter model for the NACA 4412 airfoil is given in Table 15. As we can see from this table and the convergence histories for the mean flow and turbulence modeling equations in Fig. 30, there is a significant departure from the convergence behavior observed with the 2006 Wilcox model. In particular, there is an irregularity in the convergence as well as a slowdown with mesh density. It is certainly a possibility that this slowdown is a consequence of the increased extent of upper airfoil surface flow separation relative to that with the Wilcox model. There is also the possibility that the nonlinear limiter of the numerical dissipation model is at least contributing to producing such a slowdown.

Figure 31 exhibits the surface pressure and skin-friction distributions for the same range of grid densities. These plots indicate almost no discernible difference in the distributions for the three grids. The aerodynamic coefficients computed with both the Roe and matrix form of dissipation are presented in Table 16. It is clearly seen that there are only small differences in the coefficients with the two forms of dissipation. Yet, that does not exclude the possibility of limiter effects of the Roe dissipation on convergence behavior.

Table 15: Computational performance for flow over NACA 4412 airfoil using the the 2003 Menter SST model.

Grid	MG Cycles	Convergence Rate
448×128	215	0.8719
896×256	96	0.7343
1792×512	300	0.9065

Table 16: Computed lift and drag coefficients with SST model (2003) for NACA 4412 airfoil. Numerical dissipation computed with Roe and Matrix forms. The far field vortex (FFV) effect used in outer boundary condition. No transition (Tr) set.

Dissip.	Grid	C_L	C_D	$(C_D)_p$	$(C_D)_v$	x_{sep}/c
Roe	224×64	1.526610	0.0357887	0.0294016	0.00638710	0.719688
Roe	448×128	1.603900	0.0307412	0.0239594	0.00678186	0.781613
Roe	896×256	1.622190	0.0299893	0.0230836	0.00690567	0.788752
Roe	1792×512	1.626420	0.0298628	0.0229144	0.00694844	0.794475
Mat	224×64	1.544880	0.0356976	0.0291920	0.00650563	0.744329
Mat	448×128	1.603980	0.0311452	0.0243412	0.00680401	0.781613
Mat	896×256	1.622190	0.0303632	0.0234476	0.00691556	0.788752

To uncover an enhanced understanding of how the SST model behaves, we now consider a comparison of the calculated velocity profiles with the experimental data. Profiles for an even coarser grid (224×64 mesh cells) is also considered. The x-component and y-component (u and v) velocity profiles are displayed in Figs. 32 – 35. These profiles show a consistency with respect to mesh refinement, avoiding any anomalous behavior even on the 224×64 grid. Once a grid density of 896×256 is reached, there are essentially no significant differences with refinement to a mesh density of 1792×512. This can be readily seen in Fig. 36, which directly compares the profiles on these two grids. The symbols correspond to the 896×256 solution, and the lines correspond to the 1792×512 solution. Moreover, these profiles are in very close agreement with those given on the NASA TMR website.

In addition to comparing the current results with the NASA TMR, we also consider the available computed results of Menter [8]. This comparison of the variation of surface pressures and the x-component velocity profiles indicates that these two sets of computational results also appear to have, in a general sense, good agreement. It is important to emphasize that Menter's version of the SST model used vorticity in the production term rather than the strain rate.

Additional details of the flow field are revealed by the leading edge and trailing edge pressure contours and streamlines that are depicted in Figs. 37 – 40. From these plots one sees the development of the NACA 4412 airfoil separation region on the upper surface. On the coarsest grid (224×64), in particular, there is an exaggerated extent of the trailing edge separation bubble. As we have seen already for the velocity profiles with mesh refinement, there is a significant adverse effect on the accuracy of the solution on the coarsest mesh. This is a consequence of the high value of the grid stretching due to the outer boundary being located 100 chords away from the airfoil. The streamlines for the two finest grids are essentially the same. Next, we show the eddy viscosity profiles for this range of grids in Figs. 41 and 42. These plots delineate the reduction in the turbulent viscosity in the wake region with mesh refinement.

Remark 1 *A few of what seem to be minor changes were made to the 1992 version of the SST model to obtain the 2003 model. One principal modification was the replacement of vorticity in the production term with strain rate. Menter [8, 10] performed numerical computations that indicate for several flows, including the NACA 4412 flow, essentially the same solutions are obtained with the SST model using either strain rate or vorticity. Although not included in this report, this author has also verified this for the NACA 4412 airfoil.*

Remark 2 *Clearly, in the interest of making progress to improve turbulence modeling, it is essential to delineate the effect of each change in a model. This should be done for a range of baseline turbulent flows. In addition, the effects of mesh refinement as well as full convergence should also be part of an evaluation of a turbulence model.*

7 Perspective on Solving Transport Equations

Before considering the elements of this section, we state a guideline that is followed throughout. Frequently, in the current literature on the development and improvement of the numerical algorithms for solving the RANS equations, we observe that there is a general tendency to use a descriptive word such as *robust*. This is a powerful descriptive word, and yet, the context in which it is being used is often not clearly defined. It is the viewpoint of this author that a precise definition of this adjective must be given to avoid any misinterpretation by the reader. This author defines a robust solution algorithm as one that has as a minimum the following properties:

(a) Solution is obtained for any physical problem within the range of applicability of the governing fluid dynamic equations and corresponding boundary conditions.

(b) Solution is consistent with the physics of the problem being solved.

(c) Solver produces a fully converged solution with a given set of input parameters.

In the subsequent subsection, we discuss the critical mathematical issue when solving PDEs that exemplifies why caution is imperative when using the word *robust*.

First, in the subsequent section, we delineate the fundamental theoretical subjects in the analysis of partial differential equations (PDEs). These subjects establish the requirements to prove well-posedness of a boundary-value problem. Next, we consider the current status in proving well-posedness. It should be pointed out that one of the seven Millenium Prize Problems in the field of Mathematics concerns the existence and smoothness of solutions of the incompressible Navier-Stokes equations. A description of the problem is given by C. L. Fefferman in the article "Existence and Smoothness of the Navier-Stokes Equations" of Ref. [49]. Then, we present and discuss various components to consider when designing an effective numerical algorithm for solving the RANS equations and the transport equations of a turbulence model.

7.1 Well-Posedness

As pointed out by Shearer and Levy [50], the theoretical study of PDEs generally focuses on four basic issues, and three of these are the requirements for well-posedness in the sense of Hadamard [51]. According to Hadamard, a solution to a PDE or system of PDEs must exist, be unique and depend continuously upon the initial and boundary conditions. One additional consideration is regularity (i.e., smoothness) of the solution.

It is well-known at this time there is no proof, in general, that the multidimensional, nonlinear, compressible, time-dependent Navier-Stokes equations along with appropriate boundary conditions are a well-posed problem. This statement assumes that no specific requirements are being made about the regularity of the solution. It then follows that this is also true for the corresponding RANS equations.

To ensure that we have a well-posed problem for the equations under considerations, we must first establish that the boundary conditions of the initial-boundary value problem are appropriately defined. As we discuss subsequently, the classical energy method (under the necessary restrictions) can be used to determine suitable boundary conditions. Further, such a method can reveal the minimal number of boundary conditions, which along with an estimate of the solution can lead to showing the existence and uniqueness of the solution.

Thus, the question that immediately arises is: What is necessary to establish that the physical problem being considered is well-posed on both the continuous and discrete levels? Answering this question is essential, since then we know the circumstances under which a reliable solution can be obtained.

Although proving well-posedness, in a general sense, for problems governed by the Navier-Stokes equations remains elusive, some progress has been achieved. For example, Gustafsson and

Sunström [52], Oliger and Sundström [53] and Nordstrom [54] have considered well-posedness for the linearized and constant coefficient Navier-Stokes equations. In each paper, the energy method is applied to the symmetrized form of the equations. The energy method determines an estimate that must be satisfied to bound the energy growth. This estimate is imposed to determine boundary conditions for the continuous and discretized equations necessary for a well-posed problem. In addition to the boundary conditions for the Euler equations, there are also numerical conditions required for the Navier-Stokes equations. At open boundaries of the domain, the number of boundary conditions needed for the Euler equations is based upon the number of ingoing and outgoing characteristics.

More recently, using a regularity assumption, Nordström [55] has delineated what he calls a roadmap for establishing well-posedness of the continuous time-dependent compressible Navier-Stokes equations. Part of this roadmap is to ensure a stable numerical approximation. A critical issue in considering well-posedness and a stable method for approximating the numerical solution is the boundary conditions. The number of boundary conditions and their form must be considered. The roadmap addresses these questions based on the analysis for the continuous problem given in Nordström and Svärd [56]. Moreover, it is asserted, based on the energy method, that using a summation-by-parts (SBP) form and a weak imposition of the these boundary conditions leads to stability. There are some details regarding the development of this roadmap that are of particular interest in regard to the issue of well-posedness, as will be revealed in what follows.

In constructing the roadmap of Ref. [55], the analysis starts with a frozen coefficient linearized form of the governing PDEs. The focus is on proving that the linear continuous problem is well-posed. The energy method, boundary conditions of Ref. [56] and the maximal semiboundedness of the differential operators lead to well-posedness for the smooth linear problem. According to Nordström, the principles of linearization and localization, given by Kreiss and Lorenz [57], can be used to extend the linear theory to smooth nonlinear problems. Again, it needs to be emphasized that there are assumptions of regularity and requirements for the boundary conditions. Thus, in the discrete formulations that are often considered, it may not follow that the discrete problem can be classified as well-posed. We are also confronted with the challenge of solving various complex flow problems associated with an extensive range of aerodynamic configurations. Without well-posedness of the fluid dynamics problem, we are exposed to the possibility of multiple solutions, which will be discussed for the RANS equations later in this section. Discussions of many aspects of well-possedness for initial-boundary value problems, which in some cases includes important specific theoretical considerations, are given in the Refs. [50,57–62]. A paper of particular relevance for this perspective is a recent paper by Langer and Swanson [63]. Here, a compelling argument is made that transport equations with suitable boundary conditions are not a well-posed problem.

7.2 Solving RANS and Transport Equations

When considering the RANS equations for turbulent flows, there are important issues concerning the mathematical formulation of turbulent flow problems involving transport equation models that are either not addressed or not given a complete description. One issue is that the well-posedness of the mathematical problem is generally not addressed. Another issue is that frequently there is not a complete description of the continuous and discrete problems. Such a delineation requires presenting not only the boundary conditions but also their exact implementation. A third issue is that cut-off (restriction) of certain variables in the turbulence model are often not completely identified. This is an extremely important deficiency, since limiting these variables can create serious questions about the approximate solutions of the governing equations. In addition to these issues, there is often a woeful neglect of a proper study of the mathematical characteristics (properties) of the equations in the turbulence model, even when there is an attempt to solve the equations of a model in a weakly coupled manner (i.e., RANS and transport equations solved in a sequential manner with each advancement of the iterative solution). As a result, there are often serious difficulties in solvability encountered when attempting to solve the flow and turbulence modeling equations. Even if

these essential mathematical issues are addressed, there still remains many challenging numerical difficulties that can occur when solving two or more transport equations. Furthermore, without a careful study of the mathematical properties of the equations and resolution of the key issues, there is limited possibility to build reliable transport equation models that can be used on a routine basis for industrial applications.

Conjecture 1 *The construction of a reliable and efficient algorithm for solving two or more transport equations modeling the effects of turbulence, either weakly or strongly coupled to the RANS equations, is highly unlikely, in general, without complete mathematical and numerical analysis of the system of equations.*

In general, developers of turbulence models do not give significant consideration to solving the transport equations of a tubulence model. As a consequence, even considering various implicit solution algorithms to relax or possibly eliminate stiffness of the equations due to viscous layers and source terms, there is generally inadequate convergence of the numerical solution to the transport equations. As indicated previously, the most notable exception [3, 5] concerns the effort to augment the reliability of the one-equation model of Spalart and Allmaras. The success of this model in terms of reliability and efficiency has been affected considerably by examining methodically the mathematical characteristics of the transport equation as well as the requirements for reliable numerical behavior.

When approaching the modeling of turbulence, we should keep in mind two extremely important factors. First, one must recognize that development of turbulence models generally depend to some degree upon heuristics. Also, models involving more than one transport equation are not based totally upon derivations from first principles of fluid dynamics. These factors suggest that there is some flexibility in solving the transport equations by changing the models to make them amenable to solution. Here, such improved amenability to solution is called enhanced *numerical compatibility*. Of course, with such changes in the model, there must be a concerted and careful effort to verify that the integrity of the original model has not been compromised. This means that the solutions of standard test cases used in validation of the model must be computed with the changes to demonstrate replication of the solutions used in validation.

The importance of establishing fully converged solutions in any type of modeling must be emphasized. Moreover, if we cannot solve the equations, which means that it is possible to reduce the residuals to machine zero (at the very least for canonical problems), then how can we conclude that the model improves predictions and can be applied on a reliable basis. In addition, if the equations of the model are not solvable, how can we possibly determine if the model can actually improve the predictions that are possible with other models.

There are several essential requirements for reliable numerical algorithms for solving the transport equations of turbulence models. Ideally, we would like to solve these equations and the compressible RANS equations in a fully coupled manner. This would necessarily require that we understand the mathematical characterization of the complete system of equations. While we can characterize the time-dependent RANS equations (i.e., incomplete parabolic system), the inclusion of the transport equations will change this characterization of the complete system. Thus, at this point, a much better choice is to solve the fluid dynamic and transport equations in an appropriate loosely coupled manner. There is no assertion here that solving the mean flow and turbulence model equations loosely coupled is comparable to solving the equations fully coupled. On the otherhand, Lee and Choi [64] indicate that there is no benefit in solving equations fully coupled, but they have not proven this in a mathematical sense.

7.3 Strong Solution Algorithms

The numerical algorithms for solving both the mean flow and the turbulence modeling equations should belong to the class of strong algorithms. One essential measure of a strong algorithm is that

it must be highly implicit, allowing for unconditional stability at least in a linear sense, which accounts for the effect of boundary conditions. Since the fluid dynamic equations are highly nonlinear, in general, a much stronger stability is required to establish a highly reliable algorithm that can be used on a routine basis in an industrial environment. Later, we briefly discuss an approach to produce a nonlinear stability. Both complete linear and nonlinear stability properties (that consider the eigensystems of the equations with boundary conditions) must also apply to the solution process for the nonlinear transport equations. When constructing the numerical algorithms for the mean flow and transport equations, we should keep in mind that it may be possible to improve convergence if we have an algorithm for full coupling of both sets of equations, assuming that the character of the full system of equations is completely understood.

7.4 Stiffness of Governing Equations

In addition to strong stability, the implicitness of the algorithm is absolutely essential for the effective treatment of stiffness in the governing equations. There are several reasons for such stiffness. First, there is the stiffness that is associated with the discrete mean flow equations. This type of stiffness arises due to the requirement to resolve viscous layers with an economic use of grid points (e.g., the application of grid stretching in the normal direction to a solid boundary to resolve the boundary layer). Second, there is the stiffness of the transport equations of the turbulence model. Such stiffness is primarily caused by the source terms and the disparity between the time scales of these terms and those of the convective and diffusive terms. During the initial phase of solving the equations of the turbulence model, it is these source terms that easily cause exponential growth of any disturbances in the solution field due to an imbalance between the production and destruction terms in the turbulence model. Thus, a strong numerical solver is essential. Consider, for example, the specific dissipation rate (ω) equation in the k-ω turbulence models. As pointed out by Wilcox [1], the original form of this equation was derived by Kolmogorov using the physics of the the fluid dynamics and dimensional analysis. The resulting ω equation is quite stiff, especially due to the behavior of ω in the immediate neighborhood of a solid boundary. Some undesirable properties of this transport equation may have a connection to how it was derived. Moreover, in a loose sense, this equation is kludged up, rather than being derived rigorously from first principles of fluid dynamics. For all these reasons the level of stiffness for the equations of the turbulence model is much greater than that of the mean flow equations.

7.5 Positivity and Realizability

Another important consideration when constructing a solution scheme for the mean flow and turbulence equations is positivity. Ultimately, we would like to develop positivity preserving schemes. For the mean flow equations, there is the requirement of positivity for the thermodynamic variables. In the case of a two-equation model, such as the k-ω model of Wilcox, we need to ensure positivity of both k and ω. For a Reynolds stress model, the dependent variables include the Reynolds stresses, and we must ensure positivity of the normal stresses. There are three methods that are currently used to ensure positivity of the dependent variables in turbulence models. One approach is to simply explicitly enforce the positivity, which is what we have done in the current work with the k-ω model.

Another way [65] to enforce positivity is to replace k and ω with $\ln k$ and $\ln \omega$, respectively. With this method, there is a need to introduce a wall function since k vanishes at a solid boundary. Also, as pointed out by Mor-Yossef [15], this approach can experience difficulties with an upper bound on the eddy viscosity. To remove the necessity of wall functions, while retaining a reduction in the severe variation of ω approaching the wall boundary, Bassi and Rebay [66] and Bassi et al. [67] replace only ω with $\tilde{\omega}$ that represents $\ln \omega$. However, with this method, there is then a need to ensure the positivity of k to compute a physical eddy viscosity. This is accomplished by defining

a $\bar{k} = \max(0, k)$ and computing $\bar{\mu}_t = \alpha^* \rho \bar{k} \mathrm{e}^{-\tilde{\omega}_r}$. The α^* is a closure coefficient. Realizability conditions for the normal Reynolds stresses and the shear Reynolds stresses are set by imposing a lower bound on $\tilde{\omega}$.

The third method is to construct an M-matrix, which is a semipositive matrix with positive real eigenvalues, that approximates the Jacobian of the transport equations. A nonsingular M-matrix has the desirable properties that it has a convergent regular splitting, and its inverse is positive. These properties guarantee unconditional stability (in a linear sense, depending on boundary conditions) and positivity of the dependent variables in the turbulence equations. Moreover, the M-matrix can be used to construct an implicit operator that has a positive inverse. This ensures that any update to the solution in the iterative process is positive. Mor-Yossef [15–17, 44, 45] has applied the M-matrix approach in solving the equations of the k-ω model of Wilcox and the full Reynolds stress transport (RST) model of Eisfeld. It should be pointed out that such an M-matrix approach does not appear to have a counterpart for the mean flow equations. This type of approach for just the transport equations seems to have adverse effects in solving the mean flow equations, including a significant limitation of the CFL number.

There are additional conditions that require enforcement when solving the equations of the k-ω and RST models. For example, in general, numerical difficulties can be encountered during the initial phases of a computation. Clearly, one such difficulty, as indicated previously, is the imbalance between the production and destruction terms of a turbulence model. In this report, we have applied the limiting of the production term suggested by Menter. We have also explicitly enforced the positivity of k and ω. Generally, it is not desirable to impose conditions explicitly in numerical computations, since this often has repercussions on convergence behavior. It is interesting that in the current set of problems neither the limiting of the production nor the explicit enforcement of positivity have caused any significant adverse effects on convergence. However, one cannot infer that this will always be the situation. Some recent numerical tests with the solution algorithm described in this paper have indicated the possibility that this type of limiting as well as the explicit enforcement of positivity may not be necessary for simpler flows. Without such limiting and positivity enforcement, it may be necessary for complex turbulent flows, such as multielement airfoil flows, and three-dimensional flows to control the updates of the dependent variables to ensure positivity. This type of approach has the disadvantage that it may have a substantial impact on the convergence rate.

Alternatively, one can directly ensure positivity of the dependent variables with the iterative scheme. A possible way of doing this is the M-matrix approach of Mor-Yossef, which also apparently avoids the use of the Menter limiter function. There is a necessary requirement to verify this through extensive testing. Clearly, a desirable property in developing a robust algorithm for solving both the mean flow and turbulence model equations is to ensure positivity. There remains a need to develop a solution algorithm for ensuring positivity for both the thermodynamic and the dependent variables of these equations.

For a Reynolds stress model, there are some realizability constraints that need to be enforced. These constraints are associated with the Reynolds stress tensor, which we define here as $\mathcal{R}_{ij}$. There are three constraints, which are as follows:

$$\mathcal{R}_{ij} \geq 0 \quad \text{for} \quad i = j, \tag{70a}$$

$$\mathcal{R}_{ij} \geq \tau_{ii}\,\tau_{jj} \quad \text{for} \quad i \neq j, \tag{70b}$$

$$\det\left[\mathcal{R}_{ij}\right] \geq 0, \tag{70c}$$

where $\det$ means determinant. These realizability constraints are usually explicitly enforced. Currently, there is no enforcement of the constraints that is done within the construction of the algorithm itself. While choosing an M-matrix for the Jacobian ensures positivity of the normal Reynolds stesses, it does not guarantee satisfaction of the other two constraints. Mor-Yossef enforces these two constraints explicitly.

7.6 Boundary Conditions

Consider a discrete problem and the singular type behavior of the dissipation (ω) equation when approaching a solid wall boundary. When applying the boundary condition given in (44), we currently do not subiterate with each advancement in pseudotime. Thus, we are actually not even solving a boundary value problem with each advancement in pseudotime. This could possibly introduce some numerical problems in general. For the computations presented herein, there are not any apparent difficulties resulting from the present, and usual, approach. However, one cannot assume that this will not be an issue for more complex flows.

It is possible to mitigate the effect of the strong, singular type behavior of ω near a wall boundary. The use of a $\log(\omega)$ instead of ω appears to be somewhat beneficial in this regard (see Bassi et al. [67]). However, the singular character of ω is not a removable singularity. It should be possible to remove this behavior at the wall boundary, but only to have it appear somewhere else in the flow field. Moreover, the subsequent behavior of ω may actually present even greater numerical difficulties (e.g., significantly altering behavior in the far field of the solution domain). This possibility means that it is extremely important when considering such transformations (see, for example, Ref. [68]) to verify that all boundary conditions are satisfied, and that machine zero convergence of residuals is attained (at the very least for canonical problems). It is also very important to consider the behavior of the turbulent viscosity in the solution field, since this can often provide important clues about the effects of the transformation. It should be mentioned that the manner in which ω behaves near a wall boundary can in general produce adverse effects on the convergence of the solution for k and ω, and significantly reduce the potential effectiveness of the solution algorithm. Moreover, the near-wall behavior of ω makes it difficult to obtain any significant convergence acceleration benefit when using a multigrid method.

Usually, the far-field values of k and ω (see (45)) are prescribed according to the values suggested by Menter [10], which are also given in the Turbulence Model Resource (TMR) [19]. In general, a principal factor for establishing the far-field values of these variables is the turbulence intensity (turbulence level), which is often designated by Tu. The turbulent viscosity (μ_t) is also required. Then, the turbulence kinetic energy is determined using the Tu. With a known μ_t, the ω is computed. Additional boundary conditions are required for the Reynolds stresses in the RST model (see the TMR or Mor-Yossef [44, 45]). When formulating the continuous and discrete problems, the functional dependence (such as the dependence on the Tu) of the dependent variables must also be defined completely for these problems.

Once the boundary conditions are explicitly defined, then we can proceed in considering the issue of well-posedness, in the sense of Hadamard [69]. As indicated initially, there is no proof of well-posedness of the boundary-value problem for the RANS equations when regularity (i.e., smoothness of solution and derivatives) is not assumed. This suggests that we do not have a well-posed problem for the nonlinear transport equations of the turbulence model when a regularity assumption is not imposed. Furthermore, in Ref. [63], by considering the corresponding inverse problem, a compelling case is made, although not a proof, that the problem is ill-posed. Thus, it is distinctly possible that both the continuous and discrete problems are ill-posed, resulting in the possibility of multiple solutions. Further, since the ω transport equation is kludged up, this suggests an increased possibility of multiple solutions.

Conjecture 2 *The fact that the specific dissipation rate transport equation of the RST model is not rigorously derived from first principles of fluid dynamics suggests that there may be an increased probability of multiple solutions. As the mesh densities for computations continue to grow, we may well observe such multiple solutions. Yet, we cannot dismiss the possibility that the number of multiple solutions may actually decrease with increased mesh density.*

7.7 Linear and Nonlinear Stability

Initially we discuss linear (Fourier) stability (often called von Neumann stability) analysis for a solution algorithm. For boundary value problems, a local mode analysis, which is based on the Fourier analysis (i.e., Fourier transform of linear equations), is often quite beneficial in estimating the high-frequency smoothing properties. When considering initial-boundary value problems, one can use the energy method, which allows for variable coefficients and the inclusion of boundary conditions. This method determines a sufficient condition for stability, and it gives an estimate of error growth and rate of convergence. This approach is not discussed here, but a complete discussion of this method is given in Richtmyer and Morton [60]. A somewhat more direct approach for initial-boundary value problems is an eigenvalue system analysis. This method includes boundary conditions and provides an evaluation of stability as well as a good estimate of the asymptotic convergence rate. Also, it is possible with a Krylov method, using the Arnoldi algorithm, to determine the stability behavior of the actual discrete physical problem being considered, as in Ref. [70]. In the second part of this section, we give a succinct discussion of nonlinear stability.

7.7.1 Linear stability

The first consideration of stability usually involves a linear analysis on an infinite domain. Satisfying the von Neumann stability criterion is at least a necessary condition for linear stability. In certain cases, this satisfaction of this criterion can also be sufficient (see for example proof of Lax equivalence theorem). For the RK/Implicit scheme applied in this report, unconditional stability has been demonstrated for the governing flow equations using this analysis. Since we are considering an initial-boundary value problem, an eigensystem analysis based on the Fourier approach has also been performed that shows the unconditional stability and indicates good high-frequency smoothing properties of the solution algorithm. For additional discussion, see Ref. [71]. At this time, additional analysis is required for the two-equation turbulence model. Nevertheless, as indicated previously, all the computations herein have been done with a CFL between 10^3 and and 10^6. The algorithm does not automatically ensure the positivity, which requires in general an explicit enforcement of positivity for k and and ω (or application of limitation on allowable updates). An automatic enforcement with the algorithm would be beneficial and possibly improve the viability of application in an industrial environment.

Mor-Yossef and collaborators [16,44,45] have made some nice progress in solving two-equation and RST turbulence models. They apply implicit schemes for solving both the mean flow and turbulence model equations. As indicated previously, these are not the same implicit schemes, which leads to a problem when considering the fully coupled system. Different implicit solvers [44, 45] have been considered for the mean flow equations when considering structured and unstructured grids. They have developed the unconditionally positive convergent (UPC) implicit scheme, using an M-matrix, for solving two-equation and RST turbulence modeling equations. The properties of the scheme have been discussed based upon theory and some eigenvalue analysis [16, 44]. It is interesting that when applying these algorithms for the mean flow and turbulence modeling equations, the CFL is $\mathrm{O}(10^2)$, and often between 25 and 50. Moreover, when machine zero convergence (or even approaching it) is attained, the iterative process requires about 5000 iterations or more. In many cases, the convergence level (i.e., residual reduction) is between four and five orders of magnitude. Generally, they do not employ multigrid to accelerate the convergence of the scheme, although Wasserman et al. [17] have considered multigrid for a two-equation model.

7.7.2 Nonlinear stability

Since the equations for the mean flow and turbulence model are nonlinear, and the objective is to construct a highly reliable solution algorithm, it is essential to consider nonlinear stability. The

nonlinearity can have significant effects (e.g., produce spurious oscillations) in the flow field, which can occur in underresolved regions and in the neighborhood of discontinuities such as shock waves. Here, we briefly discuss the concept of entropy stability (nonlinear stability). The purpose of this discussion is to simply suggest that work on this subject may possibly lead to substantial advances for the reliability of the solution algorithm when there is turbulence modeling.

There has been considerable work done on entropy stability by Tadmor, starting with his 1987 paper [72] on entropy stable schemes for systems of conservation laws. In a later paper, Tadmor [73] delineates approaches to analysis of entropy stability (i.e., comparison arguments, homotropy approach and kinetic formulations). Second-order finite-volume schemes were considered. A number of papers have been written since the initial work of Tadmor (e.g., Refs. [74–77] that have extended entropy stability to higher order schemes (with various forms of discretization) for solving the Navier-Stokes equations. There seems to be no work that has been performed regarding entropy stable schemes for solving the tranport equations of turbulence models.

As pointed out by Carpenter [76], entropy stability guarantees that the thermodynamic entropy is bounded for all time in L_2 under two conditions. First, the density and temperature remain positive. Second, the boundary data result in a well-posed problem and preserve the entropy estimate. To construct entropy stable schemes, a convex entropy function is required. This entropy function is a mathematical function that is the negative of the thermodynamic entropy of gas dynamics. It provides an estimator of system stability. A statement of the global conservation of the entropy is derived by transforming (contracting) the Navier-Stokes equations using this entropy function and integrating over the domain. By mimicking each term of this equation discretely, we can obtain a semidiscrete entropy estimate. Then, using the procedure of Tadmor called comparison arguments, the conditions that guarantee entropy stability can be established. Complete details of this procedure are given in Tadmor [73] and Fisher and Carpenter [77].

Clearly, the first major obstacle in considering entropy stability for an algorithm to solve the transport equations of a turbulence model is proving that the continuous and discrete problems are well-posed. Another difficulty concerns defining an appropriate mathematical entropy function. If progress can be made in establishing entropy stabilty for a solution algorithm, it could be a major advancement for turbulence modeling.

7.8 Multiple Solutions

Before concluding this section, it is essential to return to the fundamental issue of constructing a well-posed problem. This issue is existential in solving both the Navier-Stokes and turbulence modeling equations. As pointed out previously, we cannot in general establish a well-posed problem for even the Navier-Stokes equations, in the sense of Hadamard [69] and supplemented with the condition of regularity. This mathematical issue already sets the stage for the issue of an ill-posed problem for the system of transport equations. Such a consequence exposes the probability of anomalous results or multiple solutions. At this point, there has been very little documented concerning the existence of multiple solutions when considering various turbulence models. Moreover, there is currently no systematic way of demonstrating multiple discrete solutions, as well as how many such solutions may exist, when modeling turbulence.

It is important to recognize that there are examples of multiple solutions in fluid mechanics, which have occurred when solving the transonic potential flow equation [78] and the Euler equations [79]. There is also the discussion of Temam [61] concerning existence, uniqueness and regularity for the Navier-Stokes (N-S) equations. In fact, Temam shows an example of nonuniqueness of solutions for the N-S equations (i.e., regarding laminar flows) in which he provides proof based on topological arguments.

More recently, in 2014, Kamenetskiy et al. [80] presented numerical evidence of multiple solutions to the RANS equations for turbulent flows. They consider turbulent flow over an extruded two-dimensional (2-D) airfoil geometry and a trap wing configuration from the first AIAA High Lift

Workshop [81]. Computations were performed for both the one-equation model of Spalart-Allmaras and the two-equation model of Wilcox. Three primary approaches were considered to find multiple solutions, which are as follows: Varying initial conditions, applying different techniques for enforcement of solid surface boundary conditions, and using variations of implicit residual smoothing. For the trap wing case, the number of multiple solutions discovered with the methods depended on the mesh density. The meshes used (designated coarse, medium and fine) were from the AIAA High Lift Workshop. It should be pointed out that in the work of Kamenetskiy et al. numerical results are only classified as solutions when the residuals of the equations have been reduced to machine zero. As discussed previously, reduction of the residual to machine zero is essential. Otherwise, results in which the residual has only been reduced four or five orders of magnitude are affected by solver integration errors that can play a significant role in the behavior of the result, possibly making it quite different from the actual solution. Kamenetskiy et al. call such results pseudosolutions. It is interesting that on a coarse mesh eight solutions were found, while only two solutions were discovered on the fine mesh. This suggests a connection to spatial resolution. Thus, the question immediately arises as to how many multiple solutions, if any, will be obtained when all the relevant scales (i.e., dominant scales characterizing physics) of the turbulent flow are resolved. With a well resolved flow field (on a sufficiently fine mesh), it is distinctly possible that the number of multiple solutions is much greater than two solutions, which is a consequence of only small variations in the solutions. A final point is that Kamenetskiy et al. observed that the appearance of multiple solutions seems to be closely related to smooth body flow separation that occurs for flows over high-lift configurations. Here, we note that such occurrences of nonunique solutions may only be one member of the set of possible turbulent flows that have multiple solutions. This author has encountered both nonunique solutions as well as anomalous (nonphysical) results for the particular case of circulation control airfoil flows [82].

7.9 Concluding Remarks on Perspective

In this perspective on algorithmic requirements for solving the transport equations of a turbulence model, several necessary criteria have been discussed in order to develop reliable and efficient solution algorithms. The two-equation model of Wilcox (k-ω model) and the second-moment closure RST model (often called RSM) of Eisfeld [46] (see also Ref. [19]), as implemented by Mor-Yossef [44, 45], have been considered in the discussion. It is clear that to make significant progress we must understand the mathematical and numerical behavior of the transport equations, which begins with a complete delineation of the continuous and discrete problems and a proof of well-posedness. This provides a strong foundation from which to proceed.

The aspects of solution algorithms for the RANS and turbulence modeling equations that have been addressed are as follows: strong solution algorithms, stiffness of governing equations, positivity and realizability, boundary conditions, linear and nonlinear stability. Previously, we have discussed temporal and spatial discretization relevant to the RK/Implicit scheme for solving the RANS and k-ω equations. There are some possible discretization issues, such as a high-order approximation of the convective terms of the turbulence model and the application of a limiter, that have not been discussed. A principal difficulty in such a discretization is the design of an appropriate limiter to prevent oscillations when discontinuities occur. Another consideration that has not been discussed is parallel processing, which is important when solving the equations using large mesh densities (e.g., meshes with millions of grid points).

In discussing the various components of a solution algorithm, there has been considerable emphasis on convergence of the solution. This is because frequently in the literature solutions of the RANS equations are given without sufficient convergence of the residual function for the RANS equations and/or transport equations. In establishing reference solutions for a model, it should be considered necessary to ensure convergence to machine zero. Otherwise, the solution can continue to change, and possibly by a considerable amount. Thus, then and only then, the results become dis-

crete solutions, and can be considered appropriate for reference and comparison with other solutions using different turbulence models.

8 Concluding Remarks

In this report, the performance of the RK/Implicit scheme in solving the RANS equations and the transport equations of two-equation turbulence models has been investigated and evaluated. The governing equations have been solved in a weakly coupled manner, and fully converged solutions for both sets of equations have been obtained in all computations for a range of grid densities. Thus, in so doing, the turbulence models have been evaluated in the absence of numerical integration errors, which means the emphasis is on how well the turbulence models represent the physics of the flows considered. It should be emphasized that in the literature fully converged solutions are generally not obtained, especially when evaluating two-equation turbulence models.

As another principal objective, we have considered two transport-equation models that are currently being used to determine the effects of turbulence when solving the RANS equations. The 2006 Wilcox and the 2003 Menter SST models have been evaluated and compared by computing turbulent flows over the RAE 2822 and NACA 4412 airfoils. As part of the evaluation process, we have considered the effects due to variations in the models, such as using strain rate or vorticity in the turbulence production term of the turbulence models. In addition, we have discussed the production limiter, which is often applied in these models, the stress limiter in the Wilcox model, and the effects of changing the numerical dissipation scheme. It has been determined that the stress limiter of the Wilcox model has apparently eliminated any need to have a production limiter. We emphasize that any type of limiting can have adverse effects on convergence behavior when solving the governing equations.

The 2006 Wilcox and 2003 Menter SST turbulence models have been used to compute three cases (1, 9 and 10) for flow over the RAE 2822 airfoil. For both Case 1 (subcritical) and Case 9 (transonic and almost no flow separation), reasonable agreement with the experimental data has been obtained with strain rate in the production term. The flow conditions for Case 10 result in a sufficiently strong shock to cause extensive flow separation. With the Wilcox model, the shock has been predicted too far downstream of the data. The numerical solution with the Menter SST model, using either strain rate or vorticity, exhibits satisfactory agreement with the measured data. Similar results for Case 10 have been calculated with the Wilcox model when using vorticity in the production term. Clearly, some further study of the 2006 Wilcox model when using strain rate is required to flush out why the shock location is predicted too far downstream. In the calculations with the Wilcox model, we have observed that slow asymptotic convergence can occur on fine meshes (e.g., 1280×256 mesh cells) when the stress limiter of the model remains activated in the airfoil wake. It has been determined that simply deactivating the limiter in the wake can eliminate this difficulty.

Solutions have also been computed on a sequence of grids for high angle attack flow over the NACA 4412 airfoil. Comparisons of the solutions determined with all the turbulence models being considered have been presented. The computed velocity profiles with the 2006 Wilcox model have not shown good agreement with the measured data. These results are quite similar to those presented in the TMR website. Regardless of the choice, strain rate or vorticity, for the turbulence production term, the results are essentially the same. Thus, for this airfoil and flow conditions, there is not an adequate response to the adverse pressure gradients, which produce a significant trailing edge separation bubble. Additional investigation of the Wilcox model for such flows is required. With the 2003 Menter SST model, the computed velocity profiles on sufficiently fine grids have compared favorably with the measured data. The agreement with the data is quite good for the u velocity over the first three experimental locations beyond the airfoil midchord. It has been found that the solution calculated with the 2003 SST model agrees well with that presented on the NASA TMR website, and also with that of Menter [8], in which vorticity is used instead of strain rate. Even

though this particular airfoil flow has been frequently considered for evaluating turbulence models, it is important to recognize that there is considerable concern about the setup of the experiment, as pointed out by Rumsey on the NASA TMR website.

As the culminating element of this report, observations and perspectives on solving transport equations have been presented. In this element, aspects of solving stiff equations as well as various numerical difficulties and possible techniques for overcoming such issues have been considered. Due to numerous issues that arise when solving the RANS and turbulence modeling equations, significant emphasis in the discussion has been given to what can be called *numerical compatibility*. The basic idea behind numerical compatibility is to adjust the formulation of a turbulence model, without changing the integrity of the model, to make solvability possible and solution of the PDEs significantly easier. In the construction of turbulence models, there is usually little or no consideration given to numerical compatibility.

9 Acknowledgements

The author would like to express his thanks to Dr. Stefan Langer of DLR for extensive conversations related to this work. In addition, the author has benefitted from a number of discussions with Dr. Bernard Eisfeld of DLR, Dr. Rolf Radespiel of the Braunschweig Technical University, and Dr. Christopher Rumsey of NASA Langley.

References

1. D. C. Wilcox, **Turbulence Modeling for CFD** (Second Edition), DCW Industries, Inc., 1998 and 2000.

2. C. G. Speziale, Analytical methods for the development of Reynolds-stress closure in turbulence, *Annu. Rev. Fluid Mech.* 23 (1991) 107–157.

3. P. R. Spalart and S. R. Allmaras, A one-equation turbulence model for aerodynamic flows, *AIAA Paper* 92-0439, January 1992.

4. P. R. Spalart and S. R. Allmaras, A one-equation turbulence model for aerodynamic flows, *La Recherche Aerospatiale*, 1 (1994) 5–21.

5. S. R. Allmaras, F. T. Johnson and P. R. Spalart, Modifications and clarifications for the implementation of the Spalart-Allmaras turbulence model, Seventh International Conference on Computational Fluid Dynamics (ICCFD7), Big Island, Hawaii, July 2012.

6. D. C. Wilcox, **Turbulence Modeling for CFD** (Third Edition), DCW Industries, Inc., 2006.

7. D. C. Wilcox, Formulation of the k-ω turbulence model revisited, *AIAA Paper* 2007-1408, January 2007.

8. F. R. Menter, Improved two-equation k-ω turbulence models for Aerodynamic flows, NASA TM 103975, 1992.

9. F. R. Menter, Zonal two equation k-ω turbulence model for aerodynamic flows, *AIAA Paper* 93-2906, July 1993.

10. F. R. Menter, Two-equation eddy-viscosity turbulence models for engineering applications, *AIAA J.* 32(8) (1994) 1598–1605.

11. F. Menter and C. L. Rumsey, Assessment of two-equation turbulence models for transonic flows, *AIAA Paper* 94-2343, June 1994.

12. F. R. Menter, Ten years of industrial experience with the SST turbulence model, **Turbulence, Heat and Mass Transfer 4**, edited by K. Hanjalic, Y. Nagano, and M. Tummers, Begell House, Inc., 2003, 625–632.

13. F. R. Menter, Review of the shear-stress transport turbulence model experience from an industrial perspective, *Int. J. Comput. Fluid Dyn.* 23(4) (2009) 305–316.

14. A. Hellsten, New two-equation turbulence model for aerodynamic applications, Report A-21, Helsinki University of Technology (Laboratory of Aerodynamics), 1994.

15. Y. Mor-Yossef, Unconditionally positive implicit procedure for two-equation turbulence models: Application to k-ω turbulence models, *J. Comput. Phys.* 220 (2006) 88–108.

16. Y. Mor-Yossef, The unconditionally positive-convergent implicit time integration scheme for two-equation models: Revisited, *Comput. & Fluids* 38 (2009) 1984–1994.

17. M. Wasserman, Y. Mor-Yossef, I. Yavneh, and J. B. Greenberg. A robust implicit multigrid method for RANS equations with two-equation turbulence models, *J. Comput. Phys.* 229 (2010) 5820–5842.

18. M. W. Rubesin and W. C. Rose, The turbulent mean-flow, Reynolds-stress and heat-flux equations in mass-averaged dependent variables, NASA TM X-62,248, (1973), 1–29.

19. Turbulence Modeling Resource (TMR), NASA Langley Research Center website, C. L. Rumsey et al., 2013 (http://turbmodels.larc.nasa.gov).

20. P. G. Huang, Physics and computations of flows with adverse pressure gradients, *Modeling Complex Turbulent Flows*, M. Salas et al. editors, Kluwer, 1999, 245–258.

21. P. Bradshaw, D. H. Ferriss and N. P. Atwell, Calculation of boundary-layer development using the turbulent energy equation, J. Fluid Mech. 28(3) (1967) 593–616.

22. D. A. Johnson and L. S. King, A mathematically simple turbulence closure for attached and separated boundary layers, *AIAA J.* 23(11) (1985) 1684–1692.

23. S. L. Krist, R. T. Biedron, and C. L. Rumsey, CFL3D user's manual, NASA TM 1998-208444, June 1998.

24. J. O. Hinze, Gedächtniseffekte in der Turbulenz, ZAMM, 56 (1976) 403–415 (Translation: NASA TM-75516).

25. J. O. Hinze, **Turbulence**, Second Edition, McGraw-Hill, 1975.

26. R. C. Swanson and C.-C. Rossow, An efficient solver for the RANS equations and a one-equation turbulence model, *Comput. & Fluids* 42 (2011) 13–25.

27. P. L. Roe, Approximate Riemann solvers, parameter vectors and difference schemes, *J. Comput. Phys.*, 43, 357–372, 1981.

28. R. C. Swanson, R. Radespiel, and E. Turkel, On some numerical dissipation schemes, *J. Comput. Phys.* 147 (1998) 518–544.

29. C.-C. Rossow and R. C. Swanson, Efficient Flow Computation Including Turbulent Transport, Notes on Numerical Fluid Mechanics and Multidisciplinary Design, Vol. 112, New Results in Numerical and Experimental Fluid Mechanics VII: Contributions to the 16th STAB/DGLR Symposium, Aachen, Germany, 2008, Editors: A. Dillmann, G. Heller, M. Klaas, H.-P. Kreplin, W. Nitsche, W. Schroder, Springer-Verlag, (2010) 91–99.

30. J. L. Thomas and M. D. Salas, Far-field boundary conditions for transonic lifting solutions to the Euler equations, *AIAA J.* 24(7) (1986) 1074–1080.

31. A. Jameson, The evolution of computational methods in aerodynamics, *J. Appl. Mech.*, 50 (4b), 1052–1070, 1983.

32. R. C. Swanson and E. Turkel, On central difference and upwind schemes, *J. Comput. Phys.*, 101 (1992) 292–306.

33. R. C. Swanson, E. Turkel, and C.-C. Rossow, Convergence acceleration of Runge-Kutta Schemes for solving the Navier-Stokes equations, *J. Comput. Phys.* 224 (2007) 365–388.

34. C.-C. Rossow, Convergence acceleration for solving the compressible Navier-Stokes equations, *AIAA J.*, 44 (2006) 345–352.

35. J. C. Butcher, **Numerical Methods for Ordinary Differential Equations**, Wiley, 2003.

36. R. Alexander, Diagonally implicit Runge-Kutta method for stiff O.D.E.'s, *SIAM J. Numer. Anal.*, 14(6) (1977) 1006–1021.

37. S. Langer, Agglomeration multigrid methods with implicit Runge-Kutta smoothers applied to aerodynamic simulations on unstructured grids, *J. Comput. Phys.*, 277 (2014) 72–100.

38. D. J. Mavriplis, Multigrid strategies for viscous flow solvers on anisotropic unstructured meshes, *J. Comput. Phys.*, 145 (1998) 141–165.

39. C.-C. Rossow, Efficient computation of compressible and incompressible flows. *J. Comput. Phys.* 220 (2007) 879–899.

40. B. van Leer, C. H. Tai, K. G. Powell, Design of optimally smoothing multi-stage schemes for the Euler equations, *AIAA Paper* 89-1933, June 1989.

41. P. H. Cook, M. A. McDonald, and M. C. P. Firmin, Aerofoil RAE 2822 pressure distributions and boundary layer and wake measurements, AGARD-AR-138, 1979.

42. R. C. Swanson and C.-C. Rossow, An initial investigation of the effects of turbulence models on the convergence of the RK/Implicit scheme, NASA/TM-2008-215342, (2008) 1–42.

43. P. A. Durbin, On the k–3 stagnation point anomaly, *Int. J. Heat and Fluid Flow* 17 (1996) 89–90.

44. Y. Mor-Yossef, Unconditionally stable time marching scheme for Reynolds stress models, *J. Comput. Phys.* 276 (2014) 635–664.

45. Y. Mor-Yossef, Turbulent flow simulations on unstructured grids using a Reynolds stress model, *AIAA Paper* 2015-2761, June 2015.

46. B. Eisfeld, Implementation of Reynolds stress models into the DLR-FLOWer code, Deutsches Zentrum für Luft-und Raumfahrt e.V, DLR Report IB 124-200431, 2004.

47. D. Coles and A. J. Wadcock, Flying-hot-wire study of flow past an NACA 4412 airfoil, *AIAA J.* 17(4) (1979) 321–329.

48. D. Coles, Structure of the turbulent separated flow around a stalled airfoil, NASA-CR-152263, February 1979.

49. C. L. Fefferman, Existence and Smoothness of the Navier-Stokes Equations, https://www.claymath.org.

50. M. Shearer and R. Levy, Partial Differential Equations: An Introduction to Theory and Applications, Princeton University Press, 2015.

51. J. Hadamard, Lectures on Cauchy's Problem in Linear Partial Differential Equations, Dover publications, New York, 1952.

52. B. Gustafsson and A. Sundström, Incomplete pearabolic problems in fluid dynamics, *SIAM J. Appl. Math*, 35(2) (1978) 343–357.

53. J. Oliger and A. Sundström, Theoretical and practical aspects of some initial-boundary value problems in fluid dynamics, *SIAM J. Appl. Math*, 35(3) (1978) 419–446.

54. J. Nordström, Energy absorbing boundary conditions for the Navier-Stokes equation, Tenth International Conference on Numerical Methods in Fluid Dynamics, Vol. 264 (1986) 505–510.

55. J. Nordström, A roadmap to well posed and stable problems in computational physics, *J. Sci. Comput.*, 2016.

56. J. Nordström and Svärd, Well posed boundary conditions for the Navier-Stokes equation, *SIAM J. Numer. Anal.*, 43 (2005) 1231–1255.

57. H.-O. Kreiss and J. Lorenz, Initial-Boundary Value Problems and the Navier-Stokes Equations, Vol. 136, Academic Press, 1989.

58. J. C. Strikwerda, Finite Difference Schemes and Partial Equations, Second Edition, SIAM, 2004.

59. L. Evans, Partial Differential Equations, Second Edition, American Mathematical Society, 2010.

60. R. D. Richtmyer and K. W. Morton, **Difference Methods for Initial-Value Problems**, Second Edition, Interscience Publishers, John Wiley & Sons, 1967.

61. R. Temam, Navier-Stokes Equations: Theory and Numerical Analysis, AMS Chelsea Publishing, 2001.

62. B. Gustafsson, High Order Difference Methods for Time Dependent PDE, Springer Series in Computational Mathematics, Vol. 38, Springer-Verlag, Berlin, 2008.

63. S. Langer and R. C. Swanson, On boundary-value problems for RANS equations and two-equations turbulence models, *J. Sci. Comput.*, 85(20) (2020) 1–33.

64. S. Lee and D. W. Choi, On coupling the Reynolds-averaged Navier-Stokes equations with two-equation turbulence model equations, *Int. J. Numer. Meth. Fluids*, 50(2) (2006) 165–197.

65. F. Ilinca and D. Pelletier, Positivity preservation and adaptive solution of two-equation models of turbulence, *Int. J. Thermal Sciences* 38 (1999) 560–571.

66. F. Bassi and S. Rebay, A High Order Discontinuous Galerkin Method for Compressible Turbulent Flows. In: Cockburn B., Karniadakis G.E., Shu CW. (eds) **Discontinuous Galerkin Methods. Lecture Notes in Computational Science and Engineering** Vol. 11 (2000), Springer, Berlin, Heidelberg, 77–88.

67. F. Bassi, A. Crivellini, S. Rebay, and M. Savini, Discontinuous Galerkin solution of the Reynolds-averaged Navier-Stokes and k-ω turbulence model equations, *Computers & Fluids* 34 (2005) 507–540.

68. V. Togiti and B. Eisfeld, Assessment of g-equation for a second-moment Reynolds stress turbulence model, *AIAA Paper* 2015-2925, June 2015.

69. J. Hadamard, Sur les problèmes aux dérivées partielles et leur signification physique, Princeton Universiy Bulletin, Vol. 13, (1902) 49–52.

70. S. Langer, Computer aided analysis of preconditioned multistage Runge-Kutta methods applied to solve the compressible Reynolds averaged Navier-Stokes equations, In H. P. Kreplin, editor, **New Results in Numerical and Experimental Fluid Mechanics X: Contributions to the 19th STAB/DGLR Symposium Munich**, Germany, 2014, Notes on Numerical Fluid Mechanics and Multidisciplinary Design, 2015.

71. R. C. Swanson, E. Turkel, and S. Yaniv. Analysis of a RK/Implicit smoother for multigrid. In A. Kuzmin, editor, Computational Fluid Dynamics 2010: Proceedings of the Sixth International Conference on Computational Fluid Dynamics, ICCFD6, St. Petersburg, Russia, The International Conference on Computational Fluid Dynamics, pages 409–417. Springer-Verlag Berlin Heidelberg, 2011.

72. E. Tadmor, The numerical viscosity of entropy stable schemes for systems of conservation laws. I. *Math. Comput.* 49 (1987) 91–103.

73. E. Tadmor, Entropy stability theory for difference approximations of nonlinear conservation laws and related time-dependent problems, *Acta Numerica* (2003) 451–512.

74. F. Ismail and P. L. Roe, Affordable entropy-consistent Euler flux functions II: Entropy production at shocks, *J. Comput. Phys.* 228 (2009) 5410–5436.

75. U. S. Fjordholm, S. Mishra, and E. Tadmor, Arbitrarily high-order accurate entropy stable essentially nonoscillatory schemes for systems of conservation laws, *SIAM J. Numer. Anal.* 50 (2012), 544–573.

76. M. H. Carpenter and T. C. Fisher, High-order entropy stable formulations for Computational Fluid Dynamics, *AIAA Paper* 2013-2868, 21st AIAA Computational Fluid Dynamics Conference, 2013.

77. T. C. Fisher and M. H. Carpenter, High-order entropy stable finite difference schemes for nonlinear conservation laws, *J. Comput. Phys.* 252 (2013) 518–557.

78. A. Jameson, J. C. Vassberg, and K. Ou, Further studies of airfoils supporting non-unique solutions in transonic flow, *AIAA J.* 50(12) (2012) 2865–2881.

79. A. Jameson, Airfoil admitting non-unique solutions to the Euler equations, *AIAA Paper* 1991-1625, June 1991.

80. D. K. Kamenetskiy, J. Bussoletti, C. Hilmes, V. Venkatakrishnan, and L. Wigton, Numerical evidence of multiple solutions for the Reynolds-averaged Navier-Stokes equations, *AIAA J.* 52(8) (2014) 1686–1698.

81. C. L. Rumsey, J. P. Long, M. Stuever, and T. R. Wayman, Summary of the First AIAA CFD High-Lift Prediction Workshop, *AIAA J. Aircraft* 48(6) (2011) 2068–2079.

82. R. C. Swanson, C. L. Rumsey, and S. G. Anders, Aspects of numerical simulation of circulation control airfoils, Proceedings of Circulation Control Workshop, NASA CP 2005-213509, Hampton, Virginia, March 2004. Also, Chapter 18, **Applications of Circulation Control Technology**, edited by R. D. Joslin and G. S. Jones, Progress in Astronautics and Aeronautics, Vol. 214, 2006.

83. O. Reynolds, On the dynamical theory of incompressible viscous fluids and the determination of the criterion, *Phil Trans. R. Lond. Soc. A* 186 (1895) 123–164.

84. J. D. Jackson, Osborne Reynolds: scientist, engineer and pioneer *Proc. R. Soc. Lond. A* 451 (1995) 49–86.

85. J. D. Jackson and B. E. Launder, Osborne Reynolds and the publication of his papers on turbulent flow, *Ann. Rev. Fluid Mech.* 39 (2007) 19–35.

86. B. E. Launder, First steps in modelling turbulence and its origins: a commentary on Reynolds (1895) 'On the dynamical theory of incompressible viscous fluids and the determination of the criterion', *Phil. Trans. R. Soc. A* 373 (2015) 1–12.

87. A. Favre, Èquations des Gaz Turbulents Compressibles, *J. de Mecanique* 4(3) (1965) 361–390.

88. J. Boussinesq, Théorie de l'écoulement tourbillant, *Mém. prés. Acad. Sci.* XXIII, 46 (1877).

89. O. Darrigol, Joseph Boussinesq's legacy in fluid mechanics (A century of fluid mechanics: 1870–1970) *C. R. Mecanique* 345 (2017) 427–445.

90. G. I. Taylor, Eddy motion in the atmosphere, *Philos. Trans. Royal Society London Ser.* 215(1) (1915), 523–537.

91. L. Prandtl, Bericht über Untersuchungen zur ausgebildeten Turbulenz, *ZAMM* 5(2) (1925), 136–139.

92. T. Cebeci and A. M. .O. Smith, A finite-difference method for calculating compressible laminar and turbulent boundary layers, *J. Basic Eng.* 92(3) (1970) 523–535.

93. T. Cebeci and A. M. .O. Smith, **Analysis of Turbulent Boundary Layers**, Applied Mathematics and Mechanics, An International Series of Monographs, Academic Press, 1974.

94. B. S. Baldwin and H. Lomax, Thin layer approximation and algebraic model for separated flows, *AIAA Paper* 78-257, 1978.

95. L. Prandtl, Über ein neus formelsystem für ausgebildete turbulenz, *Nacr. Akad. Wiss. Góttingen, Math-Phys. Kl.* 6–19.

96. L. G. Norris and W. C. Reynolds, Turbulent channel flow with moving wavy boundary, Report No. FM-10, Stanford University, Department of Mechanical Engineering, USA (1975).

97. M. M. Rahman, J. Taghinia, A. K. M. Sadrul Islam, M. J. Lampinen and T. Siikonen, Modified Norris-Reynolds one-equation model, 6th BSME International Conference on Thermal Engineering (ICTE 2014) *Procedia Eng.* 105 (2015) 276–286.

98. M. M. Rahman, R. K. Agarwal and T. Siikonen, A modified one-equation turbulence model based on k-equation, *AIAA Paper* 2016-1598, Jan. 2016.

99. B. S. Baldwin and T. J. Barth, A one-equation turbulence transport model for high Reynolds number wall-bounded flows, *AIAA Paper* 91-0610, 1991 (See also NASA TM 102847, 1990).

100. T. J. Wray and R. K. Agarwal, Low-Reynolds-number one-equation turbulence model based on k-ω closure. *AIAA J.* 53(8) (2015) 2216–2227.

101. X. Han, M. M. Rahman and R. K. Agarwal, Development and application of a wall distance free turbulence model, r *AIAA Paper* 2018-0593, Jan. 2018.

102. A. N. Kolmogorov, Equations of turbulent motion in incompressible viscous fluids for very large Reynolds numbers. Izvestia Academy of Sciences, USSR, 6:56–58, 1942.

103. D. B. Spalding, Kolmogorov's two equation model of turbulence, *Proc. R. Soc. Lond. A* 434 (1991) 211–216.

104. P. G. Saffman, A model for inhomogeneous turbulent flow, *Proc. R. Soc. Lond. A* 317 (1970) 417–433.

105. M. Wolfshtein, The velocity and temperature variation distribution in one-dimensional flow with turbulence augmentation and pressure gradient, *Int. J. Heat and Mass Transfer*, 12 (1969) 301–318.

106. C. G. Speziale, R. Abid and E. C. Anderson, Critical evaluation of two-equation models for near wall turbulence, *AIAA J.* 30 (1992) 324–331.

107. P. S. Bernard and B. S. Berger, A method for computing three-dimensional turbulent flows, *J. Appl. Math.* 43(3) (1982) 453–470.

108. P. S. Bernard, Turbulent vorticity transport in three dimensions, *Theor. Comp. Fluid Dyn.*, 2(1) (1990) 165–183.

109. J. J. Gorski, Application of vorticity transport to the analysis of physically accurate turbulence models, Ph.D. Dissertation, University of Maryland, College Park, MD 1993.

110. D. F. Robinson, J. E. Harris and H. A. Hassan, Unified turbulence closure model for axisymmetric and planar free-shear flows, *AIAA J.* 33(12) (1995) 2325–2331.

111. P. Y. Chou, On the velocity correlations and the solution of turbulent fluctuation, *Quart. Appl. Math*, 3(1) 38–54.

112. B. I. Davydov, On the statistical dynamics of an incompressible fluid, *Dokl. Akad. Nauk SSSR* 136(1) (1961) 47–50.

113. F. H. Harlow and P. I. Nakayama, Transport of turbulence energy decay rate, Los Alamos Scientific Lab., University of California Report LA-3854, 1968.

114. W. P. Jones and B. E. Launder, The prediction of laminarization with a two-equation model of turbulence, *Int. J. Heat and Mass Transfer* 15(2) (1972) 301–314.

115. W. P. Jones and B. E. Launder, The calculation of low-Reynolds-number-phenomena with a two-equation model of turbulence, *Int. J. Heat and Mass Transfer* 16 (1973) 1119–1130.

116. B. E. Launder and D. B. Spalding, The numerical computation of turbulent flows, *Comput. Methods in Appl. Mech. Eng.* 3 (1974) 269–289.

117. D. C. Wilcox and R. M. Traci, A complete model of turbulence, *AIAA Paper* 76-0351, 1976.

118. D. C. Wilcox and M. W. Rubesin, Progress in turbulence modeling, NASA TP 1517, 1980.

119. D. C. Wilcox, A complete model of turbulence revisited, *AIAA Paper* 84-0176, 1984.

120. D. C. Wilcox, Reassessment of the scale-determining equation for advanced turbulence models, *AIAA J.* 26(11) (1988) 1299–1310.

121. D. C. Wilcox, Comparison of two-equation turbulence models for boundary layers with pressure gradient, *AIAA J.*/ 31(8) (1993) 1414–1421.

122. T. B. Gatski and C. L. Rumsey, Linear and nonlinear eddy viscosity models, **Closure Strategies for Turbulent and Transitional Flows**, Chapter 1 from Part A - Physical and Numerical Techniques, (2002) 9–46.

123. J. C. Rotta, Statistische theorie nichthomogener Turbulenz, *Z. Phys.* 129 (1951) 547–572.

124. B. J. Daly and H. A. Harlow, Transport equations in turbulence, *Phys. Fluids* 13 2634–2649.

125. C. DuP. Donaldson, Calculation of turbulent shear flows, *AIAA J.* 10 (1972) 4–12.

126. B. E. Launder, G. J. Reece, and W. Rodi, Progress in the development of Reynolds-stress closure, *J. Fluid Mech.* 68(3) (1975) 537–566.

127. U. Schumann, Realizability of Reynolds-stress turbulence models, *Phys. Fluids* 20 (1977) 721–725.

128. J. L. Lumley, Computational modeling of turbulent flows, *Adv. Appl. Mech.* 18 (1978) 123–176.

129. B. Eisfeld and O. Brodersen, Advanced turbulence modelling and stress analysis for the DLR-F6 configuration, *AIAA Paper* 2005-4727, July 2005.

130. J. C. Chassaing, G. A. Gerolymos, and I. Vallet, Efficient and robust Reynolds-stress model computation of three-dimensional compressible flows, *AIAA J.* 41(5) (2003) 763–773.

131. P. Sagaut, **Large eddy simulation for incompressible flows**, An Introduction, Third edition, Springer, 2004.

Numerical Results: RAE 2822 Airfoil

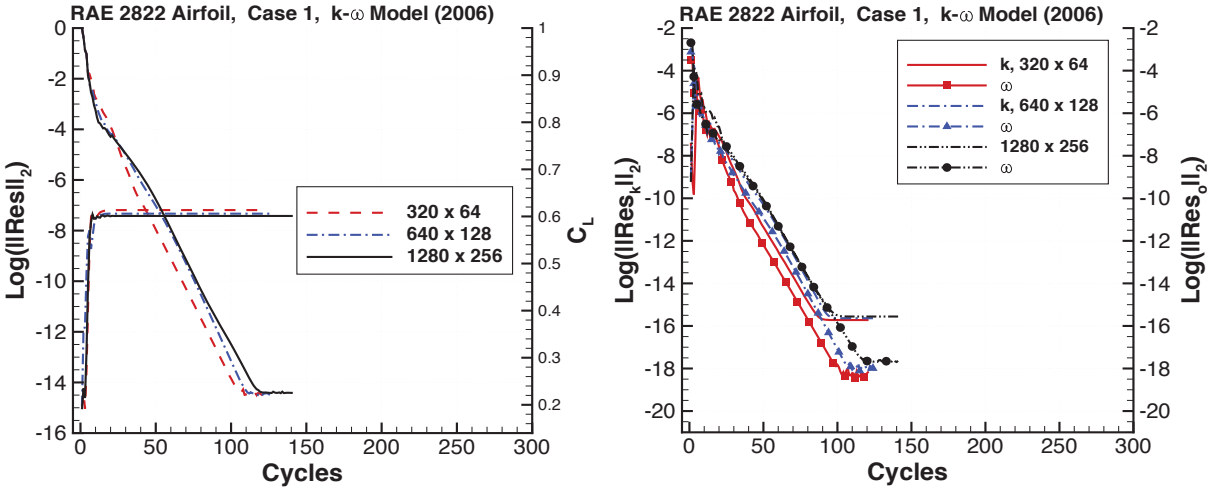

(a) (b)

Figure 1: Convergence histories for Case 1 on three grids using the 2006 Wilcox model with strain rate in production term. (a) mean flow equations, (b) k-ω equations.

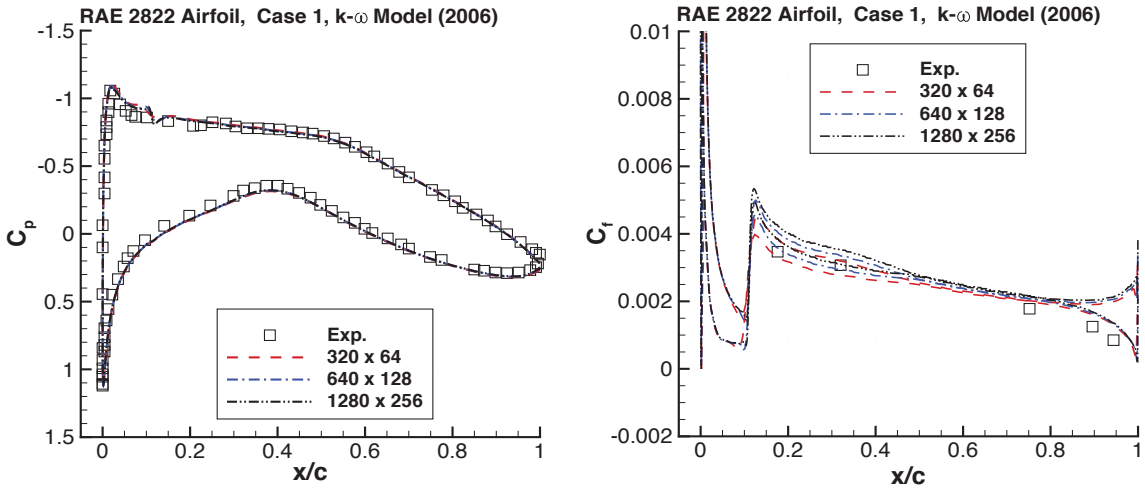

(a) (b)

Figure 2: Surface pressure and skin-friction distributions for Case 1 on three grids using the 2006 Wilcox model with strain rate in production term. (a) pressure, (b) skin-friction.

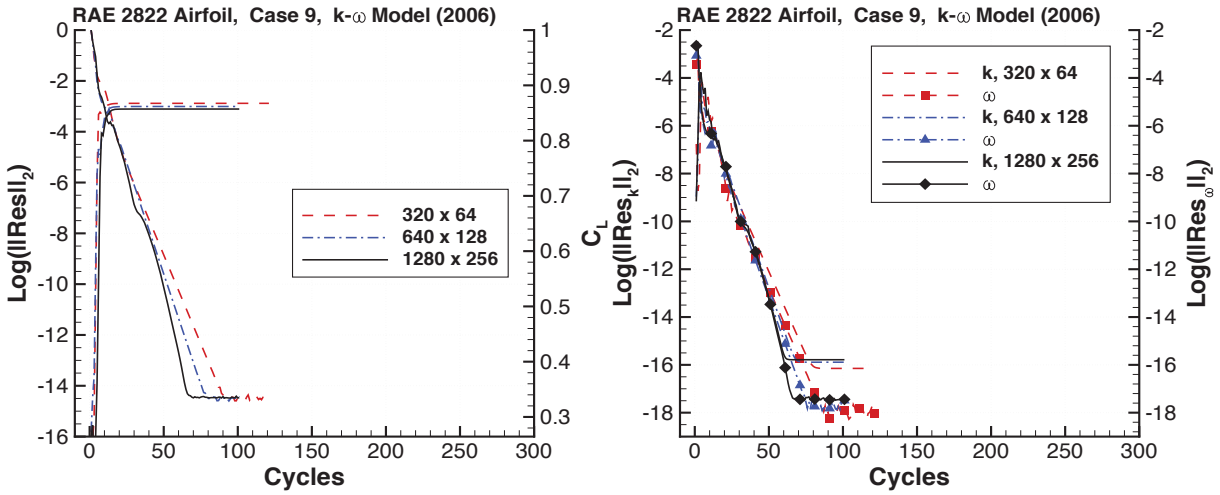

(a) (b)

Figure 3: Convergence histories for Case 9 on three grids using the 2006 Wilcox model with strain rate in production term. (a) mean flow equations, (b) k-ω equations.

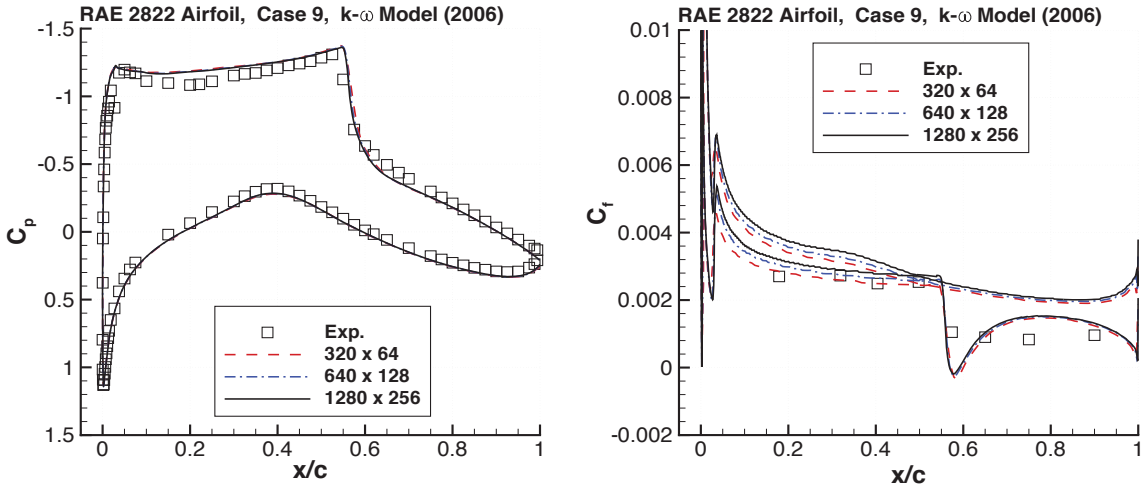

(a) (b)

Figure 4: Surface pressure and skin-friction distributions for Case 9 on three grids using the 2006 Wilcox model with strain rate in production term. (a) pressure, (b) skin-friction.

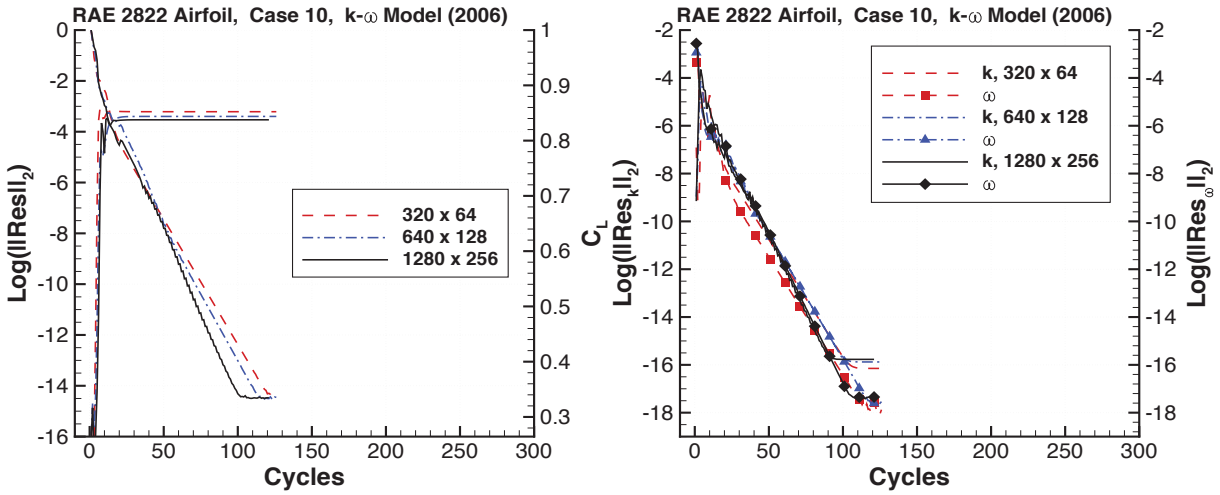

(a) (b)

Figure 5: Convergence histories for Case 10 on three grids using the 2006 Wilcox model with strain rate in production term. (a) mean flow equations, (b) k-ω equations.

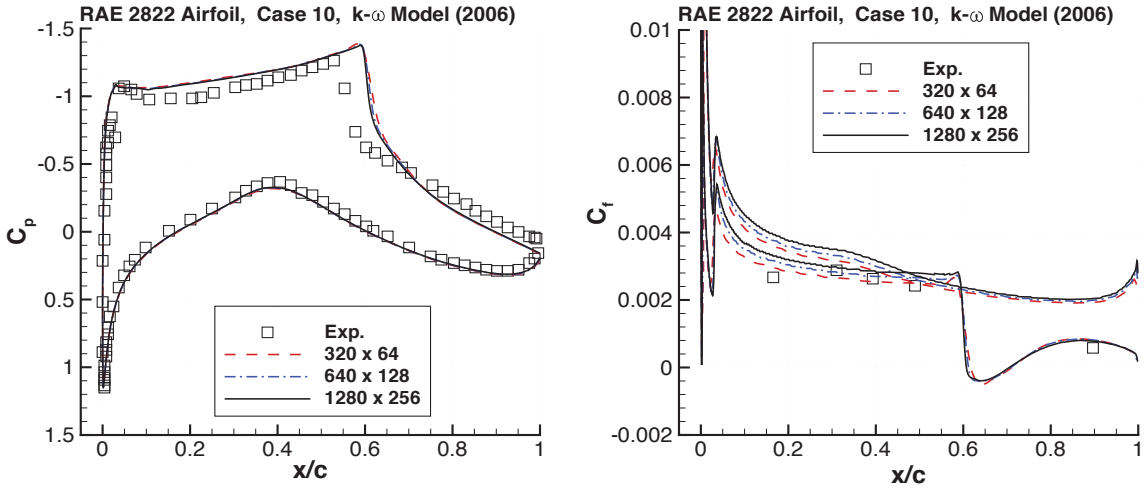

(a) (b)

Figure 6: Surface pressure and skin-friction distributions for Case 10 on three grids using the 2006 Wilcox model with strain rate in production term. (a) pressure, (b) skin-friction.

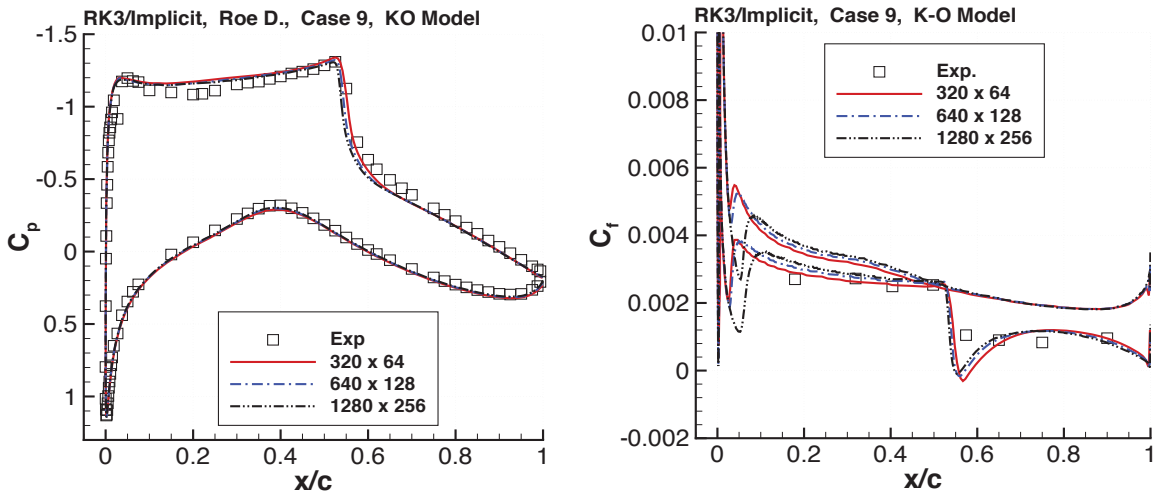

(a) (b)

Figure 7: Surface pressure and skin-friction distributions for Case 9 on three grids using the 2006 Wilcox model with vorticity in production term. (a) pressure, (b) skin-friction.

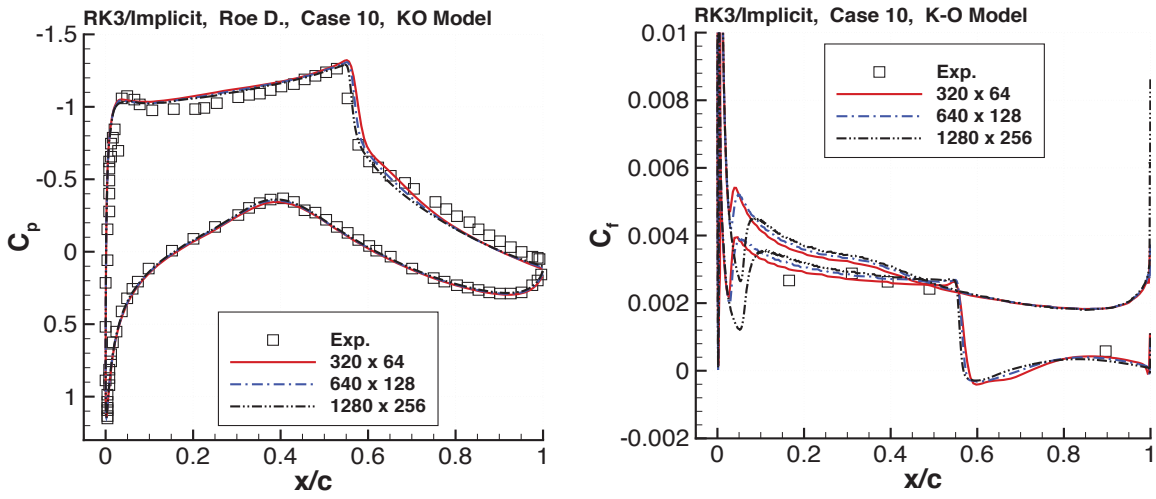

(a) (b)

Figure 8: Surface pressure and skin-friction distributions for Case 10 on three grids using the 2006 Wilcox model with vorticity in production term. (a) pressure, (b) skin-friction.

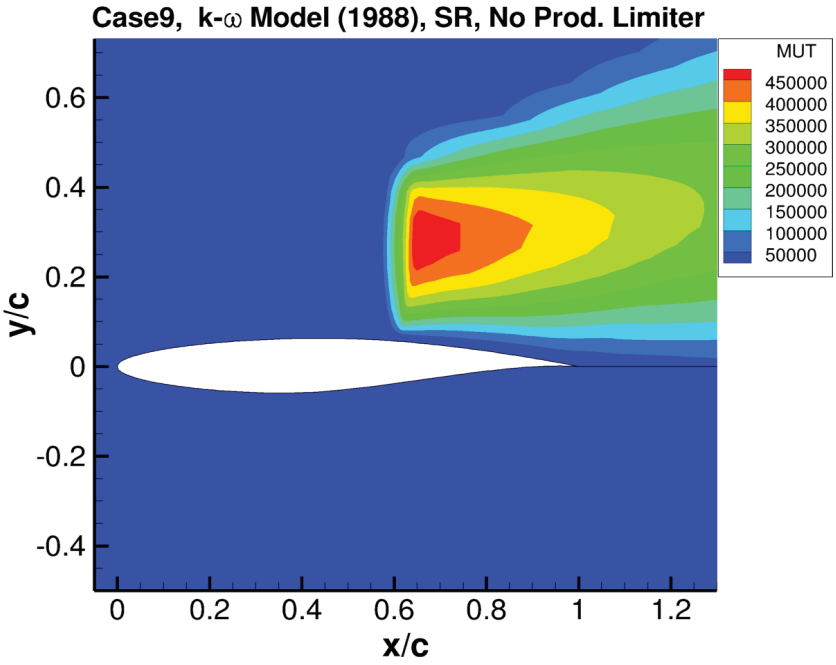

(a)

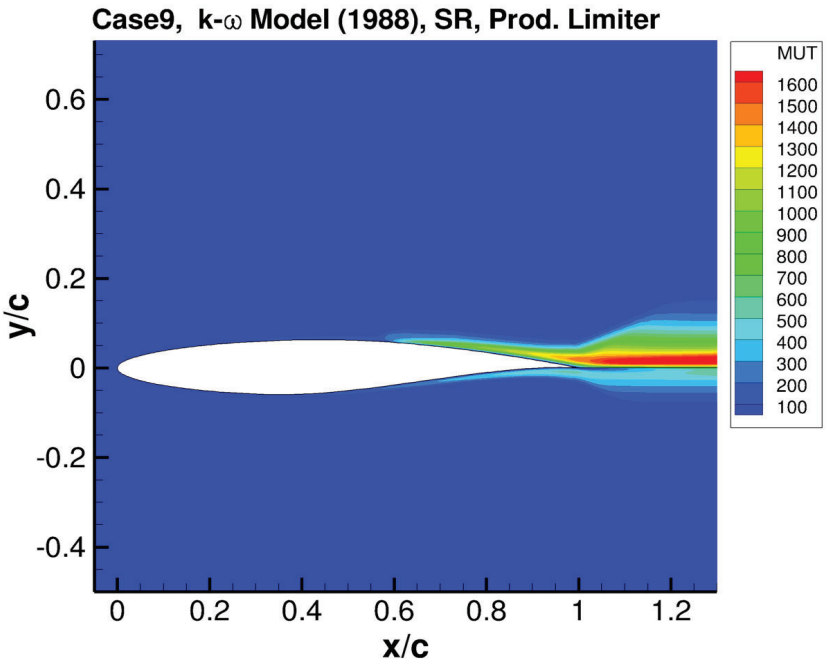

(b)

Figure 9: A comparison of eddy viscosity contours for Case 9 when using the 1988 Wilcox model with strain rate in the production term; without and with the Menter turbulence production limiter. The 320×64 grid used in the computations. (a) Without production limiter, (b) With production limiter.

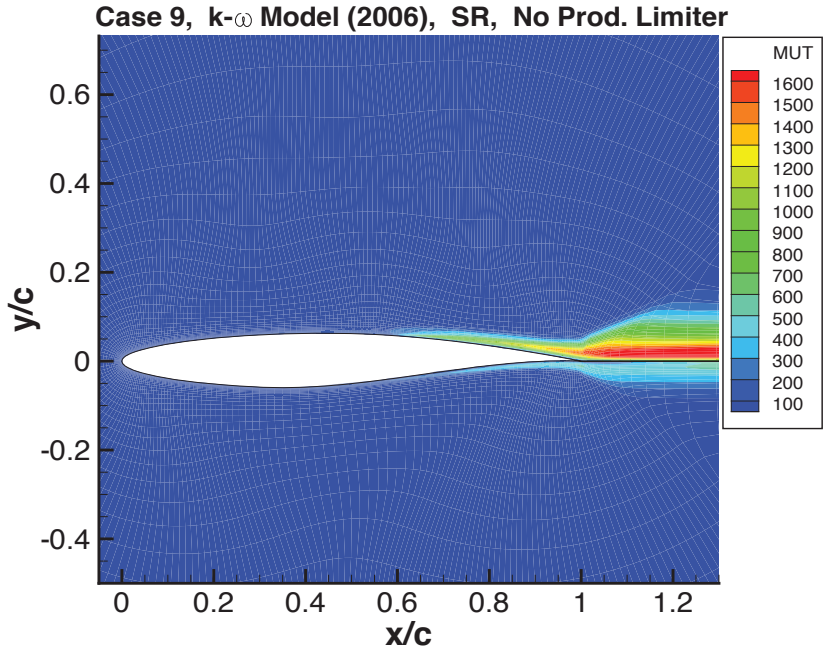

Figure 10: Eddy viscosity contours for Case 9 when using the 2006 Wilcox model with strain rate in production term. No turbulence production limiter is employed. The 320×64 grid was used in the computation.

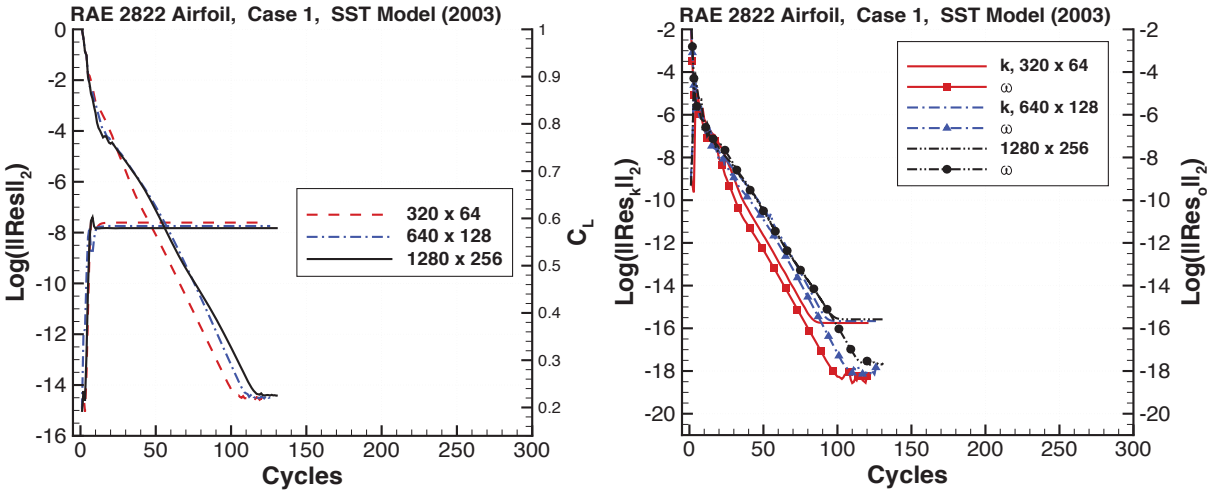

(a) (b)

Figure 11: Convergence histories for Case 1 on three grids using the 2003 Menter SST model with strain rate in production term. (a) mean flow equations, (b) k-ω equations.

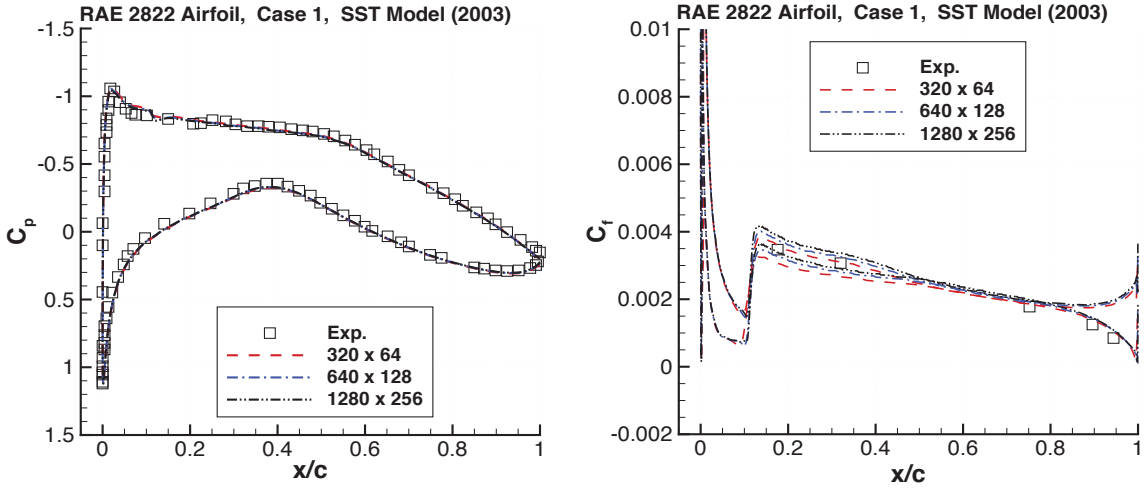

(a) (b)

Figure 12: Surface pressure and skin-friction distributions for Case 1 on three grids using the 2003 Menter SST model with strain rate in production term. (a) pressure, (b) skin-friction.

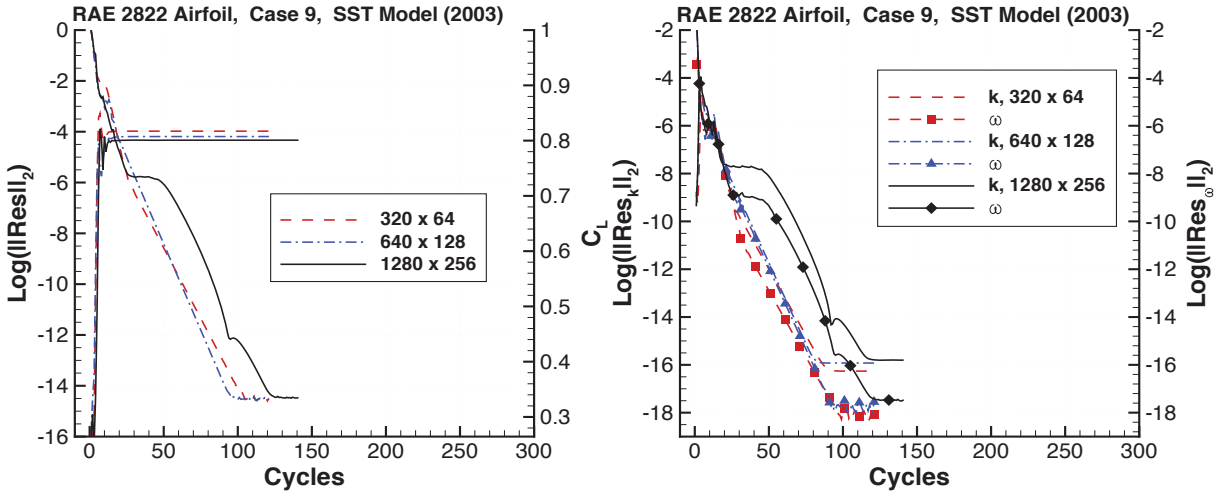

(a) (b)

Figure 13: Convergence histories for Case 9 on three grids using the 2003 Menter SST model with strain rate in production term. (a) mean flow equations, (b) k-ω equations.

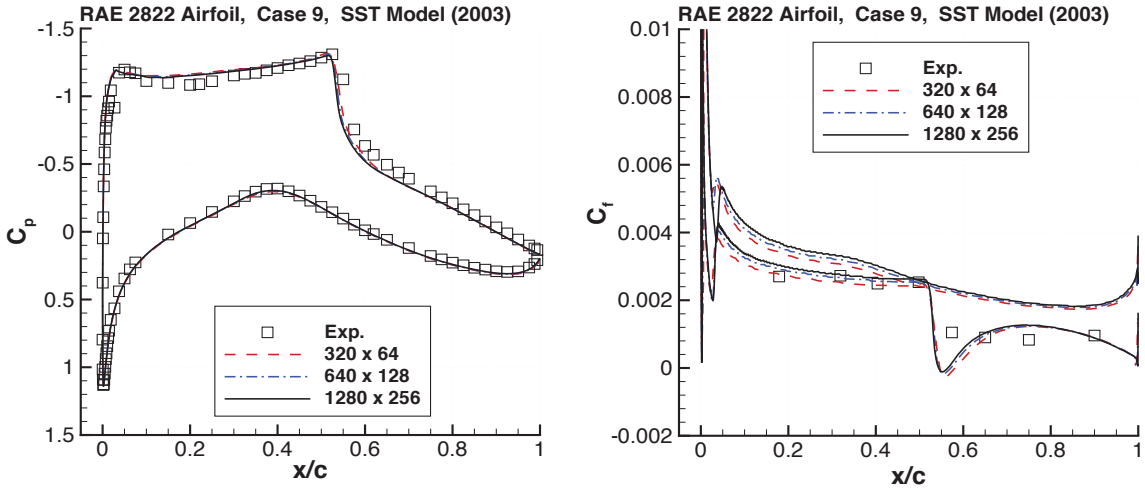

(a) (b)

Figure 14: Surface pressure and skin-friction distributions for Case 9 on three grids using the 2003 Menter SST model with strain rate in production term. (a) pressure, (b) skin-friction.

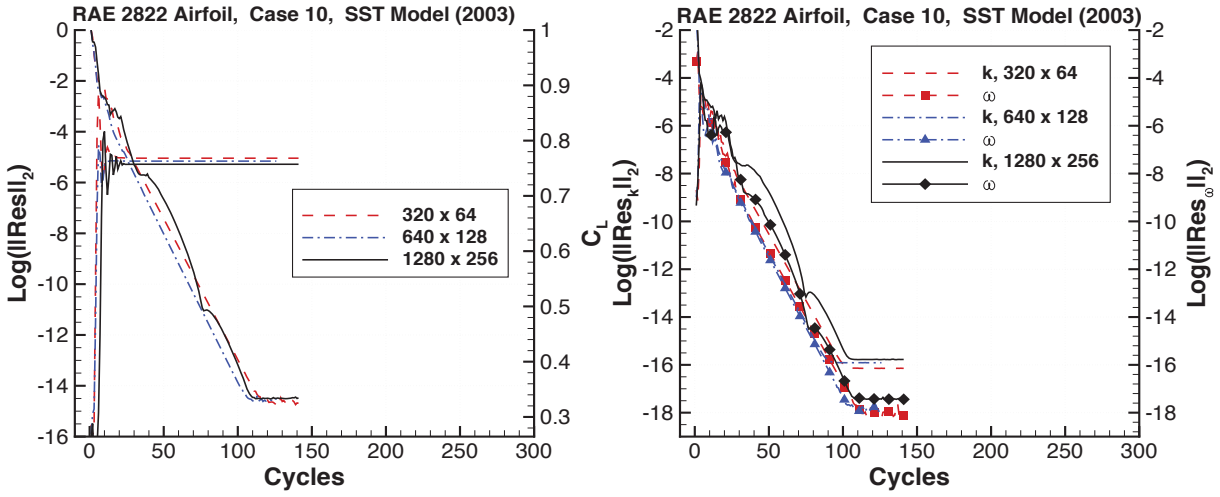

(a) (b)

Figure 15: Convergence histories for Case 10 on three grids using the 2003 Menter SST model with strain rate in production term. (a) mean flow equations, (b) k-ω equations.

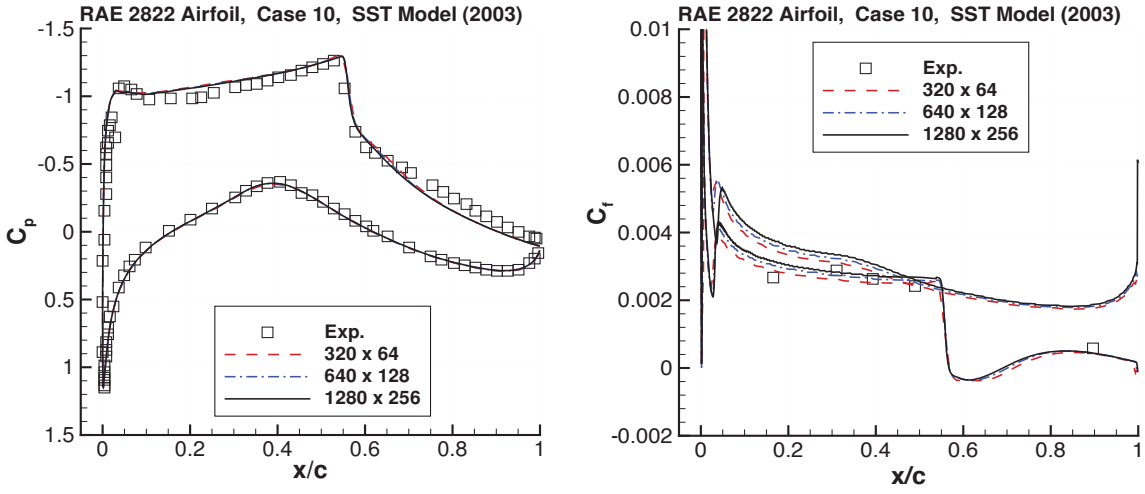

(a) (b)

Figure 16: Surface pressure and skin-friction distributions for Case 10 on three grids using the 2003 Menter SST model with strain rate in production term. (a) pressure, (b) skin-friction.

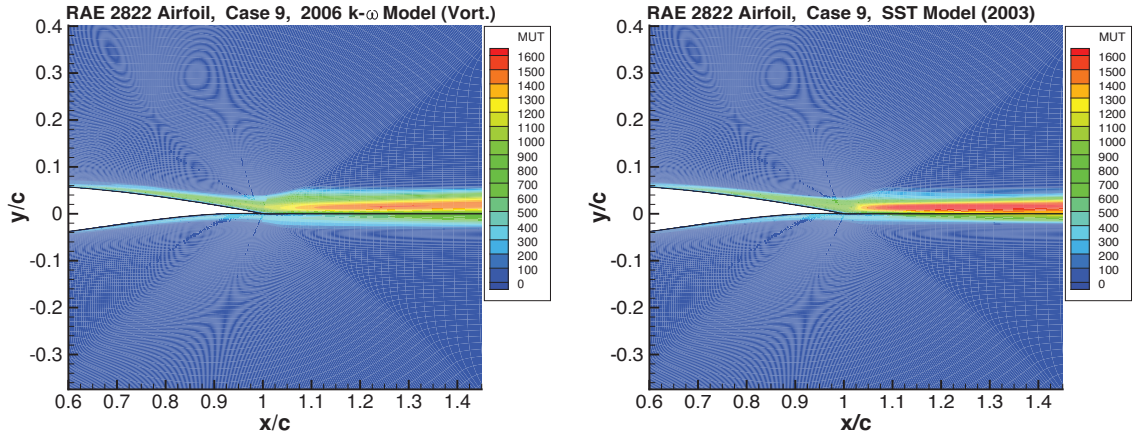

(a) (b)

Figure 17: Contours of the eddy viscosity for computations with the 2006 Wilcox model and 2003 Menter SST model. Results are for the RAE 2822 airfoil (Case 9) using the 1280×256 grid. In production term: (a) Wilcox model (vorticity), (b) Menter model (strain rate).

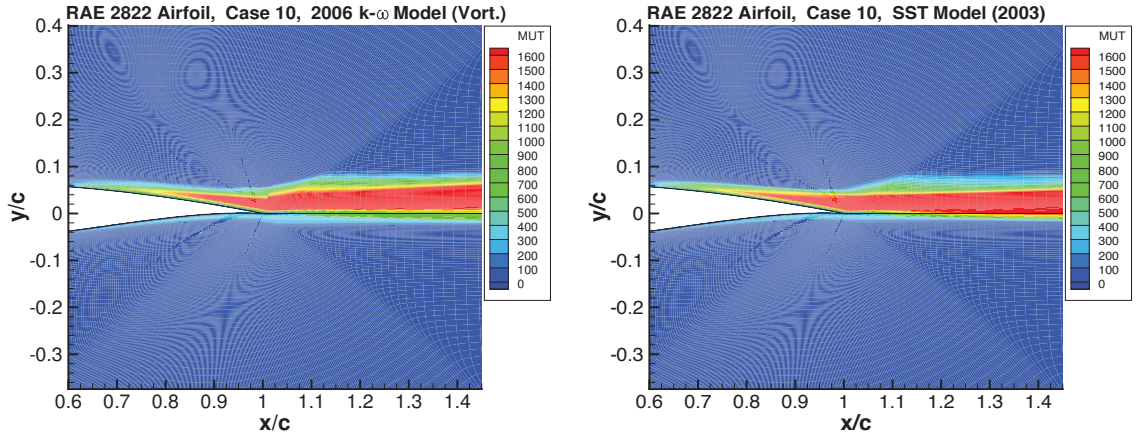

(a) (b)

Figure 18: Contours of the eddy viscosity for computations with the 2006 Wilcox model and 2003 Menter SST model. Results are for the RAE 2822 airfoil (Case 10) using the 1280×256 grid. In production term: (a) Wilcox model (vorticity), (b) Menter model (strain rate).

Numerical Results: NACA 4412 Airfoil

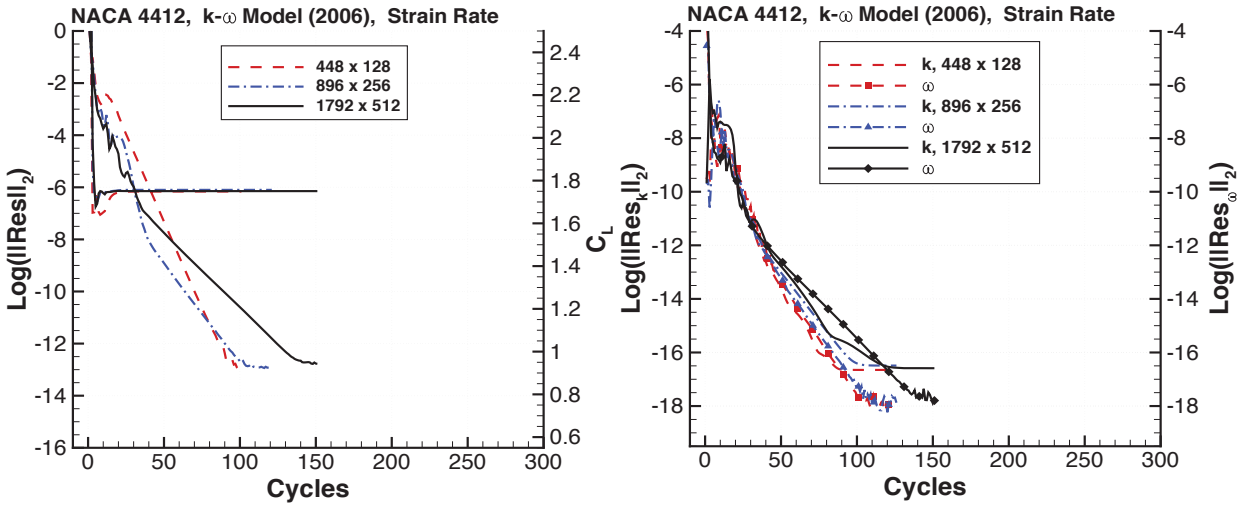

(a) (b)

Figure 19: Convergence histories for NACA 4412 airfoil on three grids using the 2006 Wilcox model with strain rate in production term. (a) mean flow equations, (b) k-ω equations.

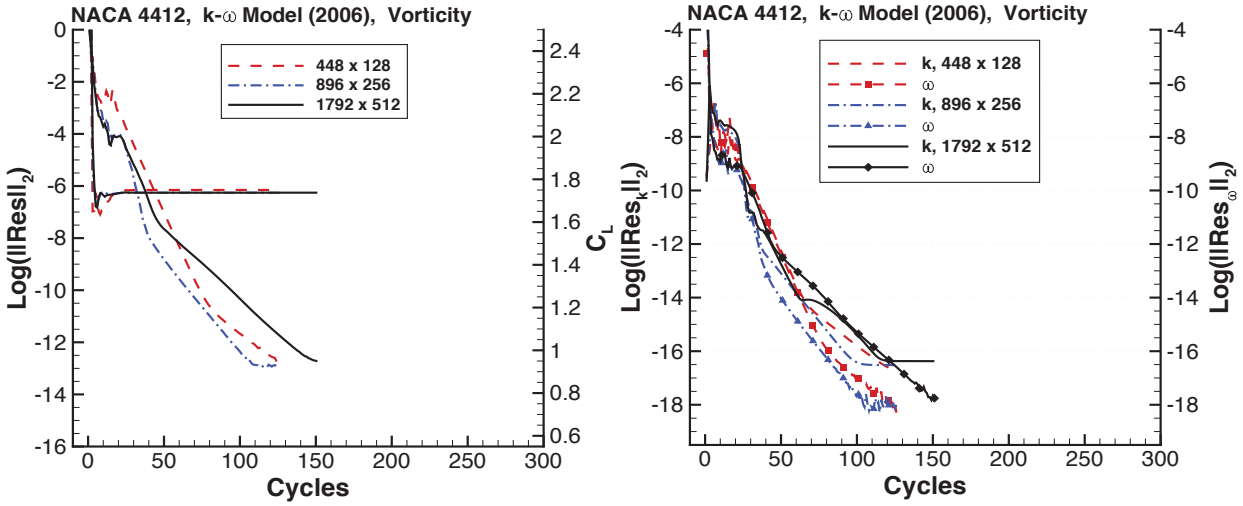

(a) (b)

Figure 20: Convergence histories for NACA 4412 airfoil on three grids using the 2006 Wilcox model with vorticity in production term. (a) mean flow equations, (b) k-ω equations.

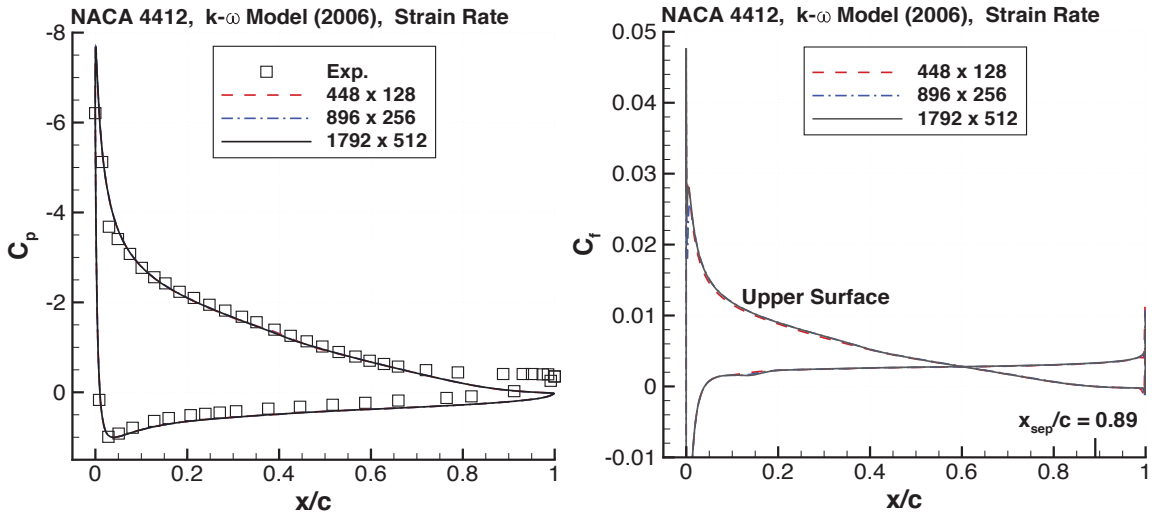

(a) (b)

Figure 21: Surface pressure and skin-friction distributions for NACA 4412 airfoil on three grids using 2006 Wilcox model with strain rate in production term. (a) pressure, (b) skin-friction.

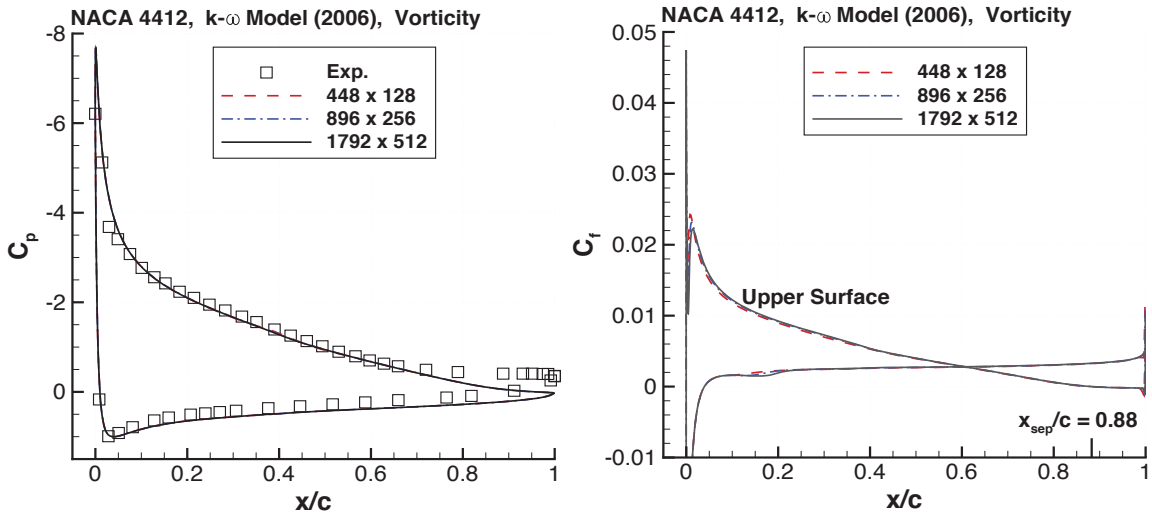

(a) (b)

Figure 22: Surface pressure and skin-friction distributions for NACA 4412 airfoil on three grids using 2006 Wilcox model with vorticity in production term. (a) pressure, (b) skin-friction.

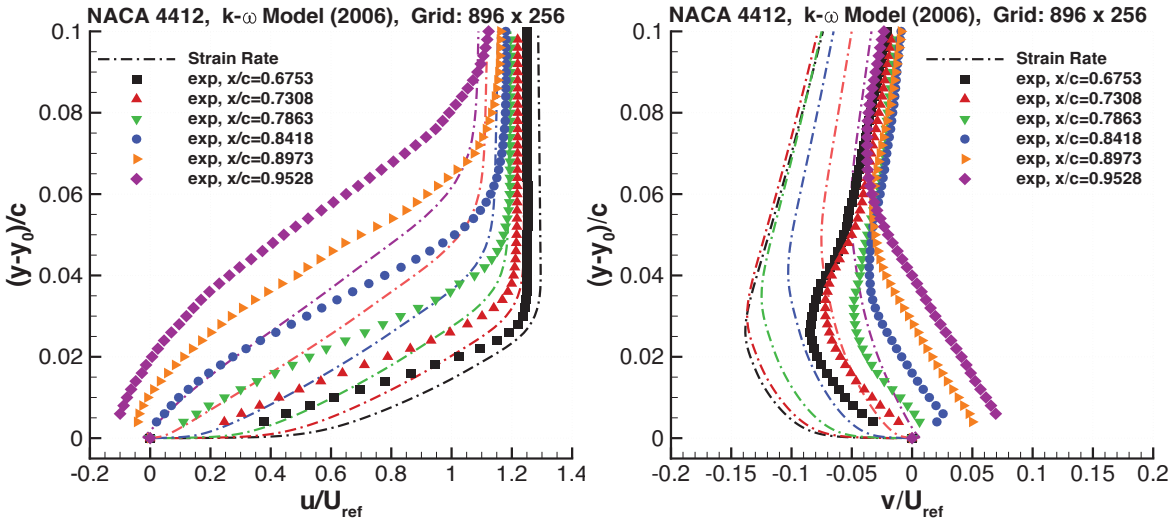

(a) (b)

Figure 23: Velocity distributions at six streamwise locations for NACA 4412 airfoil using the 896×256 grid. Computations performed with 2006 k-ω model and strain rate. (a) U velocity, (b) V velocity.

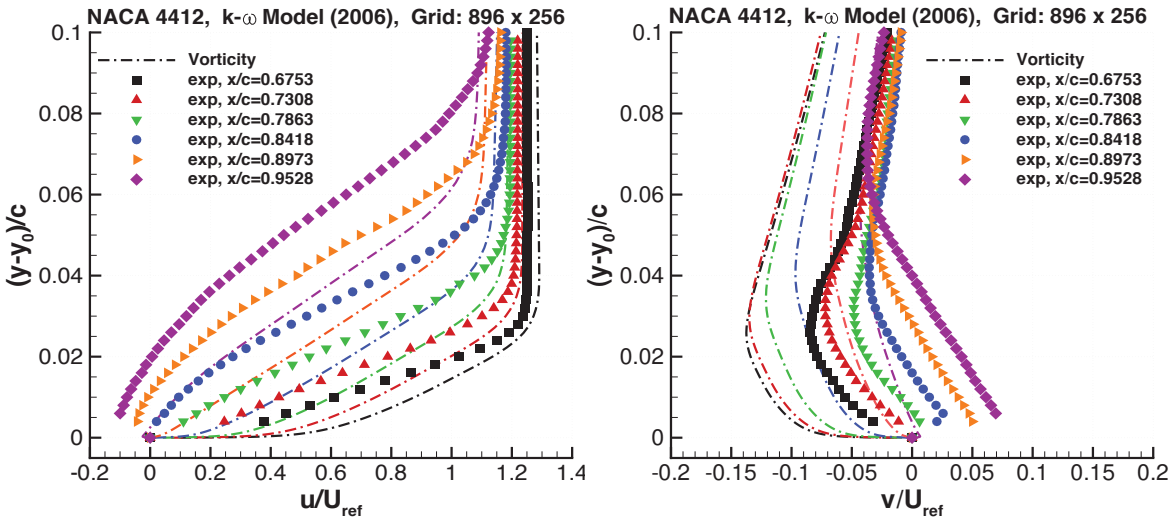

(a) (b)

Figure 24: Velocity distributions at six streamwise locations for NACA 4412 airfoil using the 896×256 grid. Computations performed with 2006 k-ω model and vorticity. (a) U velocity, (b) V velocity.

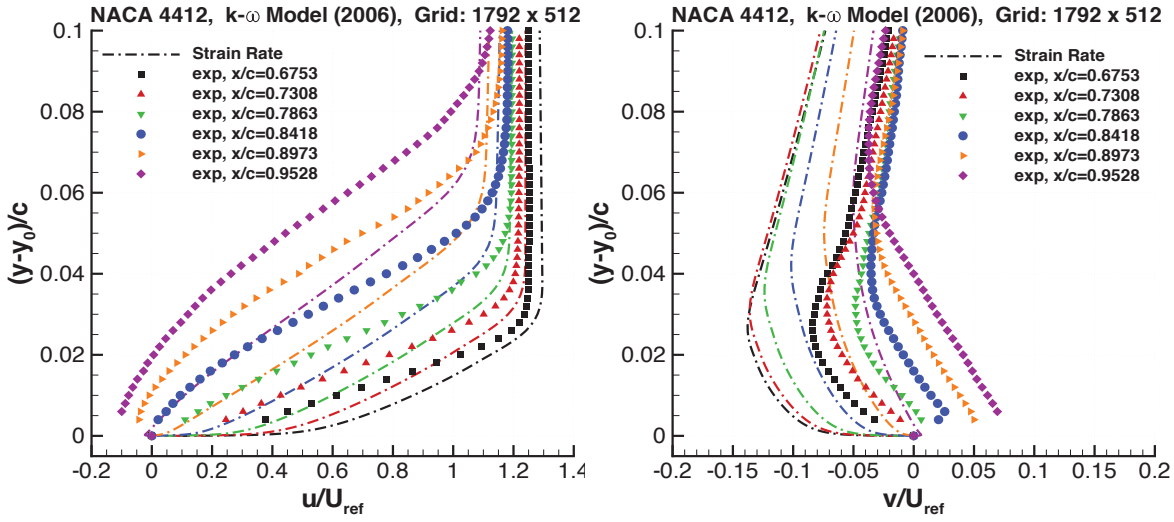

(a) (b)

Figure 25: Velocity distributions at six streamwise locations for NACA 4412 airfoil using the 1792×512 grid. Computations performed with 2006 k-ω model and strain rate. (a) U velocity, (b) V velocity.

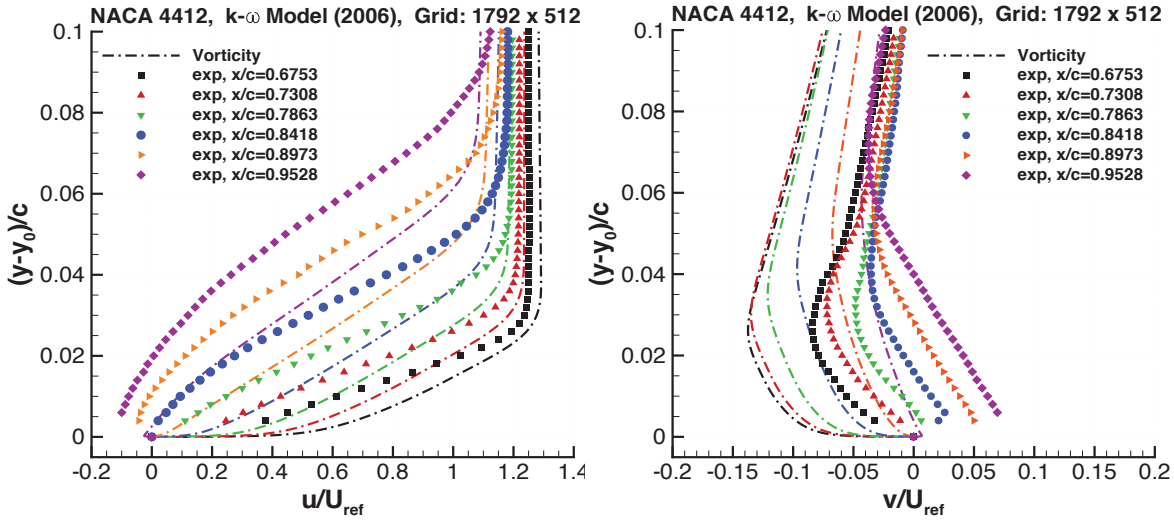

(a) (b)

Figure 26: Velocity distributions at six streamwise locations for NACA 4412 airfoil using the 1792×512 grid. Computations performed with 2006 k-ω model and vorticity. (a) U velocity, (b) V velocity.

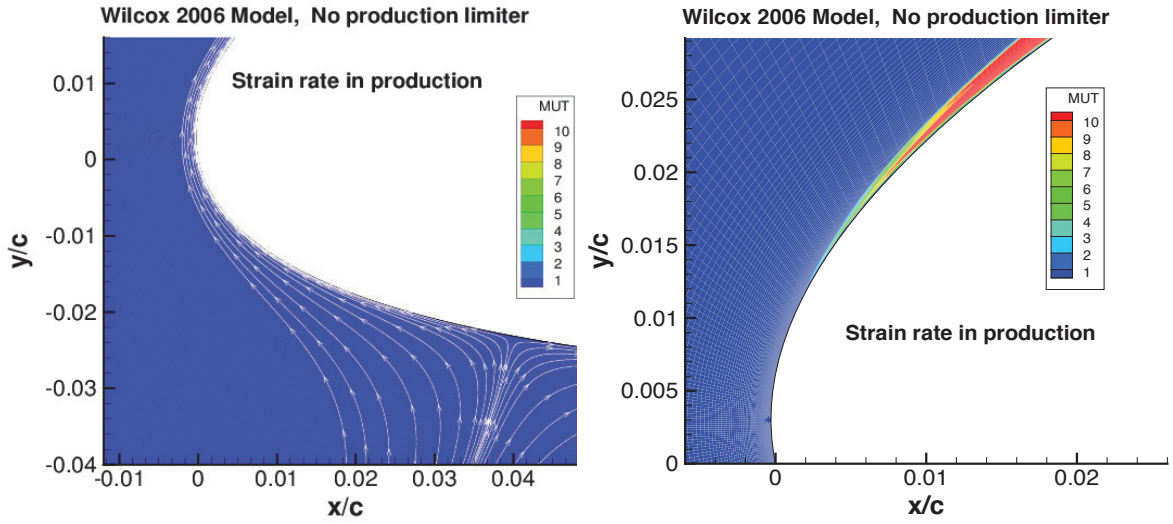

(a) (b)

Figure 27: Turbulent viscosity contours and streamlines for leading edge region of NACA 4412 airfoil computed with the 2006 Wilcox model using strain rate in production term. No production limiter used. (a) Lower region, (b) Upper region.

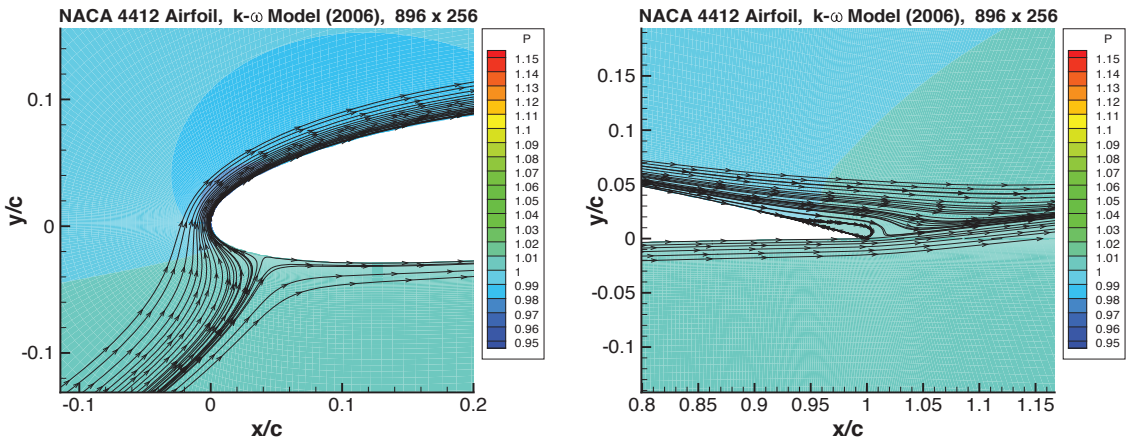

(a) (b)

Figure 28: Contours and streamlines for flow over NACA 4412 airfoil computed with the 2006 Wilcox model using strain rate in production term. No production limiter is used. Grid contains 896×256 cells. (a) Leading edge, (b) Trailing edge.

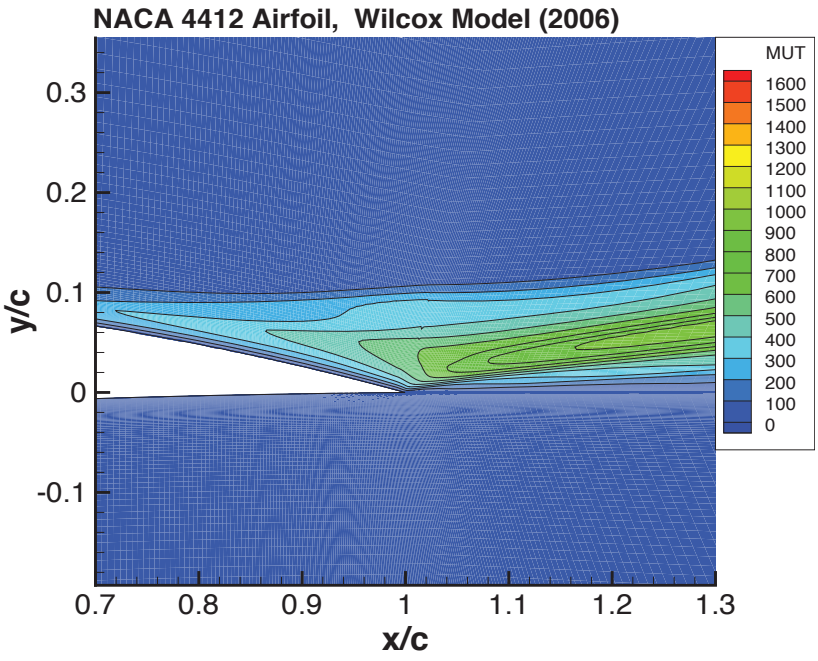

(a)

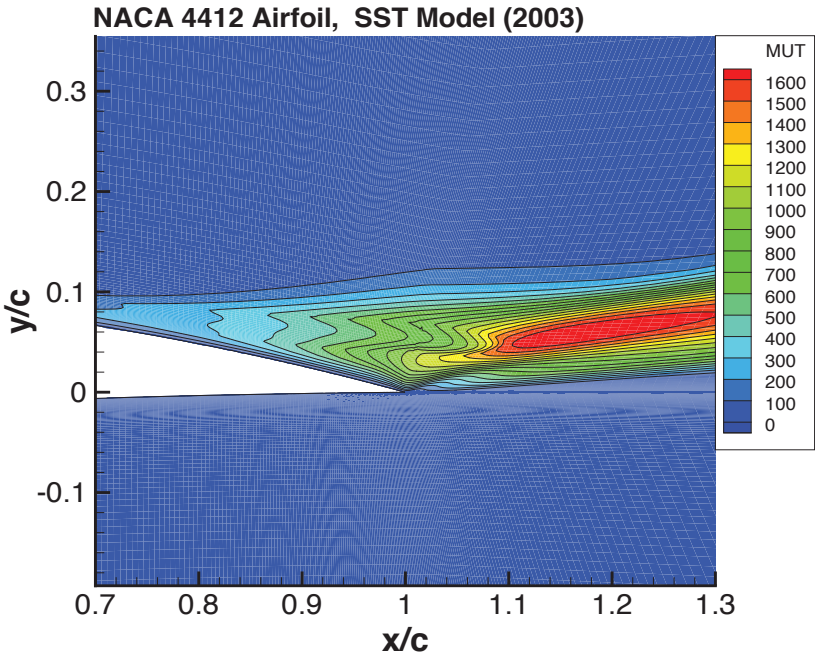

(b)

Figure 29: Contours of turbulent viscosity for flow over NACA 4412 airfoil. Grid contains 896×256 cells. (a) Wilcox model (2006), (b) Menter SST model (2003).

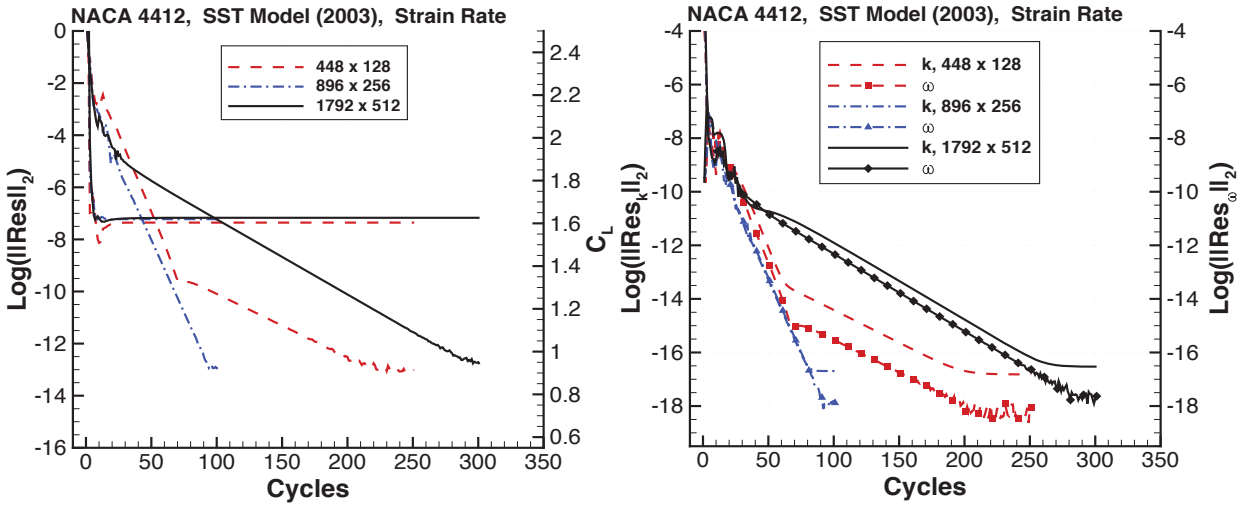

(a) (b)

Figure 30: Convergence histories for NACA 4412 airfoil on three grids using 2003 Menter model with strain rate in turbulence production term. (a) mean flow equations, (b) k-ω equations.

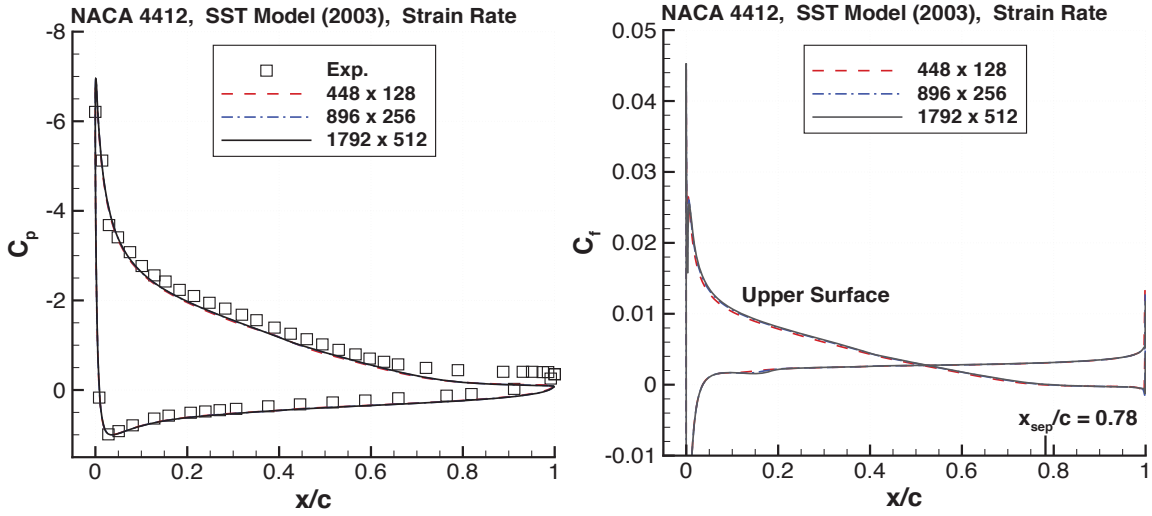

(a) (b)

Figure 31: Surface pressure and skin-friction distributions on three grids for NACA 4412 airfoil using 2003 Menter model with strain rate in production term. (a) Pressure, (b) Skin friction.

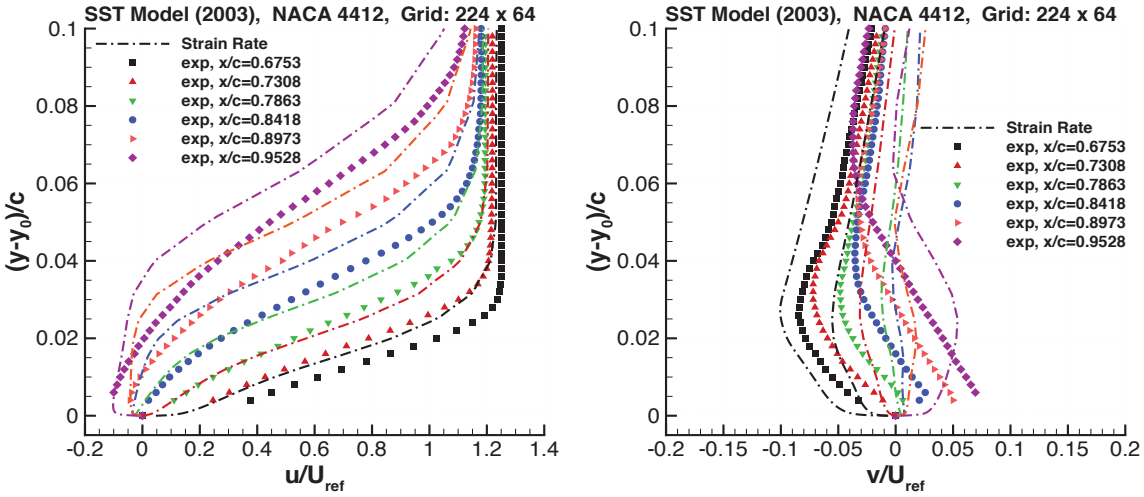

(a) (b)

Figure 32: Velocity profiles computed with SST turbulence model on a 224×64 grid and compared with the experimental data of Coles and Wadcock ($M = 0.09$, $\alpha = 13.87^o$, $Re_c = 1.52 \times 10^6$). (a) u velocity profiles, (b) v velocity profiles.

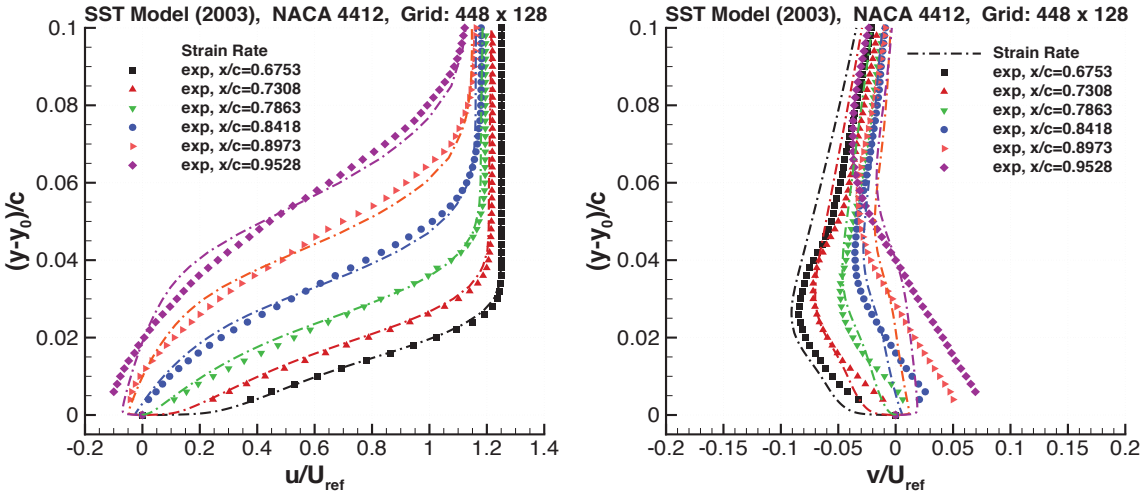

(a) (b)

Figure 33: Velocity profiles computed with SST turbulence model on a 448×128 grid and compared with the experimental data of Coles and Wadcock ($M = 0.09$, $\alpha = 13.87^o$, $Re_c = 1.52 \times 10^6$). (a) u velocity profiles, (b) v velocity profiles.

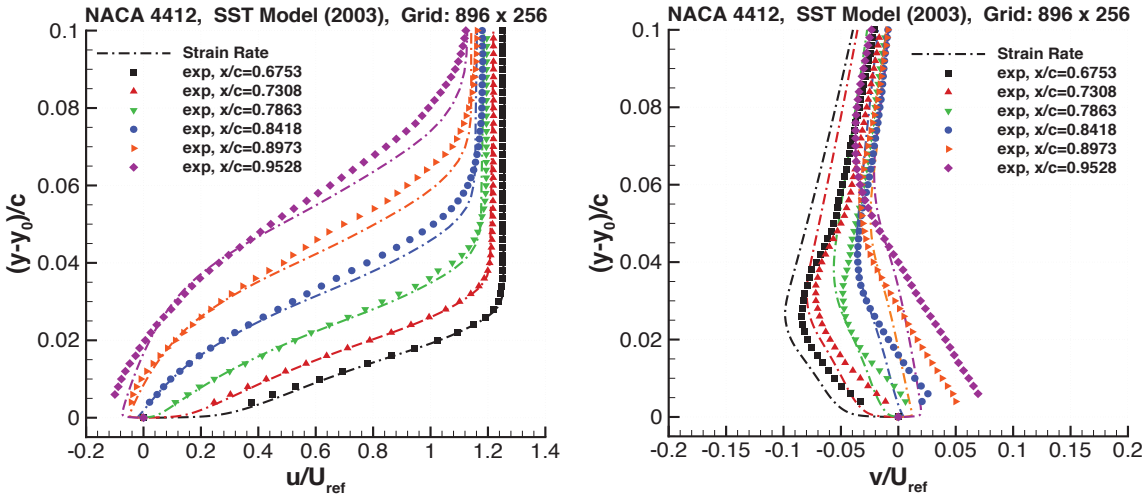

(a) (b)

Figure 34: Velocity profiles computed with SST turbulence model on a 896×256 grid and compared with the experimental data of Coles and Wadcock ($M = 0.09$, $\alpha = 13.87^o$, $Re_c = 1.52 \times 10^6$). (a) u velocity profiles, (b) v velocity profiles

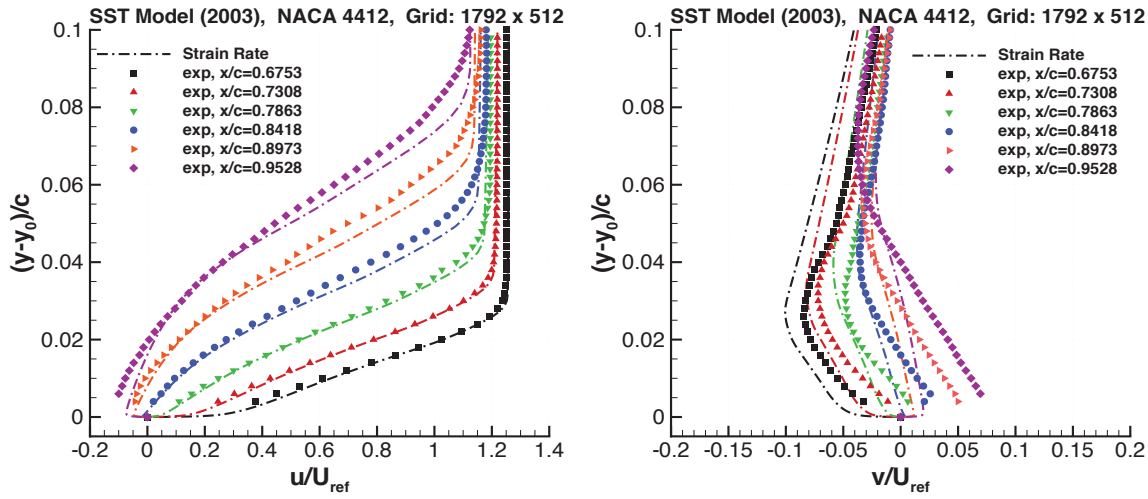

(a) (b)

Figure 35: Velocity profiles computed with SST turbulence model on a 1792×512 grid and compared with the experimental data of Coles and Wadcock ($M = 0.09$, $\alpha = 13.87^o$, $Re_c = 1.52 \times 10^6$). (a) u velocity profiles, (b) v velocity profiles.

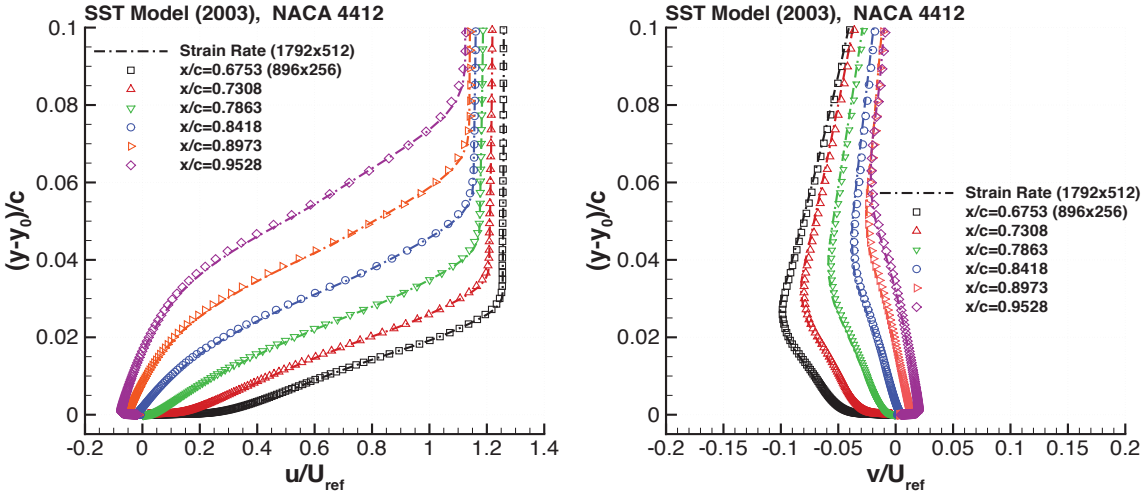

(a) (b)

Figure 36: Direct comparison of velocity profiles computed with SST turbulence model on 896×256 and 1792×512 grids ($M = 0.09$, $\alpha = 13.87^o$, $Re_c = 1.52 \times 10^6$). The dash dot lines and the symbols correspond to the solutions on the two grids. (a) u velocity profiles, (b) v velocity profiles.

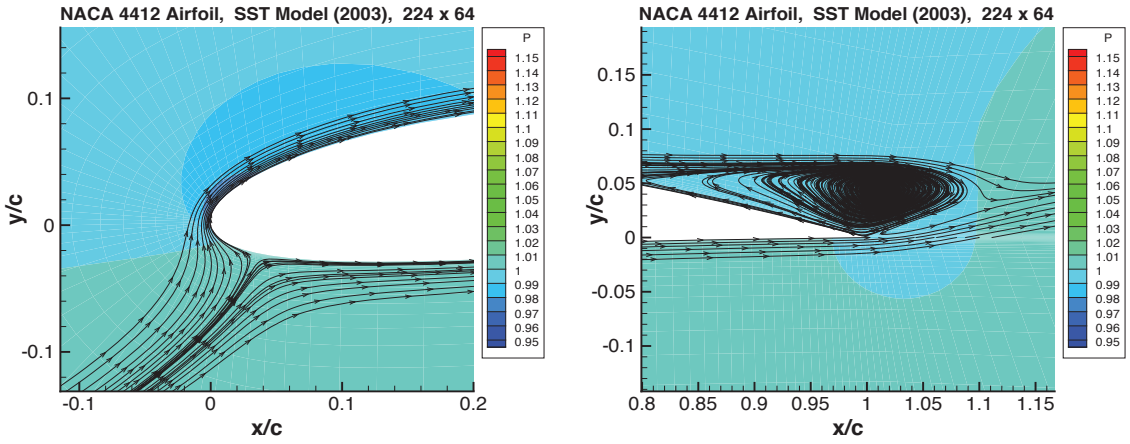

(a) (b)

Figure 37: Streamlines and pressure contours for flow over NACA 4412 airfoil computed on 224×64 grid. (a) Leading edge region, (b) Trailing edge region.

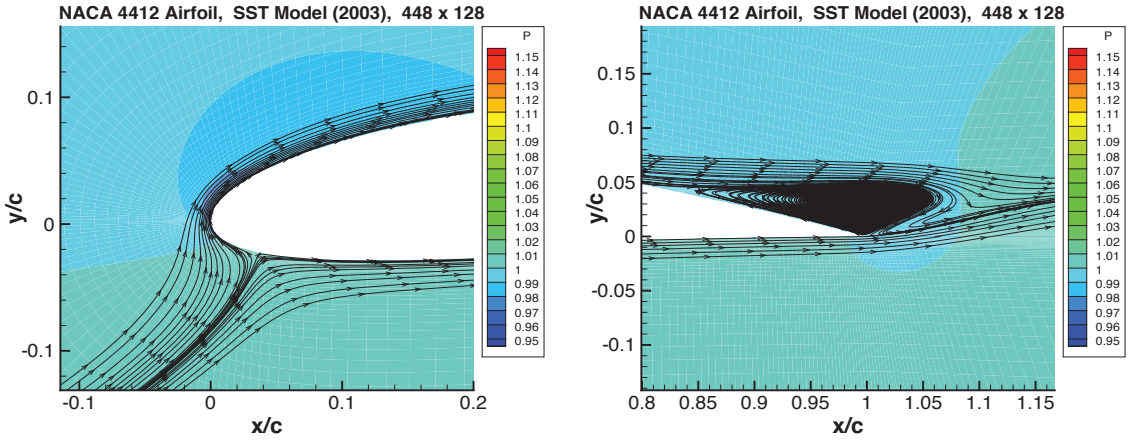

(a) (b)

Figure 38: Streamlines and pressure contours for flow over NACA 4412 airfoil computed on 448×128 grid. (a) Leading edge region, (b) Trailing edge region.

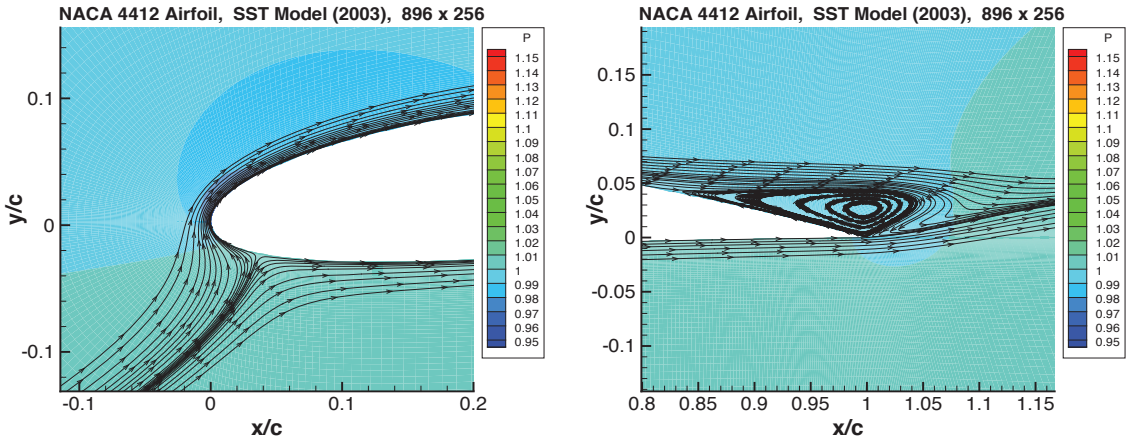

(a) (b)

Figure 39: Streamlines and pressure contours for flow over NACA 4412 airfoil computed on 896×256 grid. (a) Leading edge region, (b) Trailing edge region.

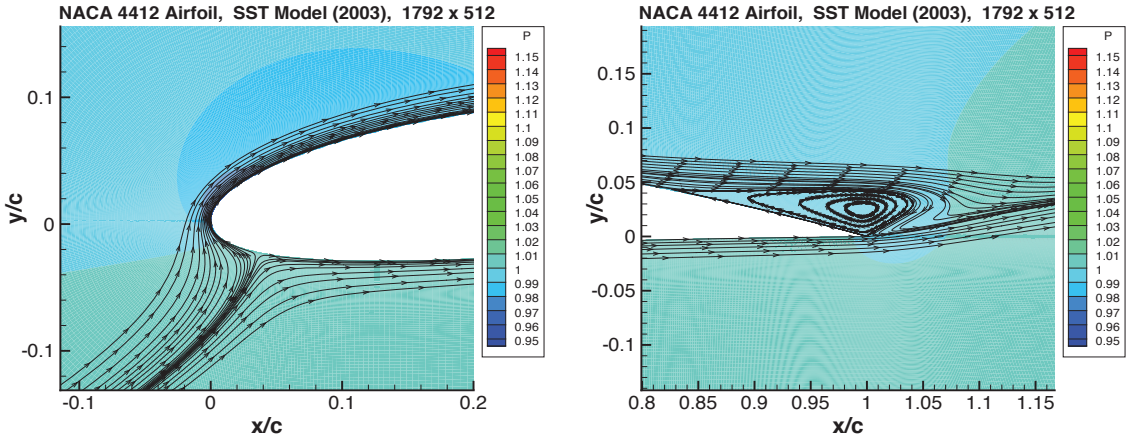

(a) (b)

Figure 40: Streamlines and pressure contours for flow over NACA 4412 airfoil computed on 1792×512 grid. (a) Leading edge region, (b) Trailing edge region.

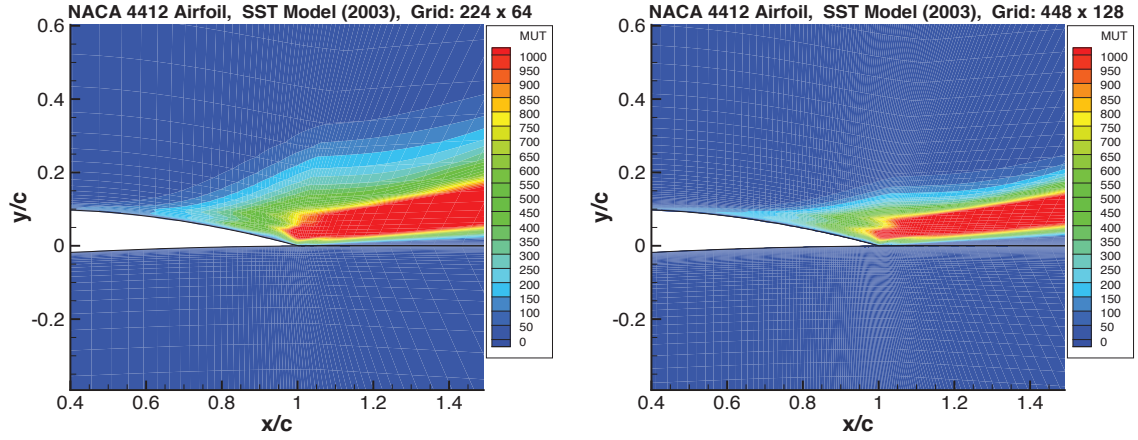

(a) (b)

Figure 41: Turbulent viscosity contours for flow over NACA 4412 airfoil computed on 224×64 and 448×128 grids.

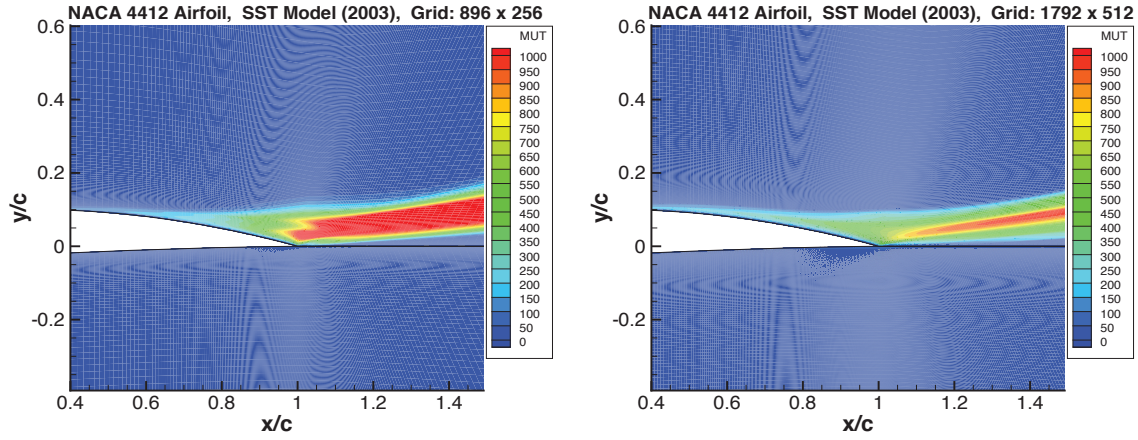

(a) (b)

Figure 42: Turbulent viscosity contours for flow over NACA 4412 airfoil computed on 896×256 and 1792×512 grids.

Appendix A

A Brief History of Turbulence Modeling

In 1895 Osborne Reynolds [83] derived a set of time-averaged equations governing turbulent flows (see also Refs. [84, 85] concerning Osborne Reynolds). These equations established the fundamental foundation for the development of turbulence modeling. They are sometimes called the Reynolds equations, but generally they are referred to as the Reynolds-averaged Navier-Stokes (RANS) equations.

Reynolds considered the instantaneous conservation equations for mass, momentum and energy. He first introduced a decomposition of the dependent into a sum of two terms. One of these terms is slowly varying (a mean value), and the other term is random varying (a fluctuating value according to the high frequencies that are characteristic of turbulence). For example, the Cartesian velocity component u_i and the pressure p are given by

$$u_i = \bar{u}_i + u_i', \quad p - \bar{p} + p' \tag{A1}$$

where the overbar indicates a mean value, and the prime means a fluctuating value. The time-averaged values of the dependent variables, for example, $\bar{u}_i$ is given by

$$\bar{u}_i(t_0) = \frac{1}{P} \int_{t_0 - P/2}^{t_0 + P/2} u_i(t) dt \tag{A2}$$

where P indicates the time interval of the averaging process. The time $t_0 - P/2$ is large compared to the time scale associated with the random fluctuations of the turbulence, and $t_0 + P/2$ is larger than the time scale corresponding any unsteady motion of the mean flow.

Since Reynolds was considering water flows, he used the incompressible form of the flow equations. Thus, the density is not contributing to the influence of the turbulence on the mean flow. This is important when using the Reynolds expansions given in (A1), since this eliminates the triple correlations (i.e., correlations that include density) of fluctuating quantities that would have otherwise appeared in the time-averaged form of the equations. If the fluid is compressible, this is not the case. As pointed out by Launder [86], Osborne originally considered mass-weighted averaging, which preceded by 70 years the paper by Favre [87] on such an approach. With such mass-weighted averaging, the resulting compressible flow equations are the same as their laminar flow counterparts with simply additional time-averaged terms due to stresses and heat fluxes associated with the turbulence. These terms are currently called the Reynolds stresses and heat fluxes). In the 1895 paper of Reynolds, however, a volume-based approach was used instead.

Another important element in the evolution of turbulence modeling was introduced by Boussinesq [88] in 1877. He assumed that the turbulent stress $\tau_t = -\bar{\rho}\overline{u'v'}$ is proportional to the mean strain rate $\partial\bar{u}/\partial y$, where y is the direction normal to the surface boundary. With this assumption (usually called the Boussinesq assumption), the Reynolds stresses of the stress tensor are simply proportional to the mean strain rate tensor. The proportionality factor is generally called the eddy viscosity. We should note that unlike the laminar viscosity, the eddy viscosity is not a property of the fluid. Note, a general discussion of the many contributions of Boussinesq in fluid mechanics is given by Darrigol [89]. While the basic assumption of Boussinesq set the stage for further developments in turbulence modeling, it does not appropriately represent the viscous forces in a turbulent flow. Moreover, such forces are actually proportional the square of the mean velocity, rather than just the mean velocity, which is the case for laminar flows. In 1915, G. I. Taylor [90] introduced the idea of representing the eddy viscosity as a product of a length scale and a velocity scale (see page 13 of that paper). Later, in 1925, Prandtl [91] refined such an approach to modify the mixing coefficient of the Boussinesq approximation. He extended the development of what is called the mixing length

concept in which the eddy viscosity is determined by

$$\mu_t = \ell \left| \frac{\partial \bar{u}}{\partial y} \right|, \tag{A3}$$

where ℓ is the mixing length. Then, the Reynolds stress can be expressed as

$$\tau_t = -\bar{\rho}\bar{u}'v' = \bar{\rho}\ell \left(\ell \left| \frac{\partial \bar{u}}{\partial y} \right| \right) \frac{\partial \bar{u}}{\partial y} \tag{A4}$$

and now the viscous force is proportional to the square of the mean velocity.

Using the Boussinesq approximation as a basis, a wide range of turbulence models have been developed to determine the eddy viscosity. We now consider the basic classes of eddy viscosity models, which are as follows: (1) Algebraic (sometimes referred to as zero-equation) model, (2) $1/2$-equation model, which is a combination of an algebraic model and an ordinary differential equation (ODE) for the principal shear stress, (3) Transport equation models: one-equation, two-equation or higher equation models. For all such models, except the two-equation and higher models, the length scale is determined algebraically.

For equilibrium boundary layers (e.g., weak interaction between the viscous and inviscid flow regions), algebraic models can often represent well the effects of turbulence on the mean flow. Two such models that have been applied frequently are the Cebeci-Smith (C-S) and Baldwin-Lomax (B-L) models [92–94]. The eddy viscosity of these two layer models is defined by

$$\mu_t = \begin{cases} (\mu_t)_{\text{inner}} & y \leq y_{\text{crossover}} \\ (\mu_t)_{\text{outer}} & y > y_{\text{crossover}} \end{cases}$$

where y is the normal distance to a wall boundary, and $y_{crossover}$ is the smallest value when the inner and outer eddy viscosities are equal. The inner μ_t is for the log-layer of the boundary layer, and the outer μ_t is for the wake region of the boundary layer. Both the inner and outer regions require appropriate length and velocity scales. The inner eddy viscosity for each model can be written as

$$\mu_{t_{\text{inner}}} = \rho\, \ell^2 F_{\text{vel}}, \tag{A5}$$

where we define the velocity scale of the model by F_{vel}. The velocity scale function for the C-S model is as follows:

$$(F_{\text{vel}})_{CS} = \sqrt{\left(\frac{\partial \bar{u}}{\partial y} \right)^2 + \left(\frac{\partial \bar{v}}{\partial x} \right)^2}, \qquad \ell = \kappa D y, \tag{A6}$$

where κ is the von Kármán and D is the van Driest damping factor that accounts for the damping of the small scale eddies near a wall boundary. The outer μ_t is proportional to the product of the edge velocity and displacement thickness of the boundary layer. A primary purpose of the B-L model is to eliminate the need to determine the edge of the boundary layer, which can be difficult, especially for three-dimensional flows. In this model, the magnitude of the vorticity replaces the $(F_{\text{vel}})_{CS}$ in the inner region, and it is used to compute the velocity scale for the μ_t in the outer region of the boundary layer as well as the wake region.

Algebraic turbulence models are not appropriate when there there are rapidly changing adverse pressure gradients to produce separation of the flow that causes significant viscous-inviscid interaction. For example, this behavior can easily occur in transonic flows in which there is interaction of a shock wave and the boundary layer. Algebraic models rely upon local flow behavior to determine the properties of the turbulence. Thus, there is no accounting of the history effects of the turbulence. It is well-known that such history effects have a profound impact on the nature of flow separation and possible reattachment. Johnson and King [22] in 1985 used the two-layer approach of the algebraic models to introduce history effects in the turbulence modeling, while at the same time avoiding

extensive additional computational effort. The basis for their model is the turbulence kinetic energy (TKE) equation. This equation is transformed to an equation for the maximum Reynolds shear stress by using the assumption of Bradshaw et al. [21] that relates the turbulence shear stress to the TKE according to

$$\tau_t = -\bar{\rho}\overline{u'v'} = \bar{\rho}a_1 k, \tag{A7}$$

where the constant $a_1 = 0.3$. The resulting equation governing the development of the maximum shear stress (velocity scale of model) is an ordinary differential equation (ODE). Baseline values of the eddy viscosity in the inner and outer regions of the boundary layer are defined in the model. That is,

$$\nu_{ti} = \kappa D^2 y\,(-\overline{u'v'})_m^{1/2}, \quad \nu_{to} = const.\gamma, \tag{A8}$$

where γ is the Klebanoff intermittency factor. The constant is determined by the value of $-\overline{u'v'}$ is computed from the solution of the ODE governing the maximum shear stress. While this model produced significant improvements in the predicted pressure distribution for transonic airfoil flows with separation, it did not reproduce in general the experimental data for weak and strong transonic flows. This model also does not overcome the computational difficulties when computing complex flows, especially three-dimensional flows.

In an effort to overcome the difficulties in applying the eddy viscosity models just described to complex flows with multiple length scales, one-equation and higher equation models have been considered. Such models include the effects of advection and diffusion turbulent flow quantities such as the turbulence kinetic energy and viscous dissipation. Currently, one-equation and two-equation models are the most frequently used in the computation of turbulent flows. For one-equation models, just as in the previous eddy viscosity models discussed, the length scale is determined algebraically. One possible starting point for developing such models is the TKE equation. The solution of this transport equation is used to compute the velocity scale of the model. Length scales are required to determine the eddy viscosity and the viscous dissipation. Prandtl [95] considered such a model in 1945. Due to his experience with a mixing length, he assumed that this mixing length could be used for the single length scale, which appears in the dissipation term of his TKE equation, and is used to define the eddy viscosity in his model. Another example of such a turbulence model is the one developed by Norris and Reynolds [96] in 1975. This is a low Reynolds number model (i.e., suitable for direct integration to a solid boundary) that attempts to include history effects on the eddy viscosity. It uses the assumption of Bradshaw [21] that the shear stress behaves like the TKE. With this model, the eddy viscosity and dissipation are given by

$$\mu_t = C_\mu \rho \sqrt{k} \ell_m u, \quad \epsilon = \frac{k^{3/2}}{\ell_\epsilon}, \tag{A9}$$

where C_μ is a constant. The length scales ℓ_μ and ℓ_ϵ are then computed using

$$\ell_\mu = C_\ell\, y \left[1 - exp\left(-\frac{Re_y)}{A_\mu}\right)\right], \quad \ell_\epsilon = \frac{C_\ell\, y}{1 + C_\epsilon / Re_y}, \tag{A10}$$

with C_μ, C_ℓ, A_μ and C_ϵ being constants. The constant C_ℓ depends on the von Kármán constant κ. As evident, the length scale ℓ_μ is quite similar to that used with the algebraic models previously described. This means that it is assumed that there is a balance between production and dissipation of turbulence. Thus, the length scales behave like $\ell = \kappa y$ in the viscous region near a solid wall boundary. In the last few years there has been some resurgence in the interest of this approach for developing a one-equation model. Rahman et al. [97, 98] modified the low Reynolds number Norris-Reynolds model to account for changes in the length scales in the near wall region. Then, these length scales have a functional dependence (a nonlinear dependence) on the invariants formed by the mean strain rate and vorticity tensors. As a consequence, this modified model is designed to have improved capability in modeling flows with separation and reattachment.

At this time, the most frequently applied one-equation model is the Spalart and Allmaras [3–5] model. There are variations of this model that account for streamline curvature and rotation effects. The Baldwin and Barth [99] and Wray and Agarwal [100] models also receive attention, but currently the frequency of application seems to be much lower. These models make a departure from building a turbulence model with the TKE equation. The Spalart-Allmaras (S-A) model constructs a single transport equation for the kinematic eddy viscosity (ν_t) predominantly using empiricism and arguments of dimensional analysis. The model is built with Galilean invariance and particular dependencies on the molecular viscosity. It is local in application with simple boundary conditions for ν_t, which faciltate integration to a wall boundary. These properties have a profound effect on the numerical solution of the transport equation. A different approach is taken to derive the Baldwin-Barth (B-B) model. A single transport equation is derived by first considering the two-equation model with dependent variables k and ϵ, which represent the TKE and its disspation rate. Then, a linear combination of these two transport equations is used to obtain a single transport equation for the quantity νR_T, where ν is the kinematic viscosity and $R_T = k^2/(\nu\epsilon)$ is the turbulence Reynolds number. The kinematic viscosity determined by,

$$\nu_t = c_\mu(\nu R_T) = c_\mu \left(\frac{k^2}{\epsilon}\right), \tag{A11}$$

where c_μ is one of four parameters required to calibrate the model. The Wray-Agarwal model is also derived from the k-ω closure (see Ref. [101] for a correction to a parameter arg_1 in the model).

A principal element in the previous models using a transport equation for k is the algebraic determination of the length scales. In summary, these scales are evaluated in the viscous region near a solid wall boundary (i.e., viscous sublayer and buffer regions of a boundary layer) by either balancing production and disspation or using a nonlinear dependence on invariants due to the turbulence variables of strain rate and vorticity. The associated length scale for the outer region of the viscous layer reflects the behavior of the boundary layer in the log-law and wake regions. Then, instead of using an algebraic determination of a length scale, a significant change occurred in turbulence modeling when Kolmogorov [102] introduced a second transport equation to govern the behavior of the length scale.

In 1941 the work of Kolmogorov set the stage for his 1942 paper [102] in which he introduced two transport equations for predicting the behavior of turbulence. These equations, along with the Navier-Stokes equations that govern a moving fluid, represent the effects of advection, diffusion and energy dissipation of turbulence on the fluid motion. One of the dependent variables in the two equations is k (quantity b in Ref. [102]), and the other is ω, which is proportional to the disspation rate of the turbulence. The velocity scale for ν_t is determined from k, and the length scale is proportional to $\sqrt{k}/\omega$. Kolmogorov did not provide the coefficients for closure of the model, and certain other details of the model are not available in his short paper. Spalding [103] provides most likely possibilites for the details that are missing in Kolmogorov's short paper. It should be pointed out that this first two-equation model does not the include terms for the production of turbulence. Even so, Kolmogorov's model is generally recognized as a major contribution in the development of two-equation turbulence models. Yet, this initial advancement of Kolmogorov set the stage in essentially all the subsequent efforts on two-equation turbulence models.

Another salient fact in the history of two-equation turbulence modeling is that Saffman [104], without previous knowledge of Kolmogorov's work, formulated a k-ω model that would be shown superior to the model of Kolmogorov. In his work, and as Wilcox [1] points out, Saffman described ω "as a frequency characteristic of the turbulence decay process under its self-interaction."

Since the introduction of a two-equation model by Kolmogorov and the subsequent developments of Saffman, numerous contributions to improve the physical modeling as well as the numerical compatibilty of such models have been made. It is important to recognize that the extensions and improvements to the initial formulations of the two-equation model have primarily focused on the choice of a different dependent variable than that used in the k-ω model of Kolmogorov, which has

the dimension of $(time)^{-1}$. The choice of this variable is critically important regarding its behavior near a solid boundary, where there is a singularity. Some examples of two-equation models that replace the specific dissipation rate ω are the following: the k-ℓ model of Wolfshtein [105], the k-ϵ model, the k-τ model of Speziale et al. [106]. For each of these two-equation models, the length scale and kinematic eddy viscosity (with units of m^2/sec) behave according to Table A1.

Table A1: Two-equation turbulence models.

Turbulence Model	Length Scale (ℓ)	Kinematic Eddy Viscosity (ν_t)
k-ℓ	$\sim k^{3/2}/\epsilon$	$\sim \sqrt{k}\ell$
k-ϵ	$\sim k^{3/2}/\epsilon$	$\sim k^2/\epsilon$
k-ω	$\sim \sqrt{k}/\omega$	$\sim k/\omega$
k-τ	$\sim \sqrt{k}\,\tau$	$\sim k\,\tau$

Another alternative for the dependent variable ω is the enstrophy (the variance of vorticity). With this approach, a length scale equation is derived based on vorticity transport theory. Several investigators [107–109] have formulated turbulence model closure with a vorticity transport equation. Robinson et al. [110] in 1995 introduced a variation of this closure using a k-ζ (or k-ω^2) equation. In addition to changing the variable for determining the length scale of the model, further efforts have also included modification of the closure constants, especialy regarding free shear flows.

Before proceeding, there are several important aspects regarding the development and application of the k-ϵ model that warrent discussion, so as to provide a clear understanding of its role in turbulence modeling. First, as pointed out by Wilcox [6], the work of Chou [111], Davydov [112] and Harlow and Nakayama [113] played a key role in developing the model. The extensive use of the model began with the version introduced by Jones and Launder [114, 115], which was further modified by Launder and Spalding [116] in 1974. This particular model is generally considered as the standard form. This model has been shown to work well for free-shear flows. Until about the 1990's the k-ϵ model was extensively used. While it continues to be applied in various industries, there has been a decrease in its usage in aerospace applications due to how well it performs in computing aerodynamic flows. In fact, Wilcox [6] gives numerous examples showing that the k-ϵ model yields inferior results when compared to the k-ω model.

Other choices, such as ω, for the dependent variable in the second transport equation were found to be much more amenable to the numerical solution process when integrating to a solid boundary, and also yielded better solution accuracy in many flows of interest. Wilcox and his various colaborators (e.g., Refs. [117] – [121]) made many extensions of the k-ω model. When modifying the model, significant emphasis has been given to establishing good agreement with the experimental data for free-shear flows. Currently, the 2006 version of the Wilcox model [6] is being used. This version is applicable to both wall-bounded and free-shear flows, which is a necessary requirement for computing complex turbulent flows. Moreover, it exhibits not only good agreement with measurements for attached boundary layers, mildly separated flows, and backward-facing steps but also for the spreading rate of free-shear flows. Relative to previous versions of the Wilcox model, the sensitivity to free-stream values of ω is significantly reduced, and the prediction of shock separated flows is also improved. Details of changes to the 2006 Wilcox model that provide such improvements are discussed in the main text of this report. As indicated in the report, there are still some concerns regarding reliability of the model for adverse pressure gradient flows.

In 1992, Menter [8] introduced a turbulence model that blends the 1988 version of the Wilcox k-ω model with the Jones and Launder [114] k-ϵ model. This blending was accomplished by first transforming the transport equations of the k-ϵ model to equations for a k-ω model. Due to this transformation, a cross-diffusion term appears in the ω equation. This term plays an important role in reducing the sensitivity of the turbulence model to the free-stream value of ω. It should be pointed out that such a term does not appear in the 1988 Wilcox model, but it is part of the 2006 Wilcox model in order to reduce significantly boundary condition sensitivity. There are two principal

reasons for this blending. The first one is to remove the difficulties of the k-ϵ model when integrating the second transport equation to a wall boundary. The second reason is the sensitivity reduction mentioned previously. An additional element in the development of this scheme is to account for the transport of the principal shear stress in adverse pressure gradient boundary layers. This means that history effects, which are important for separated flows, are included when computing turbulent flow properties, rather than simply using the instantaneous local flow properties. The impact of the history effects of the turbulence appears in the computation of the eddy viscosity using the Bradshaw assumption of the proportionality of the principal shear stress to the turbulence kinetic energy. Further details and discussion of this model in given in the main part of this report.

All of the previously mentioned first-order closure turbulence models are linear eddy viscosity models (EVMs). In general, such models cannot predict well the physics of flows in which their behavior is significantly affected due to any of the following: secondary flows induced by turbulence, streamline curvature effects, swirling or rotational effects. These models also tend to over predict turbulence energy in stagnation regions, and they predict normal stresses as isotropic in free-shear flows. To diminish some of these weaknesses, a nonlinear form for EVM has been considered. With a nonlinear EVM, the linear relationshop between the Reynolds stress tensor and mean strain rate tensor is augmented by a nonlinear function of the mean strain rate and mean rotation tensors. That is,

$$\overline{u_i u_j} = -\nu_t S_{ij} + \frac{2}{3} k \delta_{ij} + f(S_{ij}, \Omega_{ij}), \tag{A12}$$

where S_{ij} and Ω_{ij} are the mean strain rate and mean rotation tensors, respectively. The nonlinear function $f(S_{ij}, \Omega_{ij})$ represents an anisotropy tensor. Moreover, this function represents a polynomical expansion with the leading term being the strain rate tensor of a linear EVM. It allows capturing the effects of stress anisotopies that are present in second-moment closures. Further discussion on such nonlinear models is given in the book by Wilcox [1] and paper by Gatski and Rumsey [122].

A key contribution to further development of turbulence modeling is the 1951 paper of Rotta [123]. This paper set the foundation for a full Reynolds stress model (RSM), which is a second-moment closure model. A RSM includes one equation for each Reynolds stress and a length scale equation to determine the dissipation rate. Thus, there is a significant increase in complexity relative to a two-equation model. This type model abandons both the Boussinesq and isotropic turbulence assumptions, which are inhibiting factors when modeling complex turbulent flows. It incorporates non-local and history effects of the turbulence on the mean flow. As remarked previously, representing history effects is in general essential when considering flow separation. A RSM also includes streamline curvature and rotation effects, and it does not require normal stresses to be equal when the shear stresses $\partial u_i / \partial u_j$ vanish.

With this improvement in the modeling of turbulence, there are notable consequences when solving the seven equations of a RSM. In particular, when comparing with a two-equation model, the equations of a RSM are much more stiff, and the computational effort to solve the equations is much higher. The difficulties in solving the transport equations of the RSM, along with inadequate computatational capability, retarded the progress over the next several decades. By the 1970's there were many advancements in computer technology, which resulted in high-speed computer processing, and this augmented the feasibility of solving the equations of the RSM. This progress renewed interest in further developments of a second-order closure models. As indicated by Speziale [2], the work of Daly and Harlow [124] and Donaldson [125] played a key role in this revived interest. In addition, Launder et al. [126] developed a new RSM model that improved significantly the earlier formulation of Rotta and provided implementation details. This work also improved the approximation of the correlation between pressure and strain fluctuations in the stress equations. During these developments of the RSM, the necessity to impose constraints on the Reynolds stresses to ensure the realizability of the model was addressed (see Refs. [127, 128]).

Over the last 20 years efforts have continued to improve the RSM as well as the numerical solvability of its transport equations. For example, there has been the work of Eisfeld [46, 129],

Chassaing et al. [130] and Mor-Yossef [44, 45]. Eisfeld has played a key role in the developemnt of the SSGLRR-ω model, which was part of the EU-project FLOMANIA. This model extends the applicability of the Speziale-Sarkar-Gatski pressure strain model to wall bounded flows using the Launder-Reece-Rodi model. The length scale equation comes from the BSL model of Menter [8]. Mor-Yossef has developed a numerical algorithm to improve convergence behavior in solving the transport equations of this model. Even with a number of improvements to the RSM, this model is still is not widely used due to numerical difficulties (e.g., reducing residuals cannot in general be reduced to machine zero in steady-state computations), especially for complex turbulent flows. In addition, there still remains to explain why the RSM does not consistently demonstrate improved predictions relative to simpler models, even though they have a better modeling of the physics. While turbulence models, such as the algebraic RSM, have been considered to reduce the complexity of the full RSM by using algebraic constitutive equations for the Reynolds stresses, these models have not removed the aforementioned issues with the RSM.

The turbulence modeling approach currently being given considerable attention is called large eddy simulation (LES). With this type of modeling, it is required to resolve the large scale eddies of the turbulent flow and determine the small scales with either direct or indirect modeling. Direct (or explicit) modeling often means that a RANS model is used to represent how the small scales are damped in approaching a wall boundary. The indirect (or implicit) modeling (called ILES, implicit LES) assumes that the damping of the small eddies can be accomplished by choosing an appropriate numerical dissipation for the discretization of the equations. Explicit LES can easily have similar deficiencies to that of a RANS method. In general, considerable computational effort is needed due to resolution requirements with LES. Thus, this type of modeling is not attractive for routine computations of turbulent flows. Extensive discussion about the benefits and deficiencies of LES are addressed in the book by Sagaut [131].

Appendix B

RANS Equations and Nondimensionalization

In this section, we discuss the nondimensionalization of what are generally called the Reynolds-averaged Navier-Stokes (RANS) equations, which include the conservation equations of mass, momentum, and energy. Such a designation can be considered a misnomer since there is the presumption of using Reynolds expansions of the dependent variables, which is frequently not what is done. There is flexibility in choosing the expansion of the dependent variables to account for the effects of the turbulence on the fluid motion. The two principal types of expansions, which are expressed as the sum of two terms, are the Reynolds and mass-averaged expansions. One of the terms in the expansion is slowly varying with respect to the mean motion of the fluid, and the other varies at the high frequencies of the turbulence. Consider a general flow quantity b. Then, the Reynolds and mass-averaged expansions of the dependent variables can be expressed respectively as

$$b = \bar{b} + b^{'} \quad \text{and} \quad b = \tilde{b} + b^{''}, \tag{B1}$$

where the overbar denotes a mean value and the tilde indicates a density-weighted mean value. Substituting such expansions for each dependent variable (instantaneous quantities) in the governing equations and then performing a Reynolds average (i.e., time average) over a period that is long relative to the time scale of the fluctuating components but short relative to the time scale of the flow field itself yields the mean flow form of the continuity, momentum (RANS) and energy equations.

There are some important differences between the Reynolds and mass-averaged expansions. One is that in the time averaging the mean of the fluctuating components in the two expansions are as follows:

$$\bar{b^{'}} = 0, \qquad \bar{b^{''}} = -\frac{\overline{\rho^{'} b^{''}}}{\bar{\rho}}. \tag{B2}$$

In addition, there is a corresponding mass-averaged expansion for each Reynolds expansion except for the thermodynamic variables of pressure (p) and density (ρ). Additional discussion and details of the mass-averaged (Favre) variables is presented in Favre [87], Hinze [25], and Rubesin and Rose [18]. It turns out that using the Favre variables simplifies the mean-flow equations considerably. The conservation of mass equation has exactly the same form. The equations for conservation of momentum and energy retain essentially the identical form of their laminar flow counterparts except for the additional Reynolds stress, heat flux, molecular diffusion and turbulent transport of turbulence kinetic energy terms. The diffusion term contains the product of the molecular stress and fluctuating velocity of a Favre expansion. Note, the total energy also includes the turbulence kinetic energy. As pointed out in this report, it is quite usual except for high Mach number flows to neglect the molecular diffusion term as well any terms associated with the turbulence kinetic energy.

The remaining part of this section is dedicated to defining the particular nondimensionalization that is used in solving the RANS equations and the transport equations for modeling turbulence (i.e., two-equation models) considered in this report. The governing Navier-Stokes equations are nondimensionalized in the following manner, where the superscipt * refers to a dimensionless quantity, and the subscript r denotes a reference quantity.

$$\begin{aligned} {x_i}^* &= \frac{x_i}{\ell_r}, \quad \rho^* = \frac{\rho}{\rho_\infty}, \quad t^* = t\frac{u_r}{\ell_r}, \quad u_r = \sqrt{\frac{p_\infty}{\rho_\infty}} \quad {u_i}^* = \frac{u_i}{u_r}, \\ p^* &= \frac{p}{p_r}, \quad p_r = \rho_\infty u_r^2, \quad \mu^* = \frac{\mu}{\mu_\infty}, \quad E^* = \frac{E}{E_r}, \quad E_r = u_r^2, \quad T^* = \frac{T}{T_\infty}. \end{aligned} \tag{B3}$$

With this nondimensionalization, the subscript r refers to a free-stream value. Moreover, the continuity equation remains unchanged, and the momentum and energy equations are simply scaled

by the factor $\sqrt{\gamma}M_\infty/Re_\infty$, where γ is the specific heat ratio, M is the Mach number, Re is the Reynolds number, and the subscript ∞ refers to free-stream values. Thus, the only change occurs in the viscous contribution of the flux density tensor defined in (3), which becomes

$$\mathcal{F}_v = -\frac{\sqrt{\gamma}M_\infty}{Re_\infty}\begin{bmatrix} 0 \\ \bar{\tau}\cdot\mathbf{e}_x \\ \bar{\tau}\cdot\mathbf{e}_y \\ \bar{\tau}\cdot\mathbf{e}_z \\ \bar{\tau}\cdot\mathbf{q}-\nabla\cdot\mathbf{Q} \end{bmatrix}, \tag{B4}$$

where

$$\mathbf{Q} = -\left(\frac{\gamma}{\gamma-1}\,\frac{\mu}{Pr}\right)\nabla T = -\left(\frac{\gamma}{\gamma-1}\,\frac{\mu}{Pr}\right)\begin{bmatrix} \partial T/\partial x \\ \partial T/\partial y \\ \partial T/\partial z \end{bmatrix}, \tag{B5}$$

with Pr denoting the molecular Prandtl number. When using the eddy viscosity hypothesis to model turbulent flows, the molecular ratio μ/Pr is augmented by the corresponding turbulent flow ratio μ_t/Pr_t, where the subscript t indicates turbulent flow value. Here, in (B4) and (B5), as well as in subsequent equations, we suppress the symbol $*$ denoting dimensionless quantities.

Before considering the nondimensionalization for the turbulence modeling equations, we indicate the nature of the turbulence production term that appears in the equations. The production of turbulence is a measure of the kinetic energy transferred from the motion of the mean flow to the turbulence. Specfically, as indicated by Hinze [25], it is the work of deformation of the turbulence stresses per unit mass and time. Consider the following. Let $\bar{S}$ be the mean strain rate tensor as defined in Section 3.1, which is repeated here:

$$S_{ij} = \frac{1}{2}\left(\frac{\partial u_i}{\partial x_j} + \frac{\partial u_j}{\partial x_i}\right), \tag{B6}$$

A production term in the modeling equations is determined from the double-dot product (scalar product) of two second-order tensors. One is the stress tensor ($\bar{\tau}$), and the other ($\bar{V}$) represents the relative motion of one point relative to another. In Cartesian coordinates (x, y, z) and velocity components (u, v, w), the tensor $\bar{V}$ is given by

$$\bar{V} = \begin{bmatrix} \dfrac{\partial u}{\partial x} & \dfrac{\partial u}{\partial y} & \dfrac{\partial u}{\partial z} \\ \dfrac{\partial v}{\partial x} & \dfrac{\partial v}{\partial y} & \dfrac{\partial v}{\partial z} \\ \dfrac{\partial w}{\partial x} & \dfrac{\partial w}{\partial y} & \dfrac{\partial w}{\partial z} \end{bmatrix}, \tag{B7}$$

The double dot product of the turbulence production term is determined by

$$\begin{aligned}(\bar{\tau}:\bar{V}) &= (\sum_i\sum_j \delta_i\delta_j\tau_{ij} : \sum_k\sum_\ell)\delta_k\delta_\ell V_{k\ell}) \\ &= \sum_i\sum_j\sum_k\sum_\ell(\delta_i\delta_j:\delta_k\delta_\ell)\tau_{ij}V_{k\ell} \\ &= \sum_i\sum_j\sum_k\sum_\ell \delta_{i\ell}\delta_{jk}\tau_{ij}V_{k\ell} = \sum_i\sum_j \tau_{ij}V_{ji}.\end{aligned} \tag{B8}$$

Since the stress tensor is symmetric, the last expression in (B8) is equivalent to

$$(\bar{\tau}:\bar{V}) = \sum_i\sum_j \tau_{ji}V_{ji}, \tag{B9}$$

where $V_{ij} = \partial u_i/\partial x_j$. In the modeling equations, the summations are implied by imposing the Einstein convention for repeated indices.

In this report, the equations will be written in the dimensional form, while the solution algorithm implementation uses the nondimensional form.

$$k^* = \frac{k}{u_r^2}, \qquad \omega^* = \omega \frac{\mu_\infty}{\rho_\infty u_r^2}, \tag{B10}$$

Using also the definition of the turbulent viscosity ($\mu_t = \rho k/\omega$), and again suppressing the superscript $*$, the equation for the nondimensional turbulence kinetic energy per unit mass (k) can be written as

$$\frac{\partial}{\partial t}(\bar{\rho}k) + \frac{\partial}{\partial x_j}(\bar{\rho}\tilde{u}_j k) = \frac{\sqrt{\gamma}M_\infty}{Re_\infty}\left\{\bar{\rho}\tau_{ij}\frac{\partial \tilde{u}_i}{\partial x_j} - \frac{Re_\infty^2}{\gamma M_\infty^2}\beta^*\bar{\rho}k\omega + \frac{\partial}{\partial x_j}\left[\left(\mu + \sigma_k\frac{\bar{\rho}k}{\omega}\right)\frac{\partial k}{\partial x_j}\right]\right\}. \tag{B11}$$

The equation for the nondimensional specific dissipation rate (ω) is given by

$$\frac{\partial}{\partial t}(\bar{\rho}\omega) + \frac{\partial}{\partial x_j}(\bar{\rho}\tilde{u}_j\omega) = \tag{B12}$$
$$\frac{\sqrt{\gamma}M_\infty}{Re_\infty}\left\{\alpha\frac{\omega}{k}\bar{\rho}\tau_{ij}\frac{\partial \tilde{u}_i}{\partial x_j} - \frac{Re_\infty^2}{\gamma M_\infty^2}\beta\bar{\rho}\omega^2 + \sigma_d\frac{\bar{\rho}}{\omega}\frac{\partial k}{\partial x_j}\frac{\partial \omega}{\partial x_j} + \frac{\partial}{\partial x_j}\left[\left(\mu + \sigma_\omega\frac{\bar{\rho}k}{\omega}\right)\frac{\partial \omega}{\partial x_j}\right]\right\}.$$

THIS PAGE INTENTIONALLY LEFT BLANK

REPORT DOCUMENTATION PAGE	Form Approved OMB No. 0704–0188

1. REPORT DATE *(DD-MM-YYYY)*	2. REPORT TYPE	3. DATES COVERED *(From - To)*
01-10-2021	Technical Memorandum	

4. TITLE AND SUBTITLE

Solving Two-Equation Turbulence Models
With a Perspective on Solving Transport Equations

5a. CONTRACT NUMBER

5b. GRANT NUMBER

5c. PROGRAM ELEMENT NUMBER

6. AUTHOR(S)

R. C. Swanson

5d. PROJECT NUMBER

5e. TASK NUMBER

5f. WORK UNIT NUMBER

981698.01.04.23.43.03.02

7. PERFORMING ORGANIZATION NAME(S) AND ADDRESS(ES)

NASA

8. PERFORMING ORGANIZATION REPORT NUMBER

9. SPONSORING/MONITORING AGENCY NAME(S) AND ADDRESS(ES)

National Aeronautics and Space Administration
Washington, DC 20546-0001

10. SPONSOR/MONITOR'S ACRONYM(S)

NASA

11. SPONSOR/MONITOR'S REPORT NUMBER(S)

NASA/TM–20210016636

12. DISTRIBUTION/AVAILABILITY STATEMENT

Unclassified-Unlimited
Subject Category 02
Availability: NASA CASI (301) 621-0390

13. SUPPLEMENTARY NOTES

An electronic version can be found at http://ntrs.nasa.gov.

14. ABSTRACT

There are three principal objectives of this report. The first objective is to explore and evaluate the performance of the solution algorithm for the Reynolds-averaged Navier-Stokes (RANS) equations with two-equation turbulence models. The RANS and turbulence modeling equations are solved in a weakly coupled manner. A Runge-Kutta/Implicit scheme is the basis of the solution algorithm for both sets of equations. This scheme is used as a smoother for a multigrid method when solving the mean flow form of the conservation equations. Throughout this report, emphasis is given to reducing the residuals to machine zero in all flow calculations to eliminate error due to numerical integration of the discrete governing equations. The second objective of this report is to investigate frequently used two-equation models when solving the RANS equations. In this study, we consider the 2006 Wilcox and the 2003 Menter Shear Stress Transport (SST) models. Computations for flows over two different airfoils are examined to compare these turbulence models. Effects on modeling the physics of each flow due to variations in the models, such as using either strain rate or vorticity in the turbulence production term, are considered and discussed. The final objective is to provide a perspective on solving transport equations for turbulence modeling. Aspects of solving such stiff systems of equations, as well as various numerical difficulties and possible techniques to overcome them, are considered. Discussion is also provided concerning what is called 'numerical compatibility,' which is an essential requirement when designing an effective solution algorithm for solving transport equations.

15. SUBJECT TERMS

Aerodynamics, Turbulence Models

16. SECURITY CLASSIFICATION OF:			17. LIMITATION OF ABSTRACT	18. NUMBER OF PAGES	19a. NAME OF RESPONSIBLE PERSON
a. REPORT	b. ABSTRACT	c. THIS PAGE			STI Help Desk (email: help@sti.nasa.gov)
U	U	U	UU	89	19b. TELEPHONE NUMBER *(Include area code)* (301) 621-0390

THIS PAGE INTENTIONALLY LEFT BLANK